

# Depleting myeloid-biased haematopoietic stem cells rejuvenates aged immunity

<https://doi.org/10.1038/s41586-024-07238-x>

Received: 26 October 2022

Accepted: 26 February 2024

Published online: 27 March 2024

 Check for updates

Jason B. Ross<sup>1,2,3,4,9</sup>, Lara M. Myers<sup>5,9</sup>, Joseph J. Noh<sup>1,2</sup>, Madison M. Collins<sup>5,8</sup>, Aaron B. Carmody<sup>6</sup>, Ronald J. Messer<sup>5</sup>, Erica Dhuey<sup>1,2</sup>, Kim J. Hasenkrug<sup>5,10</sup> & Irving L. Weissman<sup>1,2,4,7,10</sup>

Ageing of the immune system is characterized by decreased lymphopoiesis and adaptive immunity, and increased inflammation and myeloid pathologies<sup>1,2</sup>. Age-related changes in populations of self-renewing haematopoietic stem cells (HSCs) are thought to underlie these phenomena<sup>3</sup>. During youth, HSCs with balanced output of lymphoid and myeloid cells (bal-HSCs) predominate over HSCs with myeloid-biased output (my-HSCs), thereby promoting the lymphopoiesis required for initiating adaptive immune responses, while limiting the production of myeloid cells, which can be pro-inflammatory<sup>4</sup>. Ageing is associated with increased proportions of my-HSCs, resulting in decreased lymphopoiesis and increased myelopoiesis<sup>3,5,6</sup>. Transfer of bal-HSCs results in abundant lymphoid and myeloid cells, a stable phenotype that is retained after secondary transfer; my-HSCs also retain their patterns of production after secondary transfer<sup>5</sup>. The origin and potential interconversion of these two subsets is still unclear. If they are separate subsets postnatally, it might be possible to reverse the ageing phenotype by eliminating my-HSCs in aged mice. Here we demonstrate that antibody-mediated depletion of my-HSCs in aged mice restores characteristic features of a more youthful immune system, including increasing common lymphocyte progenitors, naive T cells and B cells, while decreasing age-related markers of immune decline. Depletion of my-HSCs in aged mice improves primary and secondary adaptive immune responses to viral infection. These findings may have relevance to the understanding and intervention of diseases exacerbated or caused by dominance of the haematopoietic system by my-HSCs.

A single HSC can generate all blood cells and self-renew to maintain the stem cell pool throughout life<sup>2</sup>. HSCs demonstrate functional heterogeneity and can differ in their contribution to the lymphoid and myeloid cell lineages<sup>7–9</sup>. At least two HSC subsets exist: (1) bal-HSCs, which provide balanced production of lymphoid and myeloid cells; and (2) my-HSCs, which are biased towards predominant production of myeloid cells<sup>5,10</sup>. The frequency of my-HSCs relative to bal-HSCs increases with age<sup>1,11</sup>. This age-related shift from bal-HSCs to my-HSCs decreases lymphopoiesis and increases myelopoiesis<sup>12</sup>, thereby contributing to numerous pathologies in older individuals, including reduced adaptive immunity<sup>13</sup>, inflammaging<sup>14</sup> and several myeloid-related diseases. To address these and other age-related pathologies, we sought to develop a therapy to return the immune system to a more youthful state characterized by less my-HSCs and more HSCs with a balanced production of lymphoid and myeloid lineage cells.

To test whether antibody-mediated depletion of my-HSCs might enable bal-HSCs to reverse age-related immune decline by restoring

lymphopoiesis and limiting myeloid cell-driven inflammation, we identified distinct cell-surface markers on my-HSCs compared with bal-HSCs<sup>5,15–20</sup>, targeted and depleted my-HSCs *in vivo*, and characterized the effect of their depletion on the haematopoietic system and immune phenotypes, including functional immunity to new infections.

## Identifying surface antigens on my-HSCs

To identify candidate targets for therapeutic depletion of my-HSCs, we first established and validated a set of cell-surface antigens on my-HSCs (Fig. 1a–c and Extended Data Fig. 2a). Mouse HSCs ( $\text{Lin}^- \text{KIT}^+ \text{SCA1}^+ \text{FLT3}^- \text{CD34}^- \text{CD150}^+$ )<sup>15</sup> can be separated into my-HSCs or bal-HSCs based on their expression levels of CD150 (encoded by *Slamf1*); my-HSCs are CD150<sup>high</sup>, and bal-HSCs are CD150<sup>low</sup> (refs. 5,16). In addition to CD150, several markers of HSCs with myeloid bias have been described<sup>18,19</sup>. To identify the best target to deplete my-HSCs, we conducted a systematic search of all potential antigens increased relatively or absolutely

<sup>1</sup>Institute for Stem Cell Biology and Regenerative Medicine, Stanford University School of Medicine, Stanford, CA, USA. <sup>2</sup>Ludwig Center for Cancer Stem Cell Research and Medicine, Stanford University School of Medicine, Stanford, CA, USA. <sup>3</sup>Department of Radiation Oncology, Stanford University School of Medicine, Stanford, CA, USA. <sup>4</sup>Stanford Cancer Institute, Stanford University School of Medicine, Stanford, CA, USA. <sup>5</sup>Laboratory of Persistent Viral Diseases, Rocky Mountain Laboratories, National Institutes of Allergy and Infectious Diseases, National Institutes of Health, Hamilton, MT, USA. <sup>6</sup>Research Technologies Branch, Rocky Mountain Laboratories, National Institutes of Allergy and Infectious Diseases, National Institutes of Health, Hamilton, MT, USA. <sup>7</sup>Department of Pathology, Stanford University School of Medicine, Stanford, CA, USA. <sup>8</sup>Present address: Department of Biological and Physical Sciences, Montana State University Billings, Billings, MT, USA. <sup>9</sup>These authors contributed equally: Jason B. Ross, Lara M. Myers. <sup>10</sup>These authors jointly supervised this work: Kim J. Hasenkrug, Irving L. Weissman. e-mail: khasenkrug@nih.gov; irv@stanford.edu

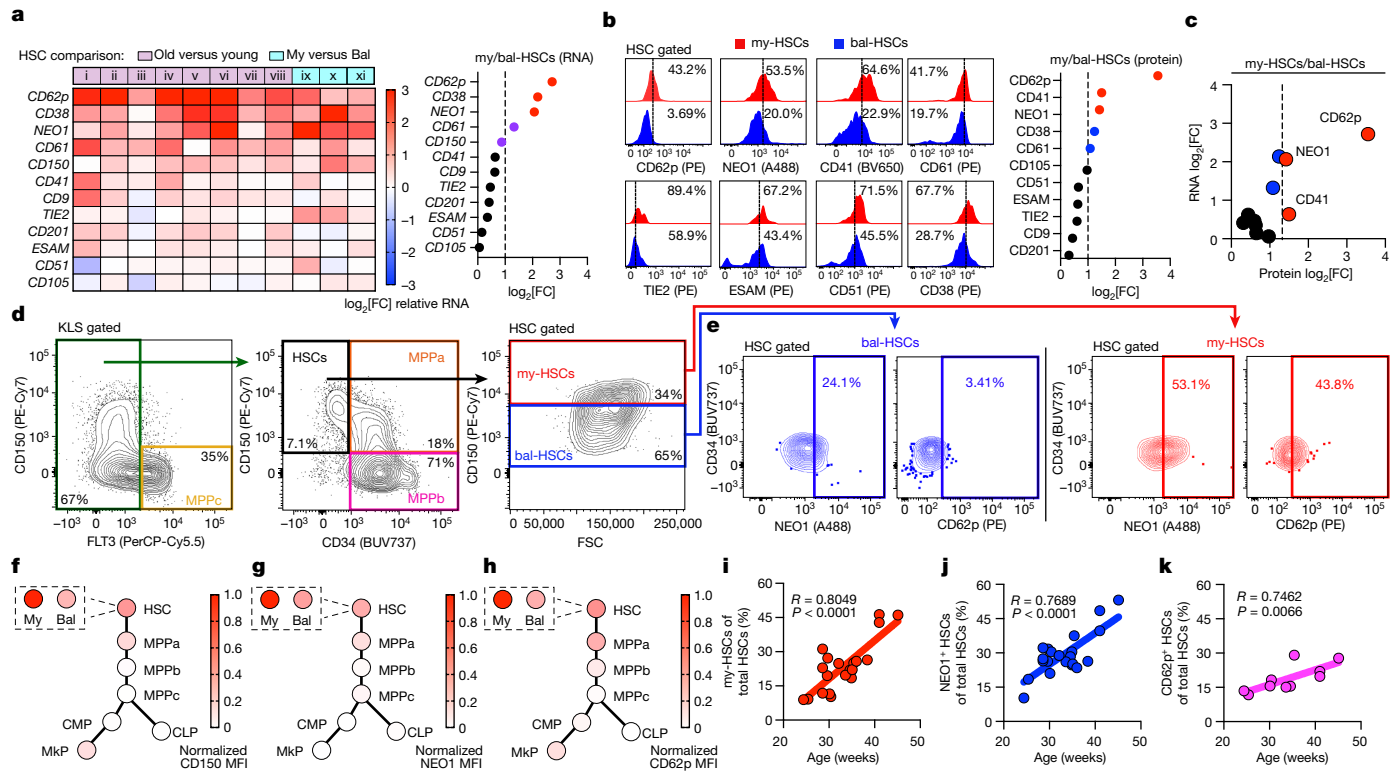


**Fig. 1 | Identification of cell-surface antigens on my-HSCs.** **a**, Candidate marker gene expression (RNA) across independent datasets (left), with the mean  $\log_2$ -transformed fold change ( $\log_2[\text{FC}]$ ; old-HSCs versus young-HSCs; my-HSCs (My) versus bal-HSCs (Bal)) (right). The following datasets were used: old HSCs versus young HSCs (i<sup>16</sup>, ii<sup>24</sup>, iii<sup>25</sup>, iv<sup>26</sup>, v<sup>27</sup>, vi<sup>28</sup>, vii<sup>29</sup>, viii<sup>30</sup>) and my-HSCs versus bal-HSCs (ix<sup>19</sup>, x<sup>22</sup>, xi<sup>21</sup>). **b**, The percentage positive for each cell surface marker on my-HSCs versus bal-HSCs (left). Right, my-HSC fold-enrichment for each marker. **c**, The my-HSC/bal-HSC  $\log_2$ -transformed fold change in RNA expression (y axis) versus cell-surface protein expression (x axis) for candidate markers. **d**, Representative flow cytometry analysis of total HSCs (KLS FLT3<sup>+</sup>CD34<sup>+</sup>CD150<sup>+</sup>), my-HSCs (KLS FLT3<sup>+</sup>CD34<sup>+</sup>CD150<sup>high</sup>) and bal-HSCs (KLS FLT3<sup>+</sup>CD34<sup>+</sup>CD150<sup>low</sup>) from mouse bone marrow, after excluding dead cells, doublets and gated on KLS. **e**, Representative flow cytometry analysis of the

percentage of bal-HSCs (left) or my-HSCs (right) that are NEO1<sup>+</sup> or CD62p<sup>+</sup>. **f–h**, The relative cell-surface expression of CD150 (f), NEO1 (g) and CD62p (h) on total HSCs (my-HSCs + bal-HSCs), my-HSCs, bal-HSCs, MPPa, MPPb, MPPc, CMPs (CMPs + GMPs), MkPs and CLPs. Flow cytometry median fluorescence intensity (MFI) values for antibodies to each marker were obtained for each population and normalized from 0 to 1 (from lowest to highest). **i–k**, The percentage of total HSCs (KLS FLT3<sup>+</sup>CD34<sup>+</sup>CD150<sup>+</sup>) that are my-HSCs (that is, CD150<sup>high</sup>) (i), NEO1<sup>+</sup> (j) or CD62p<sup>+</sup> (k) on the y axis, versus mouse age (weeks) on the x axis.  $n = 21$  (i,j) and  $n = 10$  (k) mice. Approximate mouse ages were as follows: 4–6 (b–h) and 6–12 (i–k) months. For b–k, bone marrow was KIT-enriched before analysis.  $P$  values and  $R$  values were calculated using one-tailed Pearson correlation coefficient (i–k).  $n$  values indicate independent mice.

on my-HSCs. my-HSCs are more abundant in aged animals<sup>5</sup> and in subpopulations of HSCs defined by a combination of markers and/or genetic reporters<sup>19,21,22</sup>. Thus, we reasoned that my-HSC-specific genes would be enriched in transcriptional datasets of (1) HSCs from aged animals<sup>23–31</sup>; and (2) HSCs with functional myeloid-bias<sup>19,21,22</sup> (Fig. 1a). Examination of these datasets yielded 12 candidate genes encoding cell-surface proteins that were highly enriched in aged HSCs and/or my-HSCs (Fig. 1a and Extended Data Fig. 2a). As expected, CD150 emerged from this analysis, along with several markers associated with my-HSCs: CD41<sup>17</sup>, CD61<sup>18</sup>, CD62p<sup>20</sup> and NEO1<sup>19</sup>. To validate these candidates and identify the best target on my-HSCs, we evaluated their cell-surface levels on my-HSCs and bal-HSCs using antibodies and flow cytometry.

As the ideal target antigen to deplete my-HSCs would be highly expressed on the cell surface of my-HSCs relative to bal-HSCs, we compared the cell-surface expression of each candidate antigen on my-HSCs and bal-HSCs using marker-specific antibodies (Fig. 1b). For each marker, the fold-enrichment was calculated for my-HSCs based on the proportion of my-HSCs (CD150<sup>high</sup> HSCs) relative to bal-HSCs (CD150<sup>low</sup> HSCs) that were marker positive. Antibodies against NEO1 and CD41 resulted in a substantially increased frequency of staining of my-HSCs (Figs. 1b,e), consistent with NEO1 and CD41 marking HSCs with myeloid bias<sup>17,19</sup>. Among the remaining candidates, CD62p led to

the greatest enrichment for my-HSCs (Fig. 1b–e). Overall, the most highly enriched cell-surface proteins on my-HSCs relative to bal-HSCs were CD41, CD62p and NEO1 (Fig. 1b–c). Together with CD150, we focused on these cell-surface proteins as candidate target antigens for antibody-mediated depletion of my-HSCs.

To provide insights into potential off-target effects from antibody treatment, we determined the expression of each candidate on haematopoietic progenitor cells (HPCs) and mature differentiated cells, as well as non-haematopoietic tissues. HSCs generate multi-potent progenitors (MPPs), which generate lineage-restricted common myeloid progenitors (CMPs)<sup>32</sup> and common lymphocyte progenitors (CLPs)<sup>33</sup>. Flow cytometry analysis revealed that none of the candidate surface proteins were highly expressed by these subsets, other than CD41, which was abundantly expressed in megakaryocyte progenitors (MkPs) (Fig. 1f–h and Extended Data Fig. 2b–h). These results were largely concordant with transcriptomic profiling of these same sorted populations from independent datasets<sup>31</sup> (Extended Data Fig. 1a–l). The most promising candidates—CD150, CD41, CD62p and NEO1—were not highly expressed in mature haematopoietic cells on the basis of RNA levels (Extended Data Fig. 1m) or flow cytometry analysis (Extended Data Fig. 2g,h) and were relatively specific to the haematopoietic system compared to other tissues (Extended Data Fig. 1n,o). These results demonstrated the relative specificity of these markers to my-HSCs

# Article

compared with bal-HSCs, haematopoietic progenitors and mature cells, and non-haematopoietic tissues.

Given the increased abundance of my-HSCs with age<sup>3,5</sup>, we evaluated whether HSCs isolated from aged mice demonstrated increased expression of the candidate markers we identified. We evaluated HSCs in mice spanning approximately 6 months to 1 year of age, focusing on CD41, CD62p and NEO1, which were the most highly enriched markers on my-HSCs. We observed a significant positive correlation with the proportion of my-HSCs and mouse age, consistent with the expansion of my-HSCs during ageing<sup>5</sup> (Fig. 1i and Extended Data Fig. 2j). Similarly, we also observed a strong positive correlation with age and the percentage of total HSCs that were NEO1<sup>+</sup>, CD41<sup>+</sup> or CD62p<sup>+</sup> (Fig. 1j,k and Extended Data Fig. 2i), consistent with NEO1, CD41 and CD62p marking my-HSCs that increase with age. We selected these cell-surface antigens, along with CD150, as candidate targets to deplete my-HSCs *in vivo*.

## Antibody-mediated depletion of my-HSCs

We next determined whether we could deplete my-HSCs *in vivo* by targeting these my-HSC antigens (Extended Data Fig. 5a). We focused on CD150, CD62p and NEO1, which demonstrated the greatest enrichment for my-HSCs relative to bal-HSCs and HPCs (Fig. 1b–h). We developed independent antibody-conditioning regimens to deplete my-HSCs for each target, optimizing for regulators of cell clearance, including anti-phagocytic signals<sup>34</sup>, antibody density and isotype.

To determine the effect of targeting CD150, we tested anti-CD150 antibodies for their ability to deplete my-HSCs *in vivo*. We administered rat IgG2b anti-CD150 antibodies to adult mice (aged 6–7 months) and evaluated the bone marrow after approximately 1 week<sup>35</sup> (Extended Data Fig. 5b). To control for antibody masking, whereby *in vivo* treatment with anti-CD150 antibodies might prevent the detection of target cells, we identified and validated independent non-masking antibodies to CD150 (Extended Data Fig. 3a–l). Treating mice with anti-CD150 antibodies significantly depleted my-HSCs relative to bal-HSCs both in terms of frequency (Extended Data Fig. 4a) and absolute number (Extended Data Fig. 4b,r). To verify the depletion of my-HSCs, we confirmed that HSCs expressing the independent my-HSC antigen NEO1 were also depleted after treatment with anti-CD150 antibodies (Extended Data Fig. 4c). This finding and others described below rule out single-antigen modulation as the mechanism for the lack of CD150 in the HSC analyses, but favoured depletion of cells with both markers. Consistent with rat IgG2b antibodies having greater depleting activity than IgG2a in mice, treatment with rat IgG2a anti-CD150 antibodies was only modestly effective (Extended Data Fig. 4i). Collectively, these results demonstrated that antibody targeting of CD150 was sufficient to deplete a substantial fraction of my-HSCs *in vivo*.

We optimized the my-HSC-depletion protocol by considering factors that limit *in vivo* cell clearance. As antibody-mediated depletion can be limited by the anti-phagocytic signal CD47<sup>34,36</sup>, we speculated that blocking CD47 could enhance the depletion of my-HSCs. Compared with anti-CD150 alone, dual treatment with anti-CD150 and anti-CD47 antibodies decreased the frequency of my-HSCs relative to bal-HSCs (Extended Data Fig. 4a,b). To further decrease the threshold for cell clearance, we added low doses of anti-KIT, which also depleted my-HSCs relative to bal-HSCs in the presence of anti-CD150 (Extended Data Fig. 4a,b). The addition of anti-CD47 and/or anti-KIT to anti-CD150 increased the frequency and absolute number of bal-HSCs in the bone marrow after approximately 1 week (Extended Data Fig. 4a,b), consistent with their expansion and/or redistribution after my-HSC depletion. Overall, the most effective regimen to deplete my-HSCs relative to bal-HSCs was by combining antibodies against CD150, CD47 and KIT (Fig. 2a,d and Extended Data Fig. 4a,b).

The optimized protocol that we developed to deplete my-HSCs by targeting CD150 informed our strategy to deplete my-HSCs by targeting CD62p or NEO1. To target CD62p, we used an anti-CD62p antibody

of mouse IgG2a isotype, which was predicted to have high depleting activity in mice. Indeed, administration of anti-CD62p in combination with anti-KIT and anti-CD47 significantly depleted my-HSCs in the bone marrow after approximately 1 week (Fig. 2b,e). To target NEO1, we combined goat anti-mouse NEO1 antisera with anti-CD47 and anti-KIT, which also resulted in effective depletion of my-HSCs in the bone marrow after approximately 1 week (Fig. 2c,f and Extended Data Fig. 5c–s). Similar to treatment with anti-CD150 (Extended Data Fig. 4c,d), treatment with anti-CD62p or anti-NEO1 also depleted HSCs expressing the my-HSC antigen NEO1 (Extended Data Fig. 4p,q). Taken together, these experiments established three separate antibody-conditioning regimens that deplete my-HSCs bearing two independent cell surface antigens *in vivo*. Again, depletion of cells marked by two independent surface antigens with antibodies to one marker only rules out antigenic modulation and favours my-HSC cellular depletions.

To verify changes in HSC composition after my-HSC depletion, we conducted gene expression profiling of purified total HSCs ( $\text{Lin}^- \text{KIT}^+ \text{SCA}1^+$  (KLS)  $\text{FLT3}^- \text{CD34}^- \text{CD150}^+$ ) isolated from aged (11 months) mice with or without antibody conditioning (Fig. 2g,h and Extended Data Figs. 3m,n and 4x). Gene set enrichment analysis (GSEA) revealed that HSCs isolated from mice receiving antibody conditioning were enriched in gene signatures of young HSCs and bal-HSCs (Fig. 2g,h), and were depleted in gene signatures of old HSCs and my-HSCs<sup>18–20,22,26–29,37</sup> (Fig. 2g,h and Supplementary Table 1). Thus, in addition to depleting HSCs marked by validated my-HSC cell-surface proteins, antibody conditioning altered the molecular composition of the HSC compartment by selectively depleting the my-HSC RNA ‘fingerprint’ cells and retaining or expanding the young or bal-HSC RNA fingerprints.

To functionally validate that changes in HSC potential are altered after antibody conditioning, we performed transplant experiments with purified HSCs and evaluated myeloid versus lymphoid lineage potential in recipient animals. We purified 100 total HSCs (KLS  $\text{FLT3}^- \text{CD34}^- \text{CD150}^+$ ) isolated from CD45.2 aged (11 months) mice with or without antibody conditioning and transplanted them into age-matched (2 months) CD45.1 congenic recipient irradiated mice (Extended Data Fig. 3m,n). Peripheral blood analysis revealed that mice reconstituted with HSCs isolated from antibody-conditioned mice demonstrated a significantly decreased myeloid-to-lymphoid cell ratio compared with mice reconstituted with HSCs isolated from control mice (Fig. 2i–k and Extended Data Fig. 4t–w), consistent with antibody conditioning depleting my-HSCs. Taken together, these results demonstrate that antibody conditioning depletes my-HSCs *in vivo* based on cell surface, molecular and functional phenotypes.

## my-HSC depletion rebalances progenitors

To determine the effect of depleting my-HSCs on downstream progenitors, we examined CLPs<sup>33</sup> and myeloid progenitors (CMPs + GMPs, MKPs, MEPs) in the bone marrow from mice receiving each antibody conditioning regimen (Extended Data Fig. 5a,b). Approximately 1 week after treatment, all of the antibody protocols significantly increased the frequency of CLPs or IL-7RA<sup>+</sup> lymphocyte precursors<sup>33</sup> (Fig. 2d–f and Extended Data Fig. 4j,k). Protocols targeting CD62p or NEO1 decreased the frequency of myeloid progenitors (Fig. 2e,f and Extended Data Fig. 4l,m) and increased the ratio of lymphoid progenitors (CLPs) to myeloid progenitors (CMPs + GMPs) by up to fourfold (Extended Data Fig. 4o). The increase in lymphoid progenitors and decrease in myeloid progenitors after my-HSC depletion in adult mice pointed to the potential of this treatment to reverse age-related immune decline.

## my-HSC depletion in old mice *in vivo*

To determine whether reversing the age-related shift from bal-HSCs to my-HSCs would restore cells critical for immune function and reverse

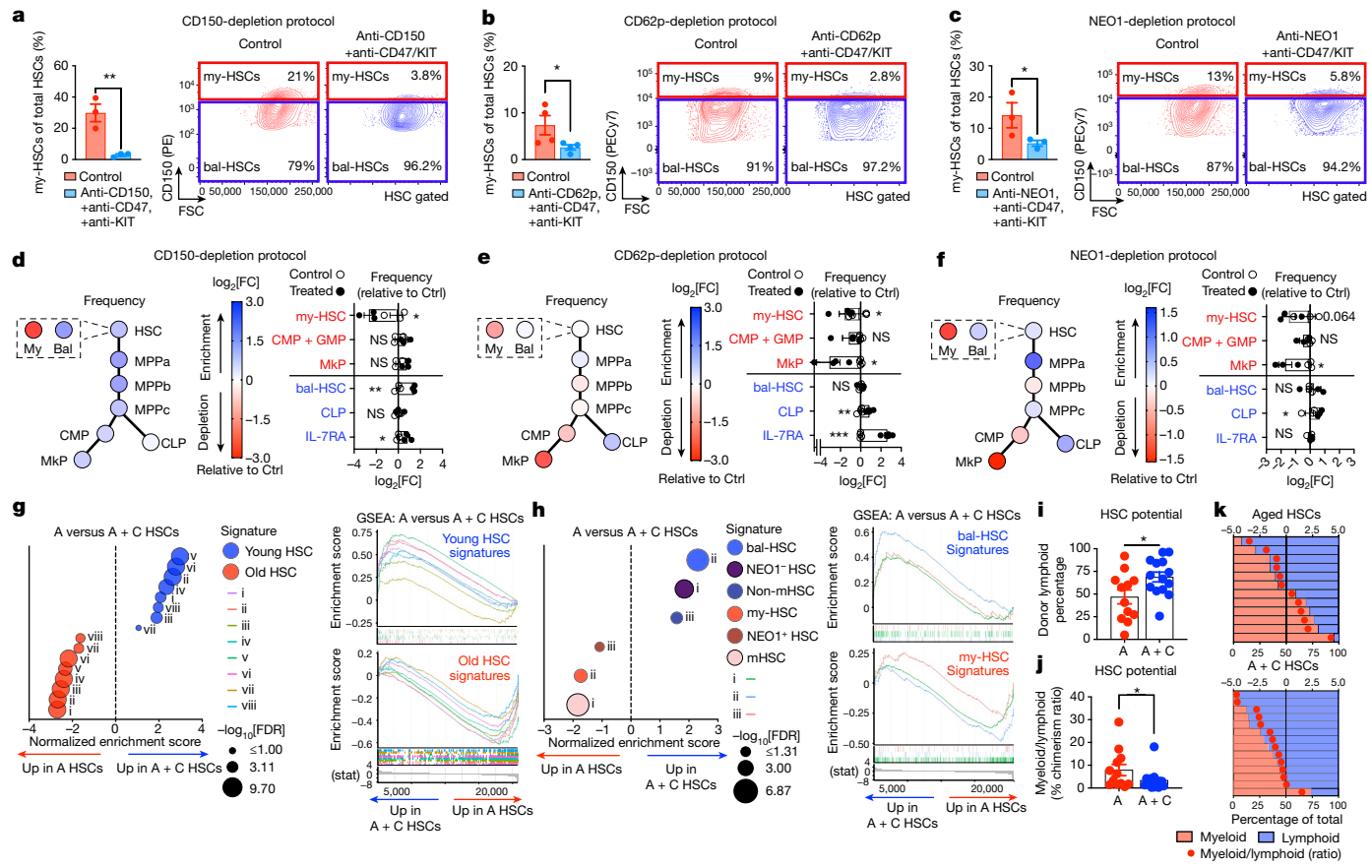


**Fig. 2 | Antibody-mediated depletion of my-HSCs in vivo.** **a–c**, The percentage of total HSCs that are my-HSCs after the anti-CD150 (**a**; \*\*P = 0.0045), anti-CD62p (**b**; \*P = 0.0374) or anti-NEO1 (**c**; \*P = 0.0465) optimized protocols (+anti-CD47 + anti-KIT), with representative flow cytometry. n = 3 (**a,c**) and n = 4 (**b**) mice per group. **d–f**, Enrichment (blue) or depletion (red) as the percentage of live cells for total HSCs (HSC), my-HSCs (My), bal-HSCs (Bal), MPPs, CLPs, CMPs + GMPs and MkPs after the anti-CD150 (**d**), anti-CD62p (**e**) or anti-NEO1 (**f**) protocols (+anti-CD47 + anti-KIT). log<sub>2</sub>-transformed treated values are shown relative to the control mean. n = 3 (**d,f**) and n = 4 (**e**) mice per group. **g–k**, Total HSCs were FACS sorted from aged mice without (aged (A)) or with my-HSC depletion (aged + conditioning (A + C)) and underwent RNA-seq (**g–h**) or transplantation (**i–k**). Depletion protocol was anti-NEO1 + anti-CD62p + anti-CD47 + anti-KIT. n = 3 (A) and n = 3 (A + C) mice. **g,h**, GSEA comparison between the A HSC versus A + C HSC groups, ranked by DESeq2 test statistic (stat), using gene signatures from young HSCs versus old HSCs (**i** (ref. 20), **ii** (ref. 37), **iii** (ref. 26), **iv** (ref. 27), **v** (ref. 22), **vi** (ref. 28), **vii** (ref. 18), **viii** (ref. 29)) (**g**) or bal-HSCs versus my-HSCs (**h**).

(**i** (ref. 18), **ii** (ref. 22) and **iii** (ref. 19)) (**h**). n = 3 (A) and n = 3 (A + C) mice. mHSC, myeloid-biased LT-HSCs, as per ref. 18. **i–k**, HSC lineage potential 16 weeks after transplantation of 100 total HSCs FACS-sorted from CD45.2 aged mice without (A) or with (A + C) my-HSC depletion into CD45.1 recipients. **i,j**, The donor lymphoid percentage (**i**; \*P = 0.0126) and the myeloid/lymphoid percentage chimerism ratio (**j**; \*P = 0.0492) at week 16. **k**, For each recipient (y axis), the percentage of donor cells (bottom x axis) that are myeloid (red bars) or lymphoid (blue bars) and the myeloid/lymphoid log<sub>2</sub>-transformed ratio (red circles) (top x axis) at week 16 are shown. n = 12 (A) and n = 14 (A + C) recipient mice. Mouse ages were as follows: 5–9 months (**a–f**), 11 months (donors, **g–k**) and 2 months (recipients, **i–k**). For **a–k**, bone marrow was KIT-enriched before analysis or sorting. P values were obtained using unpaired parametric one-tailed t-tests (**a–f,i,j**) or GSEA with false-discovery rate (FDR) adjustment (**g,h**). Data are mean ± s.e.m. n indicates independent mice. \*P < 0.05, \*\*P < 0.005, \*\*\*P < 0.0005. Exact P values are provided as source data.

age-related markers of immune decline<sup>3,5</sup>, we compared young-adult mice (aged 3–6 months) with aged mice (aged 18–24 months) with or without anti-NEO1 antibody conditioning. Analyses were conducted after around 1 week to evaluate acute effects, or after around 8 weeks or 16 weeks to evaluate persistent effects, which is after the estimated clearance of antibodies<sup>35</sup> and non-self-renewing cells<sup>38</sup> (Fig. 3a). Aged mice receiving antibody conditioning demonstrated a significant decrease in my-HSCs after approximately 1 week (Fig. 3b,c), with no significant acute effect on the frequency of mature B cells or myeloid cells (Extended Data Fig. 6h–k). Notably, 8 weeks after treatment, the frequency of my-HSCs relative to bal-HSCs was significantly reduced (Extended Data Fig. 6a), which we confirmed on the basis of the absolute numbers of cells in total bone marrow in an independent experiment (Extended Data Fig. 9c). Thus, antibody conditioning depleted my-HSCs in aged animals at least several months after a single administration. The effect on CLPs, which are non-self-renewing progenitors<sup>33</sup>, was evaluated next. Compared with young-adult mice, untreated aged

mice demonstrated a significant decrease in the frequency of CLPs (Fig. 3d), but antibody-conditioned aged mice showed increased frequencies of CLPs 8 weeks and 16 weeks after treatment (Fig. 3b,d). These results underscored the effect of a single administration of therapy to rejuvenate the haematopoietic stem cell and progenitor compartments.

## my-HSC depletion increases lymphocytes

A critical deficit of the aged immune system is the reduced generation of T and B lymphocytes capable of recognizing novel antigens<sup>13</sup>. Given that the depletion of my-HSCs in aged mice increased lymphocyte progenitors, we sought to determine whether these changes were sufficient to increase naive T and B cells. We evaluated mice after 8 weeks, as the generation of new T and B cells from HSCs peaks between 7–11 weeks<sup>15,19</sup>. Although we did not observe significant differences in thymus weight (Extended Data Fig. 6l), treated mice contained

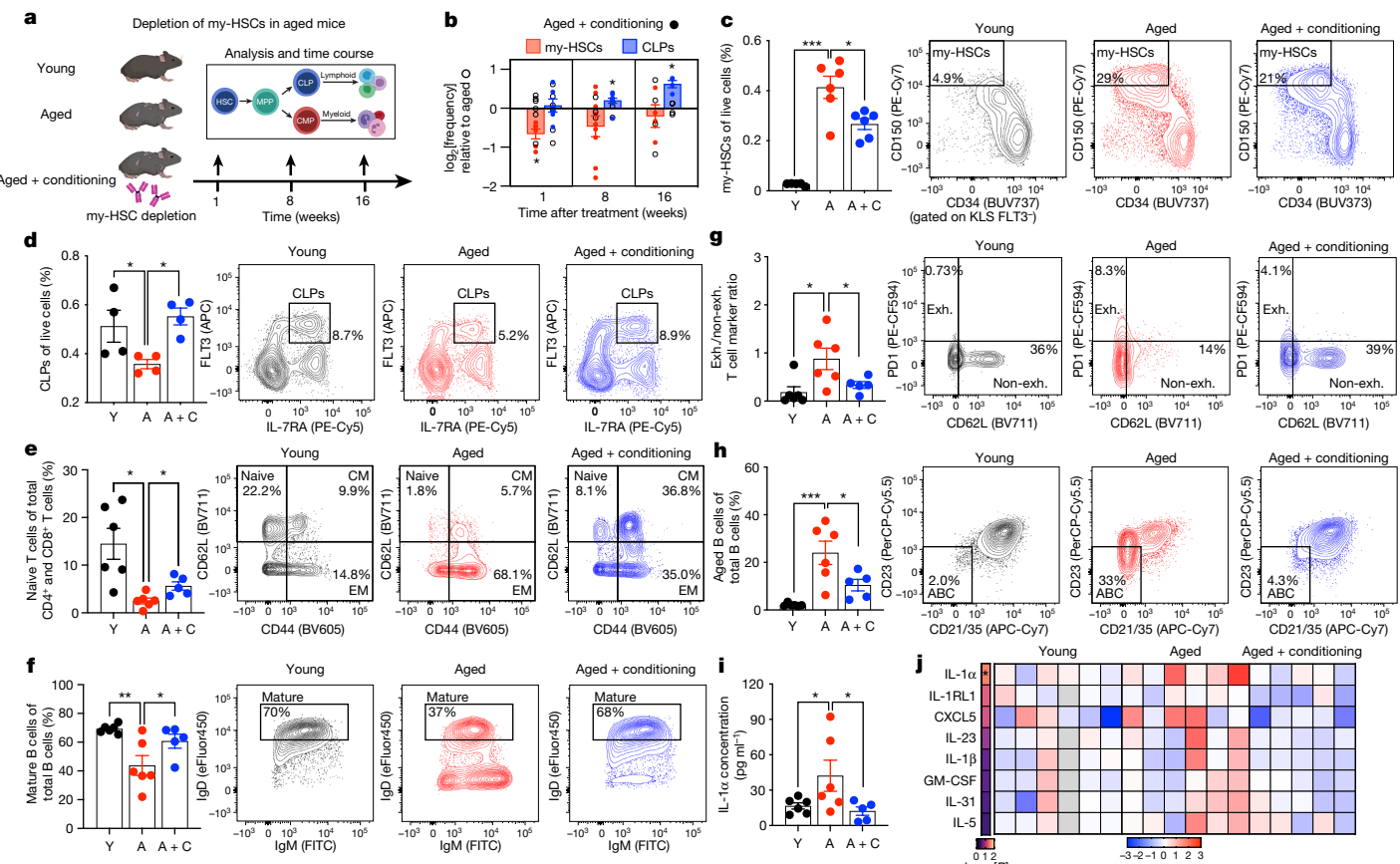


**Fig. 3 | Depletion of my-HSCs in aged mice restores youthful immune features.** **a**, Young-adult mice (Y) compared with aged mice without (A) or with anti-NEO1 conditioning (A + C), approximately 1, 8 or 16 weeks after treatment. The diagram was created using BioRender. **b**, The frequency (percentage of live cells) of my-HSCs and CLPs in the A + C group relative to the A group.  $n = 6$  (A, A + C, at 1 week),  $n = 4$  (A),  $n = 9$  (A + C, at 8 weeks) and  $n = 4$  (A, A + C, at 16 weeks).  $\log_2$ -transformed treated (A + C) values relative to mean of aged control are shown. **c**, The frequency of my-HSCs (percentage of live cells) in the bone marrow at week 1.  $n = 5$  (Y) and  $n = 6$  (A, A + C). **d**, The frequency of CLPs (percentage live) in the bone marrow at week 16.  $n = 4$  (Y, A, A + C). **e–j**, Naive T cells (CD4<sup>+</sup>CD62L<sup>+</sup>) as the percentage of total CD4<sup>+</sup> and CD8<sup>+</sup> T cells in the blood (**e**); mature B cells (IgM<sup>+</sup>IgD<sup>+</sup>) as the percentage of total B cells (CD19<sup>+</sup>B220<sup>+</sup>) in the blood (**f**); CD4<sup>+</sup>T cell ratio (percentage of PD1<sup>+</sup>CD62L<sup>+</sup> cells)/(percentage of PD1<sup>+</sup>CD62L<sup>+</sup> cells)<sup>41</sup> (**g**); aged B cells (CD21/CD35<sup>+</sup>CD23<sup>+</sup>)<sup>42</sup> as the percentage of total mature B cells (CD19<sup>+</sup>IgM<sup>+</sup>CD93<sup>+</sup>CD43<sup>+</sup>) in the blood (**h**); the plasma

concentration of IL-1 $\alpha$  (**i**); and the plasma abundance of top 17% proteins increased in the A group versus A + C group (**j**). For **e–j**, data are from week 8.  $n = 6$  (Y, A) and  $n = 5$  (A + C). For **j**, values are relative to young (Y) mean and  $\log_2$ -transformed. The grey squares indicate removed statistical outliers.  $-\log_{10}[P]$  values were calculated comparing the A group versus the A + C group. Exh., exhausted. For **b–j**, approximate mouse ages were as follows: young adult (3–6 months) and aged (18–24 months). For **b–d**, bone marrow was KIT-enriched before analysis.  $P$  values were obtained using unpaired parametric one-tailed  $t$ -tests (**b**), ordinary one-way analysis of variance (ANOVA) followed by one-tailed Dunnett's multiple-comparison test using aged as the control (**c,d,f–i**), Brown-Forsythe and Welch ANOVA followed by two-tailed Dunnett's T3 multiple-comparison test using aged as the control (**e**) and one-way ANOVA followed by Holm multiple-comparison test (**j**). Data are mean  $\pm$  s.e.m.  $n$  values represent independent mice. Exact  $P$  values are provided as source data.

all of the thymic progenitor subsets associated with thymus function<sup>39</sup> (Extended Data Fig. 6m,n). After 8 weeks, aged mice receiving antibody conditioning demonstrated a significant increase in the frequency (Fig. 3e) and absolute number (Extended Data Fig. 7a) of circulating naive (CD44<sup>−</sup>CD62L<sup>+</sup>) T cells (CD4<sup>+</sup> and CD8<sup>+</sup>) compared with age-matched controls. To further investigate T cell subsets, we examined central (stem) memory (T<sub>CM</sub>; CD44<sup>+</sup>CD62L<sup>+</sup>) and effector memory (T<sub>EM</sub>; CD44<sup>+</sup>CD62L<sup>−</sup>) cells by canonical markers or by cluster-based analysis (Extended Data Figs. 7f–j and 8a,b). Depletion of my-HSCs was associated with slightly increased T<sub>CM</sub> cells on the basis of the absolute number (Extended Data Fig. 7b), but the absolute number of T<sub>EM</sub> cells was not significantly affected (Extended Data Fig. 7c). As T<sub>CM</sub> cells are derived by expansion from activated naive T cells specific for antigens, and transition to the CD44<sup>+</sup>CD62L<sup>+</sup> state after the antigen disappears, future studies will be required to determine the CM pool to define novel antigens before and after infection. Similar to our results for T cells, aged mice receiving antibody

conditioning also demonstrated a significant increase in the frequency (Fig. 3f) and absolute numbers (Extended Data Fig. 7d) of mature circulating B cells (CD19<sup>+</sup>B220<sup>+</sup>IgM<sup>+</sup>IgD<sup>+</sup>). Antibody treatment did not significantly affect the total number of circulating CD45<sup>+</sup> leukocytes (Extended Data Fig. 7e). These results demonstrated that depletion of my-HSCs selectively increased both naive T cells and mature B cells in aged mice.

### my-HSC depletion lowers ageing phenotypes

In addition to their decreased frequency and production in aged animals, lymphocytes undergo age-related accumulation of markers of exhaustion and/or inflammation thought to contribute to immune decline<sup>41</sup>. In aged mice, CD4<sup>+</sup> T cells with an exhausted phenotype (PD1<sup>+</sup>CD62L<sup>−</sup>) increase relative to those with a non-exhausted phenotype (PD1<sup>+</sup>CD62L<sup>+</sup>)<sup>41</sup>, which we confirmed in our experimental cohort (Fig. 3g). Compared with the aged controls, antibody conditioning

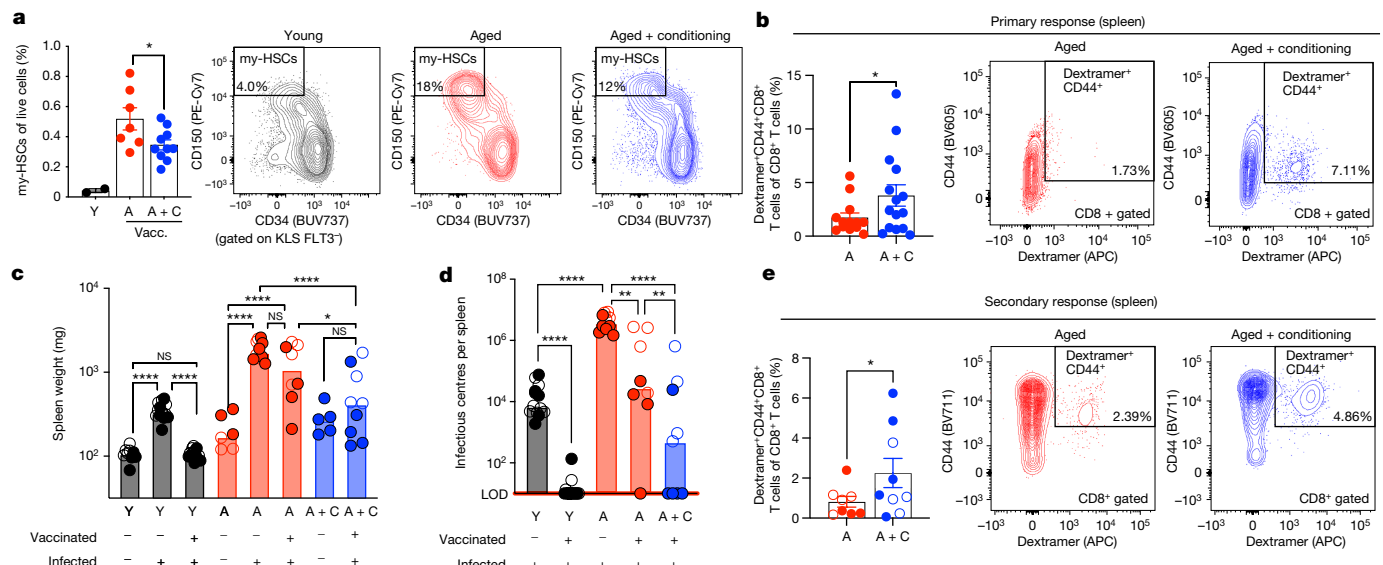


**Fig. 4 | Antibody conditioning enhances functional immunity in aged mice.**

**a**, The frequency of my-HSCs in young adult (Y) or aged mice without (A) or with (A + C) antibody conditioning 10-weeks after anti-NEO1<sup>v2</sup> treatment. Mice in the A and A + C groups were vaccinated (vacc.) 2 weeks before analysis.  $n = 2$  (Y),  $n = 7$  (A) and  $n = 10$  (A + C) mice. \* $P = 0.0159$  (A versus A + C). **b**, The percentage of splenic CD8<sup>+</sup> T cells that are dextramer<sup>+</sup>CD44<sup>+</sup> 10–14 days after vaccination in age-matched (20–26 months) mice without (A) or with (A + C) antibody conditioning. For the A + C group, my-HSC depletion was performed using anti-NEO1<sup>v2</sup> 2 months before vaccination.  $n = 13$  (A, vaccinated) and  $n = 15$  (A + C, vaccinated). \* $P = 0.0412$ . **c**, The spleen weight (mg) of naive, FV-infected or vaccinated and FV-infected mice.  $n = 9$  (Y, naive),  $n = 13$  (Y, FV-infected),  $n = 13$  (Y, vaccinated and FV-infected),  $n = 6$  (A, naive),  $n = 10$  (A, FV-infected),  $n = 8$  (A, vaccinated and FV-infected),  $n = 5$  (A + C, naive) and  $n = 9$  (A + C, vaccinated and FV-infected) mice. Data were log<sub>10</sub>-transformed. **d**, Infectious virus levels in FV-infected or vaccinated + FV-infected mice;

$n = 13$  (Y, FV-infected),  $n = 13$  (Y, vaccinated + FV-infected),  $n = 10$  (A, FV-infected),  $n = 8$  (A, vaccinated + FV-infected) and  $n = 9$  (A + C, vaccinated + FV-infected). Data are log<sub>10</sub>-transformed. The limit of detection (LOD) is indicated by a red line. **e**, The percentage of splenic CD8<sup>+</sup> T cells that are dextramer<sup>+</sup>CD44<sup>+</sup> in vaccinated + FV-infected mice.  $n = 8$  (A, vaccinated + FV-infected),  $n = 9$  (A + C, vaccinated + FV-infected). \* $P = 0.0473$ . For **a,c–e**, approximate mouse ages were as follows: 3–6 months (Y) and 21–22 months (A and A + C). For **c–e**, data from experiments with anti-NEO1<sup>v1</sup> (open circles) or anti-NEO1<sup>v2</sup> (closed circles) were combined. For **a**, bone marrow was KIT-enriched before analysis.  $P$  values were obtained using one-tailed unpaired parametric  $t$ -tests (**a,b**), ordinary one-way ANOVA followed by Tukey's multiple-comparison test (**c,d**) or one-tailed unpaired parametric  $t$ -tests with Welch's correction (**e**). Anti-NEO1<sup>v2</sup> is the same as anti-NEO1<sup>v1</sup> (anti-NEO1 + anti-CD47 + anti-KIT) but with the addition of mouse (IgG2a) anti-goat. Data are mean  $\pm$  s.e.m. (**a,b,e**) or median (**c,d**).  $n$  values represent independent mice. Exact  $P$  values are provided as source data.

decreased CD4<sup>+</sup>PD1<sup>+</sup>CD62L<sup>−</sup> cells relative to CD4<sup>+</sup>PD1<sup>−</sup>CD62L<sup>+</sup> cells (Fig. 3g). Aged mice also accumulate age-associated B cells correlated with reduced humoral immunity<sup>42</sup>. Our control cohort of aged mice had an increased frequency of age-associated B cells (CD19<sup>+</sup>IgM<sup>+</sup> CD93<sup>−</sup>CD43<sup>−</sup>CD21<sup>+</sup>CD35<sup>+</sup>CD23<sup>−</sup>)<sup>42</sup> relative to young-adult mice, which was significantly decreased after antibody conditioning (Fig. 3h). Thus, in addition to increasing naive T cells and mature B cells, antibody conditioning also suppressed lymphocyte age-related immunophenotypes. Collectively, these results suggested my-HSC depletion might enhance immune function in aged animals.

### my-HSC depletion lowers inflammatory markers

In addition to immune cell phenotypes, ageing is associated with increased levels of circulating pro-inflammatory mediators, referred to as inflammapageing, which has been linked to HSC dysfunction and myeloid bias<sup>14</sup>. To determine whether my-HSC depletion in aged animals affected pro-inflammatory mediators, we evaluated circulating proteins in plasma from young-adult and aged mice, with or without antibody conditioning, after approximately 8 weeks. The most elevated proteins in aged mice relative to young-adult mice were the pro-inflammatory factors IL-1 $\alpha$ <sup>43</sup> and CXCL5<sup>14</sup> (Extended Data Fig. 6b), which were also the most decreased proteins in aged mice receiving antibody conditioning (Fig. 3i,j and Extended Data Fig. 6c,d). Antibody conditioning decreased additional pro-inflammatory mediators in aged mice, including IL-1 $\beta$ <sup>44</sup>, CXCL2 (also known as MIP-2)<sup>14,44</sup> and IL-23 (Fig. 3j and Extended Data Fig. 6c,e). Thus, in addition to resulting in a more youthful composition of immune cells, my-HSC depletion decreased

the levels of circulating pro-inflammatory mediators several months after treatment.

### my-HSC depletion enhances aged immunity

A hallmark of immune ageing is reduced resistance to infection and responsiveness to vaccination<sup>13</sup>, as became evident during the COVID-19 pandemic<sup>45</sup>. To determine whether my-HSC depletion enhanced functional immunity to infection, we examined the immune responses of mice to live-attenuated virus and subsequent challenge with a pathogenic viral infection using the mouse Friend retrovirus (FV) model<sup>46,47</sup>. Immune protection against FV involves a complex immune response that requires B cells and CD4<sup>+</sup> and CD8<sup>+</sup> T cells, each providing indispensable and non-redundant functions<sup>48–51</sup>. The stringent immunological requirements for vaccine protection in the FV model provided a rigorous test for rejuvenation of immune responses in aged mice.

The generation of antigen-specific antiviral CD8<sup>+</sup> T cells is required for live-attenuated vaccine-induced immune protection from FV. To evaluate the primary response to vaccination, aged mice were vaccinated intravenously with live-attenuated virus approximately 8 weeks after receiving antibody conditioning containing anti-NEO1 antibodies. The spleens were collected for analysis 10–14 days later at the peak of the CD8<sup>+</sup> T cell response. Aged mice receiving my-HSC depletion demonstrated increased virus-specific CD8<sup>+</sup> T cell responses (dextramer<sup>+</sup>) in the spleen after vaccination compared with the aged controls (Fig. 4b), demonstrating that my-HSC depletion improved the primary response to live-attenuated viral infection. To evaluate immune protection, aged mice were vaccinated approximately 8 weeks after receiving anti-NEO1

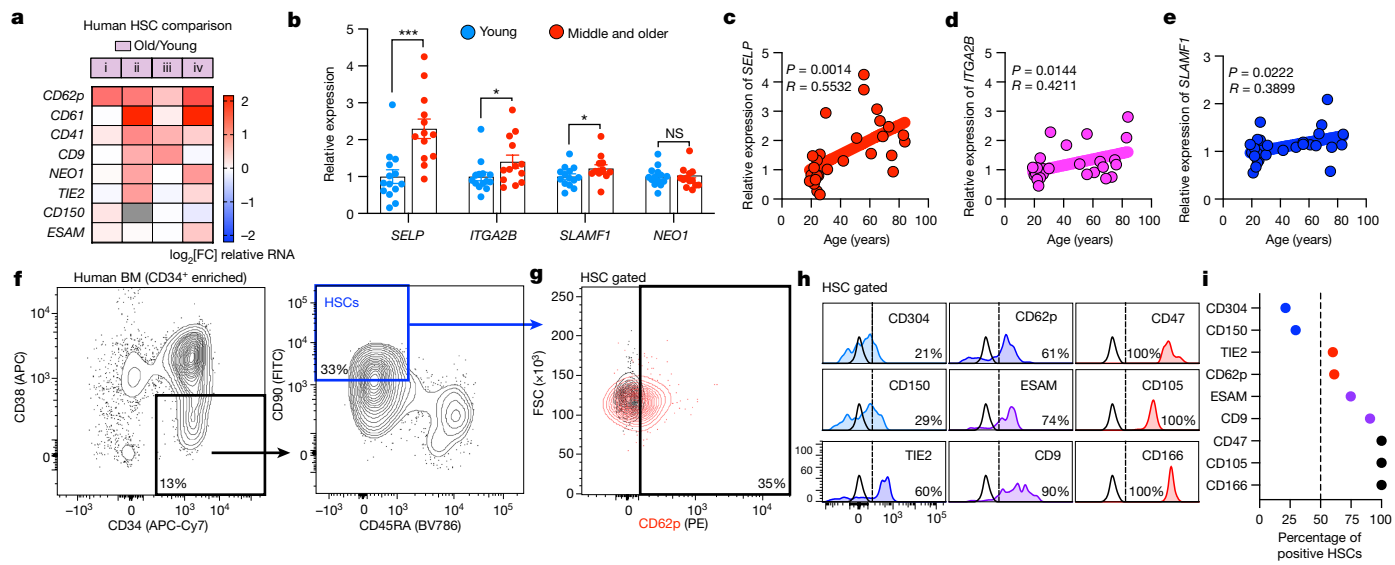


**Fig. 5 | Mouse my-HSC markers are enriched in aged human HSCs.** **a**, RNA expression of candidate human my-HSC antigens in independent datasets of human old HSCs versus young HSCs. Datasets were as follows: i<sup>3</sup>, ii<sup>53</sup>, iii<sup>54</sup> and iv<sup>55</sup>. **b**, Relative RNA expression of SELP (\*\*P = 0.000211), ITGA2B (\*P = 0.0325), SLAMF1 (\*P = 0.0359) and NEO1 (P = 0.362) in human HSCs isolated from young donors (aged 20–31 years; n = 14) and middle-aged and older donors (aged 42–85 years; n = 13) donors. Data were obtained from ref. 3 (GSE32719). **c–e**, Correlation of the relative RNA expression of SELP (**c**), ITGA2B (**d**) and SLAMF1 (**e**) in human HSCs with donor age. n = 27 donors. Data were obtained from ref. 3 (GSE32719). For **b–e**, values are relative to the mean of young donor samples. **f**, Representative flow cytometry analysis of CD34<sup>+</sup>-enriched donor

bone marrow (BM) to identify human HSCs (Lin<sup>−</sup>CD34<sup>+</sup>CD38<sup>−</sup>CD45RA<sup>−</sup>CD90<sup>+</sup>)<sup>59</sup>. **g**, Representative flow cytometry staining of human HSCs with anti-CD62p antibody (red) compared with the fluorescence minus one (FMO) control (black). n = 3 independent donors. **h,i**, Histograms for flow cytometry staining of human HSCs with antibodies to CD304, CD150, TIE2, CD62p, ESAM, CD9, CD47, CD105 and CD166. The black line represents the FMO control (**h**), with the percentage of HSCs positive for each marker (**i**). P values were obtained using unpaired parametric one-tailed t-tests (**b**); and P and R values were calculated using one-tailed Pearson correlation coefficient (**c–e**). Data are mean ± s.e.m. Exact P values are provided as source data.

antibody conditioning and were then challenged with pathogenic FV 6 weeks after vaccination (Extended Data Fig. 9a). Spleen cells were examined at 2 weeks after infection, the peak of FV replication. We verified that anti-NEO1 antibody conditioning decreased my-HSCs on the basis of both frequency and absolute number under these conditions and timepoints (Fig. 4a and Extended Data Fig. 9c–h). Control young-adult mice inoculated with FV had approximately threefold larger spleens than the naive control mice (Fig. 4c) and a per-spleen median of 7,000 infectious centres (Fig. 4d), a measure of live, infectious virus. Vaccination of young-adult mice prevented splenomegaly (Fig. 4c) and significantly reduced infectious centres (Fig. 4d). Aged infected mice fared much worse than young-adult mice. Their median increase in spleen weights was tenfold (Fig. 4c) and their median infectious centres per spleen was 4 million (Fig. 4d), more than 500-fold the median in infected young-adult mice. Vaccination of aged mice resulted in a slight but non-statistically significant decrease in splenomegaly (Fig. 4c), and only 1 out of 8 mice was able to control infection (Fig. 4d and Extended Data Fig. 9j). By contrast, mice that had been conditioned by my-HSC depletion 2 months before vaccination demonstrated significantly reduced splenomegaly (Fig. 4c), and 4 out of the 9 my-HSC-depleted mice had no detectable infectious centres in their spleens (Fig. 4d), the most stringent test of infection control. Compared with age-matched controls, vaccinated and infected aged mice receiving my-HSC depletion had increased virus-specific CD8<sup>+</sup> T cell responses (dextramer<sup>+</sup>) in the spleen (Fig. 4e), which was correlated with protection (Extended Data Fig. 9k). Taken together, these results demonstrated that my-HSC depletion in aged mice significantly improved immune responses to live viral infections.

### my-HSC genes are expressed by human HSCs

The age-associated expansion of HSCs with myeloid bias occurs in both mice and humans<sup>3</sup>. Having demonstrated that antibody-mediated

depletion of my-HSC reverses several features of age-related immune decline in mice, we investigated whether the my-HSC antigenic targets used in our conditioning protocol might be applicable to humans. First, we sought to determine whether human homologues of mouse my-HSC genes were expressed by aged human HSCs. Indeed, several mouse my-HSC genes, including *Selp* (encoding CD62p), *Slamf1*<sup>52</sup> and *Itga2b* (encoding CD41), were significantly increased in aged human HSCs from independent datasets<sup>3,53–55</sup> (Fig. 5a,b and Extended Data Fig. 10a,b) and were correlated with age across adulthood (Fig. 5c–e and Extended Data Fig. 10c–e). Moreover, genes for multiple mouse my-HSC antigens were enriched in HSCs isolated from pathologies related to ageing of the human haematopoietic system, including aberrant<sup>56,57</sup> and premalignant human HSCs<sup>58</sup> (Extended Data Fig. 10f). Notably, the most enriched gene across all datasets—in both mouse and human—was *SEL*P. Thus, several genes for mouse my-HSC antigens were also enriched in human HSCs associated with age and disease.

We next evaluated whether any candidate markers could be detected on human HSCs using antibodies. We examined the cell-surface protein expression of a subset of candidate antigens on highly pure populations of human HSCs (Lin<sup>−</sup>CD34<sup>+</sup>CD38<sup>−</sup>CD90<sup>+</sup>CD45RA<sup>−</sup>)<sup>59</sup>, which represent less than 10% of CD34<sup>+</sup> cells in the bone marrow (Extended Data Fig. 10g,h). We previously demonstrated that antibodies against NEO1 marked a subpopulation of human HSCs<sup>19</sup>. Antibodies to several cell-surface candidates—including CD62p and CD150—also separated human HSCs into two populations (Fig. 5f–i and Extended Data Fig. 10j–m). These markers were expressed with varying degrees of enrichment on HSCs relative to downstream progenitors (Extended Data Fig. 10n–s). Thus, all three mouse my-HSC markers that we demonstrated as therapeutic targets for my-HSC depletion *in vivo*—CD150, CD62p and NEO1—were also present on the cell surface of a subset of human HSCs. These experiments represent the first steps towards identifying therapeutic targets to deplete human my-HSCs and to rejuvenate the aged immune system using this strategy (Extended Data Fig. 10t).

## Discussion

The evolution of the vertebrate immune system occurred in geographically limited populations. Before machine-mediated transportation—trains, planes, boats and cars—individuals were likely to be exposed to the majority of pathogens in their local geography by the time of reproductive age. As T and B memory/stem cells can survive an individual's lifetime<sup>60,61</sup>, they should be sufficient to provide adaptive immune memory to all local pathogens. Thus, the generation of new T and B lymphocytes in later life was probably no longer advantageous, whereas the production of short-lived myeloid cells would remain important for acute innate responses, even in later life.

The requirement to maintain myeloid output for acute responses in the context of a long-lived memory T and B cell repertoire could explain the shifting of the HSC pool from bal-HSCs to my-HSCs during ageing. Although this biology has worked well throughout almost all of human evolution, the introduction of geographical migration by modern transportation created novel exposures of individuals to pathogens first encountered later in life when T and B cells are no longer efficiently produced. The haematopoietic system shift to myeloid-biased production has probably enabled novel pathogens to cause global pandemics. As the COVID-19 pandemic demonstrated, older patients are the most likely to die from SARS-CoV-2 infection<sup>62</sup>. In addition to poor adaptive immunity, the morbidity of older patients infected with new respiratory pathogens such as SARS-CoV-2 is also probably due to aberrant inflammatory responses<sup>63,64</sup>. Thus, as my-HSCs give rise to pro-inflammatory myeloid cells, we propose that their expansion in older individuals is a double-edged sword in the battle with novel pathogens, resulting not only in a poor adaptive immune response, but also in detrimental inflammatory responses. Rejuvenating the immune system by my-HSC depletion could promote more functional immune responses by increasing the generation of new T and B cells and also by reducing the production of inflammatory myeloid cells.

Our results indicate that my-HSC depletion in aged mice enabled bal-HSCs to rebalance the haematopoietic system and restore youthful immune features, including increased lymphocyte progenitors and naive cells, decreased markers of lymphocyte dysfunction/exhaustion and decreased inflammatory mediators. Importantly, HSC rebalancing also improved protective immunity in aged mice to live, pathogenic retroviral infection. The mouse my-HSC antigens mark subsets of human HSCs, implicating them as candidate targets for human rejuvenation. Further research will be required to optimize conditioning protocols, possibly using combinations of antibodies against my-HSC-specific markers while considering possible effects on differentiated cells such as regulatory T cells<sup>65</sup>.

Older humans not only have polyclonal contributions of HSCs to the blood system, but many individuals also display increases in HSC clones driven by the loss of function of epigenetic modifiers<sup>66</sup> (such as TET2<sup>67</sup> and DNMT3A<sup>68</sup>). Although such clones exist in many otherwise normal individuals, as observed in clonal haematopoiesis of indeterminate potential<sup>69</sup>, they have a higher likelihood of progressing to myeloproliferative neoplasms, myelodysplastic syndrome and acute myeloid leukaemia<sup>69</sup>, and of developing atherosclerosis<sup>70,71</sup>. It is conceivable that among my-HSCs are those that are involved in clonal haematopoiesis of indeterminate potential and could progress to these myeloid diseases, acute myeloid leukaemia and the inflammations that occur in other age-related inflammatory and fibrotic conditions<sup>71</sup>. Rejuvenating the immune system with bal-HSCs could also restore the surveillance systems required for elimination of transformed and partially transformed cells that drive cancer, and/or reduce the generation of myeloid cells that suppress tumour immunity. Such an approach could support both T-cell-based and myeloid-based immunotherapies, or reverse the inflammation and/or depletion of cells that result from cytotoxic anti-cancer therapies including chemotherapy and radiotherapy. Our study provides proof-of-principle for translational studies focused on

applying similar strategies to improve functional immunity to combat infections, chronic disease and cancer.

The conservation between mouse and humans of the expansion of my-HSCs and of the genes that increase during HSC ageing suggests that this preclinical study could support the development of clinical therapies to rejuvenate the blood-forming system in patients. These mouse studies indicate the direction of which markers on human my-HSCs may be effective or reasonable targets. Further preclinical and clinical studies will be required to determine whether such a therapy will be feasible in humans. The clinical development of safe protocols to rebalance HSCs could have broad effects on a number of age-associated issues.

## Online content

Any methods, additional references, Nature Portfolio reporting summaries, source data, extended data, supplementary information, acknowledgements, peer review information; details of author contributions and competing interests; and statements of data and code availability are available at <https://doi.org/10.1038/s41586-024-07238-x>.

1. Morrison, S. J., Wandycz, A. M., Akashi, K., Globerson, A. & Weissman, I. L. The aging of hematopoietic stem cells. *Nat. Med.* **2**, 1011–1016 (1996).
2. Rossi, D. J., Jamieson, C. H. & Weissman, I. L. Stem cells and the pathways to aging and cancer. *Cell* **132**, 681–696 (2008).
3. Pang, W. W. et al. Human bone marrow hematopoietic stem cells are increased in frequency and myeloid-biased with age. *Proc. Natl. Acad. Sci. USA* **108**, 20012–20017 (2011).
4. Yamamoto, R. & Nakuchi, H. In vivo clonal analysis of aging hematopoietic stem cells. *Mech. Ageing Dev.* **192**, 111378 (2020).
5. Beerman, I. et al. Functionally distinct hematopoietic stem cells modulate hematopoietic lineage potential during aging by a mechanism of clonal expansion. *Proc. Natl. Acad. Sci. USA* **107**, 5465–5470 (2010).
6. Rossi, D. J. et al. Cell intrinsic alterations underlie hematopoietic stem cell aging. *Proc. Natl. Acad. Sci. USA* **102**, 9194–9199 (2005).
7. Muller-Sieburg, C. E., Cho, R. H., Karlsson, L., Huang, J. F. & Sieburg, H. B. Myeloid-biased hematopoietic stem cells have extensive self-renewal capacity but generate diminished lymphoid progeny with impaired IL-7 responsiveness. *Blood* **103**, 4111–4118 (2004).
8. Sudo, K., Ema, H., Morita, Y. & Nakuchi, H. Age-associated characteristics of murine hematopoietic stem cells. *J. Exp. Med.* **192**, 1273–1280 (2000).
9. Sieburg, H. B. et al. The hematopoietic stem compartment consists of a limited number of discrete stem cell subsets. *Blood* **107**, 2311–2316 (2006).
10. Dykstra, B. et al. Long-term propagation of distinct hematopoietic differentiation programs in vivo. *Cell Stem Cell* **1**, 218–229 (2007).
11. Dykstra, B., Olthof, S., Schreuder, J., Ritsema, M. & de Haan, G. Clonal analysis reveals multiple functional defects of aged murine hematopoietic stem cells. *J. Exp. Med.* **208**, 2691–2703 (2011).
12. Min, H., Montecino-Rodriguez, E. & Dorshkind, K. Effects of aging on the common lymphoid progenitor to pro-B cell transition. *J. Immunol.* **176**, 1007–1012 (2006).
13. Montecino-Rodriguez, E., Berent-Maoz, B. & Dorshkind, K. Causes, consequences, and reversal of immune system aging. *J. Clin. Invest.* **123**, 958–965 (2013).
14. Yang, D. & de Haan, G. Inflammation and aging of hematopoietic stem cells in their niche. *Cells* **10**, 1849 (2021).
15. Chen, J. Y. et al. Hoxb5 marks long-term hematopoietic stem cells and reveals a homogenous perivascular niche. *Nature* **530**, 223–227 (2016).
16. Beerman, I. et al. Proliferation-dependent alterations of the DNA methylation landscape underlie hematopoietic stem cell aging. *Cell Stem Cell* **12**, 413–425 (2013).
17. Gekas, C. & Graf, T. CD41 expression marks myeloid-biased adult hematopoietic stem cells and increases with age. *Blood* **121**, 4463–4472 (2013).
18. Mann, M. et al. Heterogeneous responses of hematopoietic stem cells to inflammatory stimuli are altered with age. *Cell Rep.* **25**, 2992–3005 (2018).
19. Gulati, G. S. et al. Neogenin-1 distinguishes between myeloid-biased and balanced. *Proc. Natl. Acad. Sci. USA* **116**, 25115–25125 (2019).
20. Flohr Svendsen, A. et al. A comprehensive transcriptome signature of murine hematopoietic stem cell aging. *Blood* **138**, 439–451 (2021).
21. Sanjuan-Pla, A. et al. Platelet-biased stem cells reside at the apex of the hematopoietic stem-cell hierarchy. *Nature* **502**, 232–236 (2013).
22. Montecino-Rodriguez, E. et al. Lymphoid-biased hematopoietic stem cells are maintained with age and efficiently generate lymphoid progeny. *Stem Cell Rep.* **12**, 584–596 (2019).
23. Zaro, B. W. et al. Proteomic analysis of young and old mouse hematopoietic stem cells and their progenitors reveals post-transcriptional regulation in stem cells. *eLife* **9**, e62210 (2020).
24. Bersenev, A. et al. Lnk deficiency partially mitigates hematopoietic stem cell aging. *Aging Cell* **11**, 949–959 (2012).
25. Flach, J. et al. Replication stress is a potent driver of functional decline in ageing hematopoietic stem cells. *Nature* **512**, 198–202 (2014).
26. Maryanovich, M. et al. Adrenergic nerve degeneration in bone marrow drives aging of the hematopoietic stem cell niche. *Nat. Med.* **24**, 782–791 (2018).
27. Nordahl, G. L. et al. Accumulating mitochondrial DNA mutations drive premature hematopoietic aging phenotypes distinct from physiological stem cell aging. *Cell Stem Cell* **8**, 499–510 (2011).

28. Wahlestedt, M. et al. An epigenetic component of hematopoietic stem cell aging amenable to reprogramming into a young state. *Blood* **121**, 4257–4264 (2013).
29. Renders, S. et al. Niche derived netrin-1 regulates hematopoietic stem cell dormancy via its receptor neogenin-1. *Nat. Commun.* **12**, 608 (2021).
30. Sun, D. et al. Epigenomic profiling of young and aged HSCs reveals concerted changes during aging that reinforce self-renewal. *Cell Stem Cell* **14**, 673–688 (2014).
31. Seita, J. et al. Gene Expression Commons: an open platform for absolute gene expression profiling. *PLoS ONE* **7**, e40321 (2012).
32. Akashi, K., Traver, D., Miyamoto, T. & Weissman, I. L. A clonogenic common myeloid progenitor that gives rise to all myeloid lineages. *Nature* **404**, 193–197 (2000).
33. Kondo, M., Weissman, I. L. & Akashi, K. Identification of clonogenic common lymphoid progenitors in mouse bone marrow. *Cell* **91**, 661–672 (1997).
34. George, B. M. et al. Antibody conditioning enables MHC-mismatched hematopoietic stem cell transplants and organ graft tolerance. *Cell Stem Cell* **25**, 185–192 (2019).
35. Czechowicz, A., Kraft, D., Weissman, I. L. & Bhattacharya, D. Efficient transplantation via antibody-based clearance of hematopoietic stem cell niches. *Science* **318**, 1296–1299 (2007).
36. Jaiswal, S. et al. CD47 is upregulated on circulating hematopoietic stem cells and leukemia cells to avoid phagocytosis. *Cell* **138**, 271–285 (2009).
37. Kurabayashi, W. et al. Limited rejuvenation of aged hematopoietic stem cells in young bone marrow niche. *J. Exp. Med.* **218**, e20192283 (2021).
38. Morrison, S. J. & Weissman, I. L. The long-term repopulating subset of hematopoietic stem cells is deterministic and isolatable by phenotype. *Immunity* **1**, 661–673 (1994).
39. Akashi, K., Kondo, M. & Weissman, I. L. Two distinct pathways of positive selection for thymocytes. *Proc. Natl Acad. Sci. USA* **95**, 2486–2491 (1998).
40. Gattinoni, L. et al. A human memory T cell subset with stem cell-like properties. *Nat. Med.* **17**, 1290–1297 (2011).
41. Elyahu, Y. et al. Aging promotes reorganization of the CD4 T cell landscape toward extreme regulatory and effector phenotypes. *Sci. Adv.* **5**, eaaw8330 (2019).
42. Hao, Y., O'Neill, P., Naradikian, M. S., Scholz, J. L. & Cancro, M. P. A B-cell subset uniquely responsive to innate stimuli accumulates in aged mice. *Blood* **118**, 1294–1304 (2011).
43. Pioli, P. D., Casero, D., Montecino-Rodriguez, E., Morrison, S. L. & Dorshkind, K. Plasma cells are obligate effectors of enhanced myelopoiesis in aging bone marrow. *Immunity* **51**, 351–366 (2019).
44. Kovtonyuk, L. V. et al. IL-1 mediates microbiome-induced inflammatomaging of hematopoietic stem cells in mice. *Blood* **139**, 44–58 (2022).
45. Collier, D. A. et al. Age-related immune response heterogeneity to SARS-CoV-2 vaccine BNT162b2. *Nature* **596**, 417–422 (2021).
46. Myers, L. & Hasenkrug, K. J. Retroviral immunology: lessons from a mouse model. *Immunol. Res.* **43**, 160–166 (2009).
47. Dittmer, U. et al. Friend retrovirus studies reveal complex interactions between intrinsic, innate and adaptive immunity. *FEMS Microbiol. Rev.* **43**, 435–456 (2019).
48. Dittmer, U., Brooks, D. M. & Hasenkrug, K. J. Requirement for multiple lymphocyte subsets in protection by a live attenuated vaccine against retroviral infection. *Nat. Med.* **5**, 189–193 (1999).
49. Dittmer, U., Brooks, D. M. & Hasenkrug, K. J. Characterization of a live-attenuated retroviral vaccine demonstrates protection via immune mechanisms. *J. Virol.* **72**, 6554–6558 (1998).
50. Dittmer, U., Brooks, D. M. & Hasenkrug, K. J. Protection against establishment of retroviral persistence by vaccination with a live attenuated virus. *J. Virol.* **73**, 3753–3757 (1999).
51. Hasenkrug, K. J. & Dittmer, U. The role of CD4 and CD8 T cells in recovery and protection from retroviral infection: lessons from the Friend virus model. *Virology* **272**, 244–249 (2000).
52. Larochelle, A. et al. Human and rhesus macaque hematopoietic stem cells cannot be purified based only on SLAM family markers. *Blood* **117**, 1550–1554 (2011).
53. Adelman, E. R. et al. Aging human hematopoietic stem cells manifest profound epigenetic reprogramming of enhancers that may predispose to leukemia. *Cancer Discov.* **9**, 1080–1101 (2019).
54. Rundberg Nilsson, A., Soneji, S., Adolfsson, S., Bryder, D. & Pronk, C. J. Human and murine hematopoietic stem cell aging is associated with functional impairments and intrinsic megakaryocytic/erythroid bias. *PLoS ONE* **11**, e0158369 (2016).
55. Henrich, M. L. et al. Cell-specific proteome analyses of human bone marrow reveal molecular features of age-dependent functional decline. *Nat. Commun.* **9**, 4004 (2018).
56. Tong, J. et al. Hematopoietic stem cell heterogeneity is linked to the initiation and therapeutic response of myeloproliferative neoplasms. *Cell Stem Cell* **28**, 502–513 (2021).
57. Woll, P. S. et al. Myelodysplastic syndromes are propagated by rare and distinct human cancer stem cells in vivo. *Cancer Cell* **25**, 794–808 (2014).
58. Corces, M. R. et al. Lineage-specific and single-cell chromatin accessibility charts human hematopoiesis and leukemia evolution. *Nat. Genet.* **48**, 1193–1203 (2016).
59. Park, C. Y., Majeti, R. & Weissman, I. L. In vivo evaluation of human hematopoiesis through xenotransplantation of purified hematopoietic stem cells from umbilical cord blood. *Nat. Protoc.* **3**, 1932–1940 (2008).
60. Bhattacharya, D. et al. Transcriptional profiling of antigen-dependent murine B cell differentiation and memory formation. *J. Immunol.* **179**, 6808–6819 (2007).
61. Luckey, C. J. et al. Memory T and memory B cells share a transcriptional program of self-renewal with long-term hematopoietic stem cells. *Proc. Natl Acad. Sci. USA* **103**, 3304–3309 (2006).
62. Saggau, C. et al. The pre-exposure SARS-CoV-2-specific T cell repertoire determines the quality of the immune response to vaccination. *Immunity* **55**, 1924–1939 (2022).
63. Merad, M., Blish, C. A., Sallusto, F. & Iwasaki, A. The immunology and immunopathology of COVID-19. *Science* **375**, 1122–1127 (2022).
64. Jaiswal, S. & Weissman, I. L. Hematopoietic stem and progenitor cells and the inflammatory response. *Ann. N. Y. Acad. Sci.* **1174**, 118–121 (2009).
65. Hirata, Y. et al. CD150<sup>high</sup> bone marrow Tregs maintain hematopoietic stem cell quiescence and immune privilege via adenosine. *Cell Stem Cell* **22**, 445–453 (2018).
66. Jamieson, C. H. M. & Weissman, I. L. Stem-cell aging and pathways to precursor evolution. *N. Engl. J. Med.* **389**, 1310–1319 (2023).
67. Busque, L. et al. Recurrent somatic TET2 mutations in normal elderly individuals with clonal hematopoiesis. *Nat. Genet.* **44**, 1179–1181 (2012).
68. Jan, M. et al. Clonal evolution of preleukemic hematopoietic stem cells precedes human acute myeloid leukemia. *Sci. Transl. Med.* **4**, 149ra118 (2012).
69. Jaiswal, S. & Ebert, B. L. Clonal hematopoiesis in human aging and disease. *Science* **366**, eaan4673 (2019).
70. Jaiswal, S. et al. Clonal hematopoiesis and risk of atherosclerotic cardiovascular disease. *N. Engl. J. Med.* **377**, 111–121 (2017).
71. Majeti, R. et al. Clonal expansion of stem/progenitor cells in cancer, fibrotic diseases, and atherosclerosis, and CD47 protection of pathogenic cells. *Annu. Rev. Med.* **73**, 307–320 (2022).

**Publisher's note** Springer Nature remains neutral with regard to jurisdictional claims in published maps and institutional affiliations.

Springer Nature or its licensor (e.g. a society or other partner) holds exclusive rights to this article under a publishing agreement with the author(s) or other rightsholder(s); author self-archiving of the accepted manuscript version of this article is solely governed by the terms of such publishing agreement and applicable law.

© The Author(s), under exclusive licence to Springer Nature Limited 2024

## Methods

### Animal Experiments

All mice were C57BL/6 or (C57BL/10 × A.BY) F<sub>1</sub> (H-2<sup>b/b</sup>, Fv1<sup>b</sup>, Rfv3<sup>l/s</sup>) and were aged between 8 weeks and 120 weeks. For transplant experiments, C57BL/6J (Jackson Labs, 000664) CD45.2 mice were donors and B6.SJL-Ptprc<sup>a</sup>Pepc<sup>b</sup>/BoyJ (Jackson Labs, Strain 002014) CD45.1 mice were recipients. Mouse ages are described in the figure legends. Mice were routinely monitored, and sick or diseased mice were excluded from further analysis. Mice were housed in individually ventilated cages, same-sex under a 12 h–12 h light–dark cycle, with temperature and humidity control, enrichment material and ab libitum rodent chow and water. Mice were bred and maintained at Stanford University's Research Animal Facility or at the Rocky Mountain Laboratories. All of the animal experiments were performed according to guidelines established by the Administrative Panel on Laboratory Animal Care of Stanford University or on an Animal Study Proposal approved by the Animal Care and Use Committee of the Rocky Mountain Laboratories (RML 2018-058, RML 2021-046) and performed by certified staff in an Association for Assessment and Accreditation of Laboratory Animal Care International-accredited facility according to the institution's guidelines for animal use, the basic principles in the NIH Guide for the Care and Use of Laboratory Animals, the Animal Welfare Act and the US Department of Agriculture and the US Public Health Service Policy on Humane Care and Use of Laboratory Animals.

### Bone marrow cell isolation

Mice were euthanized and bone marrow was collected according to one of two methods. The unilateral or bilateral femurs, tibias and pelvises were dissected, cleaned and collected in a mortar bowl containing PBS supplemented with 2% FBS (FACS-buffer) and DNase I (LS002007, Worthington). Bones were crushed, and the resulting cell suspension was passed through a 40 µm filter. Alternatively, the femurs and tibias were dissected, cleaned and cut at the joints, and the bone marrow was flushed using an inserted 25 gauge needle and phosphate-buffered balanced salt solution (PBBS), with cells passed through a 100 µm filter. Cells were collected by centrifugation and washed multiple times with FACS buffer. Red blood cells were depleted by ACK lysis or by KIT enrichment. For ACK lysis, cells were resuspended in 1 ml ACK lysing buffer (A1049201, Thermo Fisher Scientific) and incubated for 10 min at room temperature. For KIT enrichment, cells were Fc-blocked by incubation with 1 mg ml<sup>-1</sup> rat IgG (ab37361, Abcam) for 30 min on ice, followed by the addition of anti-KIT APC-eFluor780 (47-1171-82, Thermo Fisher Scientific) for 30 min. Cells were collected by centrifugation and resuspended in FACS buffer containing 10 µl anti-APC Micro-Beads (130-090-855; Miltenyi Biotec) and incubated for 20 min on ice. Cells were then washed and isolated with LS Columns (130-042-401; Miltenyi Biotec) using a MACS Separator (Miltenyi Biotec) according to the manufacturer's instructions.

### Flow cytometry

Flow cytometry was performed on the FACS Aria II (BD Biosciences) or FACS Symphony (BD Biosciences) system and data were collected using FACSDiva (BD). For absolute cell counts, cells were counted before flow cytometry, or a known volume of Precision Count Beads (424902, BioLegend) was added to a known volume of cells, and calculations were performed according to the manufacturer's instructions. For all experiments using Precision Count Beads, the stock concentration was assumed to be 1 × 10<sup>6</sup> particles per ml according to the manufacturer. For mouse flow cytometry, analysis was performed on whole-bone marrow or on KIT-enriched cells, isolated as described above. Before antibody staining, cells were Fc-blocked by incubation with 1 mg ml<sup>-1</sup> rat IgG (ab37361, Abcam) for 30 min on ice. Antibody staining was performed in FACS-buffer solution (PBS with 2% FBS and DNase I). Incubations were performed on ice for at least 30 min. For HSC and

progenitor analysis<sup>72–75</sup>, cells were stained with combinations of the following antibodies (hereafter, HSPC stain): anti-FLT3 APC (Thermo Fisher Scientific, 17-1351-82, 1:50) or anti-FLT3 PerCP-eFluor710 (eBioscience, 46-1351-82, 1:50), goat anti-mouse NEO1 (R&D, AF1079, 15 µg ml<sup>-1</sup>), anti-CD150 PE-Cy7 (BioLegend, 115914, TC15-12F12.2, 1:50), anti-IL-7RA PE-Cy5 (Thermo Fisher Scientific, 15-1271-82 or BioLegend, 135016, 1:25) or anti-IL7Ra APC (BioLegend, 135012, 1:25), anti-CD16/32 BV510 (BioLegend, 101308, 1:50), anti-KIT APC-eFluor780 (Thermo Fisher Scientific, 47-1171-82, 1:50), anti-mouse lineage cocktail (includes anti-CD3, anti-Ly-6G/C, anti-CD11b, anti-CD45R, anti-Ter-119) AF700 (BioLegend, 133313, 1:10), anti-CD48 BV711 (BD, 740687, 1:50), anti-CD41 BV650 (BD, 740504, 1:50), anti-CD34 biotin (Thermo Fisher Scientific, 13-0341-85, 1:50), anti-SCA1 BUV395 (BD, 744328, 1:50), followed by Streptavidin BUV737 (BD, 612775, 1:50) and donkey anti-goat IgG H&L AF488 (Abcam, ab150129, 1:100). In some instances, anti-CD150 clone mShad150 PE 1:50 (eBioscience, 12-1502-80) or PE-Cy7 (eBioscience, 25-1502-82), anti-CD150 clone 9D1 PE (eBioscience, 12-1501-80, 1:50), anti-CD150 clone Q38-480 PE (BD, 562651, 1:50), anti-CD62p PE (BioLegend, 148308, 1:50) or anti-Ly6D PE (eBioscience, 12-5974-80, 1:50) were included. For testing of candidate my-HSC markers, the following antibodies were used: anti-CD51 PE (12-0512-81, Thermo Fisher Scientific, 1:50), anti-CD61 PE (561910, BD, 1:50), anti-CD31 PE (561073, BD, 1:50), anti-CD38 PE (12-0381-81, Thermo Fisher Scientific, 1:50), anti-CD47 clone MIAP301 PE (127507, BioLegend, 1:50), anti-CD47 clone MIAP410 PE (LS-C810701-25, LSBio, 1:50), anti-CD62p PE (148305, BioLegend, 1:50), anti-ALCAM PE (12-1661-82, Thermo Fisher Scientific, 1:50), anti-CD9 PE (124805, BioLegend, 1:50), anti-ESAM PE (136203, BioLegend, 1:50), anti-TIE2 PE (124007, BioLegend, 1:50), anti-CD201 PE (141503, BioLegend, 1:50) or anti-KIT ACK2 PE (135105, BioLegend, 1:50). The my-HSC fold-enrichment for each marker was calculated as (percentage marker positive of my-HSC)/(percentage marker positive of bal-HSC). To calculate the absolute number of HPCs (for example, CMP + GMP, MkP, MEP, CLP and so on) the absolute numbers of cells was quantified in total bone marrow (non-KIT enriched). To quantify the absolute number of HSCs and HSC subsets (for example, my-HSCs, bal-HSCs and so on), the absolute numbers of cells was quantified in total bone marrow (non-KIT enriched) or the percentage of HSC/HSC subsets per KLS (Lin<sup>+</sup>KIT<sup>+/-</sup>SCA1) cells was calculated in the KIT-enriched fraction and multiplied by the total number of KLS cells quantified in a paired sample of total bone marrow (non-KIT enriched).

For T cell analysis, cells were stained with the following antibodies: anti-Helios AF647 (BD, 563951, 1:200), anti-CD3 APC-Cy7 (BioLegend, 100222, 1:200), anti-Ki-67 R718 (BD, 566963, 1:150), anti-CD43 AF488 (BioLegend, 121210, 1:400), anti-CD8 BUV395 (BD, 563786, 1:400), anti-FOXP3 eF450 (Invitrogen, 48-5773-82, 1:150), anti-CD4 BV510 (BioLegend, 100559, 1:400), anti-CD44 BV605 (BD, 563058, 1:400), anti-CD62L BV711 (BioLegend, 104445, 1:1,000), anti-EOMES PE (Invitrogen, 12-4875-82, 1:200), anti-PD1 PE-CF594 (BD, 562523, 1:200), anti-TBET PE-Cy7 (Invitrogen, 25-5825-82, 1:200), anti-CD25 PerCP-Cy5.5 (BioLegend, 102030, 1:200). FV-specific CD8<sup>+</sup> T cells were identified using H-2D<sup>b</sup>/Abu-Abu-L-Abu-LTVFL APC- or PE-D<sup>b</sup>gagL-MHC Dextramer (ImmuDex) at 1:25 during surface staining. For B cells analysis, cells were stained with the following antibodies: anti-CD43 APC (BioLegend, 121214, 1:400), anti-CD21/CD35 APC-Cy7 (BioLegend, 123418, 1:400), anti-CD5 AF700 (BioLegend, 100636, 1:200), anti-IgM FITC (Invitrogen, 11-5790-81, 1:400), anti-CD19 BUV395 (BD, 563557, 1:400), anti-IgD eFluor450 (eBioscience, 48-5993-82, 1:400), anti-CD11b BV510 (BioLegend, 101245, 1:400), anti-MHCII BV605 (BD, 563413, 1:400), anti-CD40 BV711 (BD, 740700, 1:400), anti-PDL1 PE (Invitrogen, 12-5982-82, 1:200), anti-CD93 PE-Cy7 (BioLegend, 136506, 1:400), anti-CD23 PerCP-Cy5.5 (BioLegend, 101618, 1:200) and anti-CD45R/B220 PE-CF594 (BD, 562290, 1:800). Intracellular staining was performed as described previously<sup>76</sup>.

For peripheral blood chimerism analysis, cells were stained with the following antibodies: anti-CD8a Spark UV387 (BioLegend, 100797, 1:50), anti-CD4 BUV737 (BD, 612843, 1:200), anti-GR1 Pacific Blue

# Article

(BioLegend, 108429, 1:100), anti-CD3 BV711 (BioLegend, 100241, 1:100), anti-CD44 BV785 (BioLegend, 103059, 1:300), anti-CD45.2 AF488 (BioLegend, 109815, 1:100), anti-FOXP3 PE (eBioscience, 12-5773-82, 1:100), anti-CD62L PE/Dazzle 594 (BioLegend, 104447, 1:200), anti-CD19 PE-Cy7 (BioLegend, 115519, 1:100), anti-CD45.1 APC (BioLegend, 110713, 1:50), anti-CD11b APC-Cy7 (BioLegend, 101225, 1:100). Intracellular staining was performed using the FOXP3 Transcription Factor Staining Buffer Set (eBioscience, 00-5523-00) according to the manufacturer's protocol. Red blood cells were removed with ACK lysis buffer (Gibco, a1049201). Non-specific binding was prevented with TruStain FcX PLUS (BioLegend, 156604). To determine the viability of fixed cells, cells were incubated in buffer containing LIVE/DEAD Fixable Aqua Dead Cell (Thermo Fisher Scientific, L34957).

For erythroid cell analysis, spleen cells were first incubated for 30 min with mAb 34, a mouse IgG2b specific for the FV glycoGag protein expressed on infected cells<sup>77</sup>, then stained with anti-mouse IgG2b FITC (BD, 553395) and anti-TER119 PE-Cy7 (Invitrogen, 25-5921-82). Cells from uninfected controls were used for gating strategy. For non-fixed cells, to determine viability, cells were incubated in buffer containing SYTOX Red Dead Cell Stain (Life Technologies) or SYTOX Blue Dead Cell Stain (Thermo Fisher Scientific, S34857).

For flow cytometry computational analysis<sup>78,79</sup>, samples were first analysed in FlowJo v.10 (BD Life Sciences) and the T cell (CD4<sup>+</sup> and CD8<sup>+</sup>) gated events were downsampled to an equivalent number of cells per condition (young, aged, aged + conditioning), and the channel data for each sample were exported as CSV files. The Spectre package<sup>80</sup> was applied to data from all samples using R (v.4.2.2), which were annotated and merged, and clusters were assigned with PhenoGraph<sup>81</sup>, followed by dimensionality reduction using uniform manifold approximation and projection (UMAP)<sup>82</sup> for visualization. Cluster assignments were annotated and/or merged based on previous knowledge of phenotypes for naïve, T<sub>CM</sub> and T<sub>EM</sub> T cell subtypes.

To identify anti-CD150 antibodies that are not blocked by anti-CD150 antibody clone 1 (TC15-12F12.2, TC15), bone marrow HSPC-stained cells were incubated with saturating concentrations (200 µg ml<sup>-1</sup>) of unlabelled anti-CD150 antibody clone TC15 and then stained with PE-conjugated anti-CD150 clones 2 (Q38), 3 (9D1) or 4 (mShad150); PE-Cy7 conjugated anti-CD150 clone TC15 was used as a control. To confirm whether any anti-CD150 clones identify the same population of cells as anti-CD150 antibody clone 1 (TC15) by flow cytometry, bone marrow HSPC-stained cells were incubated with PECy-7 anti-CD150 antibody clone 1 (TC15) and with either PE-conjugated anti-CD150 clone 2 (Q38), 3 (9D1) or 4 (mShad150). To confirm that anti-CD150 antibody clone 4 (mShad150) does not block anti-CD150 clone 2 (Q38), bone marrow cells were incubated with saturating concentrations (200 µg ml<sup>-1</sup>) of unlabelled anti-CD150 clone mShad150 and then stained with PE-conjugated anti-CD150 clone Q38; PE-Cy7 conjugated anti-CD150 clone mShad150 was used as a control. To confirm that anti-CD150 clone mShad150 and clone Q38 identify the same populations by flow cytometry, bone marrow cells were incubated with PECy-7 anti-CD150 clone mShad150 and with PE anti-CD150 clone 2 (Q38).

To confirm that mouse IgG2a (SB115d, SouthernBiotech) and IgG2b (SB115h, SouthernBiotech) anti-goat antibodies do not block donkey anti-goat IgG AF488 (Abcam, ab150129), bone marrow HSPC-stained cells were incubated with saturating concentrations (100 µg ml<sup>-1</sup>) of unlabelled mouse IgG2a (6158-01, SouthernBiotech) or IgG2b (6157-01, SouthernBiotech) anti-goat antibodies and then stained with donkey anti-goat AF488. To confirm that mouse IgG2a and IgG2b anti-goat antibodies identify the same populations as donkey anti-goat IgG AF488 by flow cytometry, bone marrow HSPC-stained cells were incubated with mouse IgG2a AF555 (6158-32, SouthernBiotech, 1:100) or IgG2b PE (6157-09, SouthernBiotech, 1:100) anti-goat antibodies, and with donkey anti-goat AF488.

For human HSC<sup>83</sup> flow cytometry analysis, bone marrow mononuclear cells from young-adult donors (aged 26–33 years) were commercially

obtained (AllCells). CD34<sup>+</sup> cells were enriched using the CD34 Micro-Bead Kit (130-046-702, Miltenyi Biotec) according to the manufacturer's instructions. Antibody staining was performed in FACS-buffer solution (PBS with 2% FBS and DNase I) at a 1:1 ratio to Brilliant Stain Buffer (563794, BD Biosciences). Non-specific binding was blocked with FcR Blocking Reagent (130-059-901, Miltenyi Biotec) for 5 min on ice, followed by the addition of the following antibodies: anti-lineage panel PE-Cy5: (anti-CD3 (BD, 555341, 1:200), anti-CD4 (BD, 555348, 1:200), anti-CD8 (BD, 555368, 1:200), anti-CD11b (BD, 555389, 1:200), anti-CD14 (Thermo Fisher Scientific, MHCD1406, 1:200), anti-CD19 (BD, 555414, 1:200), anti-CD20 (BD, 555624, 1:200), anti-CD56 (BD, 555517, 1:200), anti-CD235a (BD, 559944, 1:200)), anti-CD34 APC-Cy7 (343514, BioLegend, 1:25), anti-CD45RA BV-785 (304139, BioLegend, 1:25), anti-CD38 APC (555462, BD, 1:10), anti-CD90 FITC (328107, BioLegend, 1:50) and one of anti-human PE: anti-CD62P clone AK4 (304905, BioLegend, 1:20), anti-CD62P clone Psel.KO2.3 (12-0626-82, eBioscience, 1:20), anti-CD62P clone AC1.2 (550561, BD, 1:5), anti-CD150 (306307, BioLegend, 1:20), anti-TIE2 (CD202b, 334205, BioLegend, 1:20), anti-ESAM (408519, Novus, 1:10), anti-CD166 (ALCAM, 343903, BioLegend, 1:20), anti-CD9 (312105, BioLegend, 1:20), anti-CD105 (Endoglin, 800503, BioLegend, 1:20) or anti-CD304 (neuropilin-1, 354503, BioLegend, 1:20). All flow cytometry data were analysed using FlowJo v.10 (BD Life Sciences).

## Antibody conditioning

For antibody conditioning experiments, mice received injections of antibodies resuspended in PBS intraperitoneally. Control animals received an equivalent volume of PBS or an equivalent amount of isotype control antibodies: mouse IgG1 (MOPC-21, Bio X Cell), rat IgG2b (LTF-2, Bio X Cell) or rat IgG2a (RTK2758, BioLegend). Given that isotype control antibodies demonstrated no effect on phenotype, PBS was used as a control in many experiments, as described previously<sup>84</sup>. my-HSC-specific antibodies (anti-CD150, anti-CD62p or anti-NEO1) were injected on day -9. For CD150, 200 µg rat IgG2b anti-CD150 (mShad150, eBioscience) for the CD150<sup>v1</sup> protocol, or 200 µg rat IgG2a anti-CD150 (TC15-12F12.2, BioLegend) for the CD150<sup>v2</sup> protocol, was administered on day -9. For CD62p, 200 µg mouse anti-CD62p (RMP-1, BioLegend) was administered on day -9. For NEO1, 30 µg, 90 µg or 200 µg goat anti-NEO1 (polyclonal, AF1079, R&D)<sup>19,85–92</sup> was administered on day -9 for the NEO1<sup>v1</sup> protocol and, when indicated, 150 µg mouse IgG2a (SB115d, SouthernBiotech) or IgG2b (SB115h, SouthernBiotech) anti-goat was administered 24 h later<sup>93–95</sup> on day -8 for the NEO1<sup>v2</sup> protocol. For CD47 blockade, mouse IgG1 anti-CD47 (MIAP410, Bio X Cell) was administered on day -11 (100 µg) and on day -9 to day -5 (500 µg daily), as previously described<sup>34,96</sup>. For KIT, rat anti-KIT (ACK2, Bio X Cell) was injected retro-orbitally on day -9 (30 µg, 50 µg or 100 µg), and mice were administered 400 µg of diphenhydramine at least 30 min before administration, as previously described<sup>34,96</sup>. Mice were euthanized for bone marrow analysis on day 0 (that is, approximately 1 week), at approximately 8–10 weeks or at approximately 14–16 weeks.

## Blood cell isolation and plasma immunoassays

For blood cell isolation and plasma immunoassays, mouse peripheral blood was collected in EDTA tubes after removal of cells through centrifugation at 500 r.c.f. for 10 min; plasma was then transferred to a clean tube and centrifuged for an additional 10 min at 13,000 r.c.f., while the red blood cells were depleted with ACK lysis, followed by a PBS wash and then stained for flow cytometry as described above. For absolute cell counts per ml, the volume of blood obtained per animal was recorded and a known volume of Precision Count Beads (424902; BioLegend) was added to a known volume of cells, and calculations were performed according to the manufacturer's instructions assuming a Precision Count Beads stock concentration of  $1 \times 10^6$  particles per ml. Plasma was frozen at -80 °C until processing by the Stanford Human

Immune Monitoring Center (HIMC), as described previously<sup>84</sup>. The samples were run in technical triplicate using the 48-Plex Mouse ProcartaPlexPanel (EPX480-20834-901; Thermo Fisher Scientific) or the Mouse Acute Phase Magnetic Bead Panel 2 (MAP2MAG-76K; Millipore Sigma). MFI average value were compared after removal of statistical outliers using the extreme studentized deviate (ESD) Grubbs statistical test ( $\alpha = 0.0001$ )<sup>97</sup>. For comparison of estimated concentrations, values below the limit of detection were assigned the value equal to this lower limit.

## FV mouse model

**Ethics and biosafety statement.** All in vivo experiments were performed in accordance with Animal Study Proposal approved by the Animal Care and Use Committee of the Rocky Mountain Laboratories (RML 2018-058, RML 2021-046) approved by the Institutional Animal Care and Use Committee of Rocky Mountain Laboratories (National Institutes of Health (NIH)) and carried out by certified staff in an Association for Assessment and Accreditation of Laboratory Animal Care International-accredited facility, according to the institution's guidelines for animal use, following the guidelines and basic principles in the NIH Guide for the Care and Use of Laboratory Animals<sup>98</sup>, the Animal Welfare Act and the US Department of Agriculture and the US Public Health Service Policy on Humane Care and Use of Laboratory Animals.

**Vaccination and virus challenge.** The FV retrovirus stock used in these experiments was FV-NB, a lactate dehydrogenase virus-free<sup>99</sup> complex containing NB-tropic Friend murine leukaemia helper virus (F-MuLV) and polycythaemia-inducing spleen focus-forming virus (SFFV)<sup>100</sup> generated as a spleen cell homogenate from infected BALB/C mice. The live attenuated vaccine was an NB-tropic F-MuLV helper stock, which replicates poorly without SFFV-induced proliferation, generated as a supernatant from infected *Mus dunni* cells<sup>101</sup>. *M. dunni* cells were obtained from the American Type Culture Collection (ATCC), tested negative for mycoplasma after receipt and were not independently authenticated beyond the provided identity. Mice of the (C57BL/10 × A.BY) F<sub>1</sub> background were vaccinated by 0.1 ml intravenous injection of 10<sup>5</sup> focus-forming units (FFU) of virus in phosphate-buffered, balanced salt solution (PBBS). For challenge, mice were injected intravenously with 0.2 ml PBBS containing 20,000 spleen FFU of FV-NB complex.

**Infectious centre assay.** Titrations of single-cell spleen suspensions were plated onto susceptible *M. dunni* cells and allowed to incubate in vitro for 2 days at 37 °C under 5% CO<sub>2</sub>. The plates were then fixed with 95% ethanol, stained with F-MuLV envelope-specific Mab 72015<sup>102</sup>, followed by goat anti-mouse (H+L) HRP (EMD Millipore, AP308P), and then developed with aminoethylcarbazol substrate to detect foci.

**Antigen-expressing cells in vivo.** To quantify AG34<sup>+</sup> expressing cells in vivo, AG34 expression was determined by mAb 34 antibody staining using flow cytometry<sup>77</sup>. Cells from uninfected controls were used to define the background level of staining. A positive versus negative threshold was set equal to the highest level of background staining observed in non-infected animals, and only samples with values higher than this threshold were considered to be positive<sup>103</sup>. Samples with values equal to or lower than the background level in non-infected animals were considered to be negative and their level of staining was set to a value of 0%. Both positive and negative samples were included in the statistical analysis for comparison. To obtain the absolute number of AG34<sup>+</sup>TER119<sup>+</sup> cells per samples, an equivalent number of cells was analysed for each mouse using flow cytometry, and the frequency of AG34<sup>+</sup>TER119<sup>+</sup> cells (as defined by the positive and negative thresholds) per total cells was multiplied by the total number of cells counted per spleen.

## Transcriptomic analysis

**Murine and human HSCs.** The following publicly available datasets were used to compare mouse old versus young HSCs: ref. 16 (i, GSE43729), ref. 24 (ii, GSE39553), ref. 25 (iii, GSE48893), ref. 26 (iv, GSE109546), ref. 27 (v, GSE27686), ref. 28 (vi, GSE44923), ref. 29 (vii, GSE128050), ref. 30 (viii, GSE47819). The following datasets were used to compare mouse my-HSCs versus bal-HSCs: ref. 19 (ix, GSE130504), ref. 22 (x, GSE112769) ref. 21 (xi, E-MEXP-3935). The following publicly available datasets were used to compare human old HSCs versus young HSCs: ref. 3 (i, GSE32719), ref. 53 (ii, GSE104406), ref. 54 (iii, GSE69408), ref. 55 (iv, GSE115348). Additional transcriptional publicly available datasets related to human HSCs included: ref. 104 (e, HMGA2<sup>+</sup> versus HMGA2<sup>-</sup>CD34<sup>+</sup> cells, GSE107594), ref. 56 (f, essential thrombocythaemia and polycythaemia vera versus normal HSCs, GSE111410), ref. 57 (g, MDS versus normal HSCs, GSE55689), ref. 58 (h, pre-leukaemic versus normal HSCs, GSE74246). Data were processed and analysed with GREIN<sup>105</sup> or GEO2R<sup>106,107</sup>.

**Mouse progenitors, mature cells and tissues.** To determine gene expression of mouse progenitors and mature cells, processed data were obtained directly from supplementary table 1 of ref. 19 on 23 haematopoietic phenotypes based on 64 microarray expression profiles extracted by the Gene Expression Commons<sup>31</sup>. Publicly available gene expression data from bulk mouse tissues were obtained from: *Tabula Muris* (GSE132040)<sup>108</sup> and ref. 109 (GSE87633). Data were processed using Phantasma (v.1.19.3)<sup>110</sup>.

**RNA-seq analysis of FACS-purified mouse HSCs.** For RNA-seq analysis of purified mouse HSCs, approximately 1,000 total HSCs (KLS FLT3<sup>-</sup>CD34<sup>-</sup>CD150<sup>+</sup>) were FACS-sorted from aged control mice or aged mice that received antibody conditioning 9 days earlier and were immediately added to lysis buffer. Libraries were prepared using the Takara SMART-Seq v4 Ultra low Input RNA kit and sequencing was performed using the NovaSeq system with approximately 20 million paired reads per sample by MedGenome. Differential gene expression was performed using DESeq2<sup>111</sup> with fold change shrinkage. Heat maps were generated using Phantasma<sup>110</sup> (v.1.21.5) with all protein-coding FPKM values filtered by minimum > 0 as input and Limma<sup>112</sup> to define differentially expressed genes. GSEA<sup>113</sup> was conducted on genes ranked using the DESeq2 test statistic using the WEB-based GEne SeT AnaLysis Toolkit<sup>114</sup> (WebGestalt 2019) with the default parameters using a custom list of curated gene signatures. The following publicly available datasets was used to obtain gene signatures for young versus old HSCs: ref. 20 (i), ref. 37 (ii), ref. 26 (iii, GSE109546), ref. 27 (iv, GSE27686), ref. 22 (v, GSE112769), ref. 28 (vi, GSE44923), ref. 18 (vii, GSE100428), ref. 29 (viii, GSE128050). The following datasets were used to obtain gene signatures of mouse my-HSCs versus bal-HSCs: ref. 18 (i, GSE100428), ref. 22 (ii, GSE112769), ref. 19 (iii, GSE130504). Gene signatures were obtained directly from these studies or were generated by identifying statistically significant differentially expressed genes between cell populations. Data were processed and analysed using GREIN<sup>105</sup> or GEO2R<sup>106,107</sup>.

## HSC transplant experiments

For HSC transplant experiments, 100 total HSCs (KLS FLT3<sup>-</sup>CD34<sup>-</sup>CD150<sup>+</sup>) were FACS-sorted from CD45.2 aged control mice, or CD45.2 aged mice that received antibody conditioning 9 days earlier, and were injected retro-orbitally into 2-month-old recipient CD45.1 mice together with 1 × 10<sup>6</sup> whole-bone marrow CD45.1 support cells in 100 µl PBS. Recipient mice received split-dose irradiation 24 h before transplantation with 2 doses of 4.5 Gy 4 h apart. For chimerism analysis, peripheral blood was collected from the facial vein. HSC-derived donor cells were identified on the basis of CD45.2 expression and host recipient cells were identified on the basis of CD45.1 expression.

# Article

All transplanted mice with chimerism above 0.05% were analysed. Myeloid cells were defined as CD11b<sup>+</sup>CD3<sup>-</sup>CD19<sup>-</sup> and lymphoid cells were defined as CD19<sup>+</sup> or CD3<sup>+</sup>. The CD45.2 HSC donor-derived myeloid-to-lymphoid cell ratio was calculated as: (the number of CD45.2 myeloid cells)/(the number of CD45.2 lymphoid cells). The myeloid-to-lymphoid percentage of donor cell chimerism ratio was calculated as: (the percentage of all myeloid cells that are CD45.2)/(the percentage of all lymphoid cells that are CD45.2).

## Statistics and reproducibility

All exact *P* values are provided as source data. For all experiments, *n* indicates the number of biologically independent replicates. The sample size for in vivo experiments, including antibody depletion, viral infection and transplantation was selected on the basis of previous publications with similar experiments<sup>5,19,34,35,48,49,51,96</sup>. For all experiments, allocation of mice into experimental groups was randomized after matching for age and sex. Investigators were not blinded during data collection or analysis. All experiments involved internal control groups. Experimental and control animals were treated equally. All attempts at replication were successful. Replicated experiments were identically or similarly designed. Some experiments were replicated at independent institutions and with independent mouse strains. Data depict combined results of at least two independent experiments (Figs. 1b,c,i–k, 3b, 4b–e and 5h,i and Extended Data Figs. 2g–j, 4j–q, 7a–c, 9b, i–k and 10s), or are representative of four or more experiments (Fig. 1d–h and Extended Data Fig. 2b,c), three experiments (Figs. 2c,f and 5f–g and Extended Data Fig. 10g–j and Extended Data Fig. 10o), two experiments (Fig. 3c–e,g and Extended Data Figs. 7f–j, 8a–c and 10k–m,p) or one experiment (Figs. 2a–b,d,e,g–k, 3f,h–j and 4a and Extended Data Figs. 2d–f,k, 3a–n, 4a–i,r–x, 5c–s, 6a–n, 7d,e, 8d–l, 9c–h and 10q,r). Biological replicates (*n* represents individual mice) are reported in the figure legends. All statistical analysis was performed using GraphPad Prism (GraphPad Software) or SPSS Statistics (IBM) unless otherwise specified. The statistical tests used (parametric or nonparametric *t*-tests, one-way ANOVA, Pearson or Spearman correlation) and details (sample size, one- or two-tailed, multiple-comparison adjustment) are noted in the figure legends. Error bars denote mean  $\pm$  s.e.m. unless otherwise specified.

## Reporting summary

Further information on research design is available in the Nature Portfolio Reporting Summary linked to this article.

## Data availability

Data for all graphical representations are provided as source data. RNA-seq data have been deposited at the GEO under accession code GSE252062 and the Sequence Read Archive (SRA) under BioProject PRJNA1054066. The following publicly available datasets were used: GSE43729 (ref. 16), GSE39553 (ref. 24), GSE48893 (ref. 25), GSE109546 (ref. 26), GSE27686 (ref. 27), GSE44923 (ref. 28), GSE128050 (ref. 29), GSE47819 (ref. 30), GSE130504 (ref. 19), GSE112769 (ref. 22), E-MEXP-3935 (ref. 21), GSE32719 (ref. 3), GSE104406 (ref. 53), GSE69408 (ref. 54), GSE115348 (ref. 55), GSE107594 (ref. 104), GSE111410 (ref. 56), GSE55689 (ref. 57), GSE74246 (ref. 58), GSE132040 (ref. 108), GSE87633 (ref. 109) and GSE100428 (ref. 18). Source data are provided with this paper.

72. Spangrude, G. J., Heimfeld, S. & Weissman, I. L. Purification and characterization of mouse hematopoietic stem cells. *Science* **241**, 58–62 (1988).
73. Osawa, M., Hanada, K., Hamada, H. & Nakuchi, H. Long-term lymphohematopoietic reconstitution by a single CD34-low/negative hematopoietic stem cell. *Science* **273**, 242–245 (1996).
74. Smith, L. G., Weissman, I. L. & Heimfeld, S. Clonal analysis of hematopoietic stem-cell differentiation in vivo. *Proc. Natl Acad. Sci. USA* **88**, 2788–2792 (1991).
75. Yamamoto, R. et al. Large-scale clonal analysis resolves aging of the mouse hematopoietic stem cell compartment. *Cell Stem Cell* **22**, 600–607 (2018).
76. Myers, L. M. et al. A functional subset of CD8<sup>+</sup> T cells during chronic exhaustion is defined by SIRPa expression. *Nat. Commun.* **10**, 794 (2019).
77. Chesebro, B. et al. Characterization of mouse monoclonal antibodies specific for Friend murine leukemia virus-induced erythroleukemia cells: friend-specific and FMR-specific antigens. *Virology* **112**, 131–144 (1981).
78. Marsh-Wakefield, F. M. et al. Making the most of high-dimensional cytometry data. *Immunol. Cell Biol.* **99**, 680–696 (2021).
79. Liechti, T. et al. An updated guide for the perplexed: cytometry in the high-dimensional era. *Nat. Immunol.* **22**, 1190–1197 (2021).
80. Ashhurst, T. M. et al. Integration, exploration, and analysis of high-dimensional single-cell cytometry data using Spectre. *Cytometry A* **101**, 237–253 (2022).
81. Levine, J. H. et al. Data-driven phenotypic dissection of AML reveals progenitor-like cells that correlate with prognosis. *Cell* **162**, 184–197 (2015).
82. McInnes, L., Healy, J. & Melville, J. UMAP: uniform manifold approximation and projection for dimension reduction. Preprint at arxiv.org/abs/1802.03426 (2018).
83. Baum, C. M., Weissman, I. L., Tsukamoto, A. S., Buckle, A. M. & Peault, B. Isolation of a candidate human hematopoietic stem-cell population. *Proc. Natl. Acad. Sci. USA* **89**, 2804–2808 (1992).
84. Yiu, Y. Y. et al. CD47 blockade leads to chemokine-dependent monocyte infiltration and loss of B cells from the splenic marginal zone. *J. Immunol.* **208**, 1371–1377 (2022).
85. Brignani, S. et al. Remotely produced and axon-derived Netrin-1 instructs GABAergic neuron migration and dopaminergic substantia nigra development. *Neuron* **107**, 684–702 (2020).
86. Hadi, T. et al. Macrophage-derived netrin-1 promotes abdominal aortic aneurysm formation by activating MMP3 in vascular smooth muscle cells. *Nat. Commun.* **9**, 5022 (2018).
87. König, K. et al. The axonal guidance receptor neogenin promotes acute inflammation. *PLoS ONE* **7**, e52145 (2012).
88. Li, N. et al. Upregulation of neogenin-1 by a CREB1-BAF47 complex in vascular endothelial cells is implicated in atherogenesis. *Front. Cell Dev. Biol.* **10**, 803029 (2022).
89. Robinson, R. A. et al. Simultaneous binding of guidance cues NET1 and RGM blocks extracellular NEO1 signaling. *Cell* **184**, 2103–2120 (2021).
90. Schlegel, M. et al. Inhibition of neogenin dampens hepatic ischemia-reperfusion injury. *Crit. Care Med.* **42**, e610–e619 (2014).
91. Schlegel, M. et al. Inhibition of neogenin fosters resolution of inflammation and tissue regeneration. *J. Clin. Invest.* **128**, 4711–4726 (2019).
92. van den Heuvel, D. M., Hellemons, A. J. & Pasterkamp, R. J. Spatiotemporal expression of repulsive guidance molecules (RGMs) and their receptor neogenin in the mouse brain. *PLoS ONE* **8**, e55828 (2013).
93. Keren, Z. et al. B-cell depletion reactivates B lymphopoiesis in the BM and rejuvenates the B lineage in aging. *Blood* **117**, 3104–3112 (2011).
94. Säwén, P. et al. Mitotic history reveals distinct stem cell populations and their contributions to hematopoiesis. *Cell Rep.* **14**, 2809–2818 (2016).
95. Boivin, G. et al. Durable and controlled depletion of neutrophils in mice. *Nat. Commun.* **11**, 2762 (2020).
96. Chhabra, A. et al. Hematopoietic stem cell transplantation in immunocompetent hosts without radiation or chemotherapy. *Sci. Transl. Med.* **8**, 351ra105 (2016).
97. Iglewicz, B. & Hoaglin, D. C. *How to Detect and Handle Outliers* (Asq Press, 1993).
98. *Guide for the Care and Use of Laboratory Animals* (National Research Council, 2010).
99. Robertson, S. J. et al. Suppression of acute anti-friend virus CD8<sup>+</sup> T-cell responses by coinfection with lactate dehydrogenase-elevating virus. *J. Virol.* **82**, 408–418 (2008).
100. Chesebro, B., Wehrly, K. & Stimpfling, J. Host genetic control of recovery from Friend leukemia virus-induced splenomegaly: mapping of a gene within the major histocompatibility complex. *J. Exp. Med.* **140**, 1457–1467 (1974).
101. Lander, M. R. & Chattopadhyay, S. K. A *Mus dunni* cell line that lacks sequences closely related to endogenous murine leukemia viruses and can be infected by ectropic, amphotropic, xenotropic, and mink cell focus-forming viruses. *J. Virol.* **52**, 695–698 (1984).
102. Robertson, M. N. et al. Production of monoclonal antibodies reactive with a denatured form of the Friend murine leukemia virus gp70 envelope protein: use in a focal infectivity assay, immunohistochemical studies, electron microscopy and western blotting. *J. Virol. Methods* **34**, 255–271 (1991).
103. Horton, H. et al. Optimization and validation of an 8-color intracellular cytokine staining (ICS) assay to quantify antigen-specific T cells induced by vaccination. *J. Immunol. Methods* **323**, 39–54 (2007).
104. Kumar, P. et al. HMGA2 promotes long-term engraftment and myeloerythroid differentiation of human hematopoietic stem and progenitor cells. *Blood Adv.* **3**, 681–691 (2019).
105. Mahi, N. A., Najafabadi, M. F., Pilarczyk, M., Kouril, M. & Medvedovic, M. GREIN: an interactive web platform for re-analyzing GEO RNA-seq data. *Sci. Rep.* **9**, 7580 (2019).
106. Barrett, T. et al. NCBI GEO: archive for functional genomics data sets-update. *Nucleic Acids Res.* **41**, D991–D995 (2013).
107. Edgar, R., Domrachev, M. & Lash, A. E. Gene Expression Omnibus: NCBI gene expression and hybridization array data repository. *Nucleic Acids Res.* **30**, 207–210 (2002).
108. The Tabula Muris Consortium. Single-cell transcriptomics of 20 mouse organs creates a *Tabula Muris*. *Nature* **562**, 367–372 (2018).
109. Kadoki, M. et al. Organism-level analysis of vaccination reveals networks of protection across tissues. *Cell* **171**, 398–413 (2017).
110. Kleverov, M. et al. Phantasma: web-application for visual and interactive gene expression analysis. Preprint at bioRxiv <https://doi.org/10.1101/2022.12.10.519861> (2022).
111. Love, M. I., Huber, W. & Anders, S. Moderated estimation of fold change and dispersion for RNA-seq data with DESeq2. *Genome Biol.* **15**, 550 (2014).
112. Ritchie, M. E. et al. limma powers differential expression analyses for RNA-sequencing and microarray studies. *Nucleic Acids Res.* **43**, e47 (2015).
113. Subramanian, A. et al. GSEA: gene set enrichment analysis: a knowledge-based approach for interpreting genome-wide expression profiles. *Proc. Natl. Acad. Sci. USA* **102**, 15545–15550 (2005).
114. Liao, Y., Wang, J., Jaehnig, E. J., Shi, Z. & Zhang, B. WebGestalt 2019: gene set analysis toolkit with revamped UIs and APIs. *Nucleic Acids Res.* **47**, W199–W205 (2019).

115. Seita, J. & Weissman, I. L. Hematopoietic stem cell: self-renewal versus differentiation. *Wiley Interdiscip. Rev. Syst. Biol. Med.* **2**, 640–653 (2010).
116. Helbling, P. M. et al. Global transcriptomic profiling of the bone marrow stromal microenvironment during postnatal development, aging, and inflammation. *Cell Rep.* **29**, 3313–3330 (2019).
117. Akashi, K. & Weissman, I. L. The c-kit<sup>+</sup> maturation pathway in mouse thymic T cell development: lineages and selection. *Immunity* **5**, 147–161 (1996).
118. Loder, F. et al. B cell development in the spleen takes place in discrete steps and is determined by the quality of B cell receptor-derived signals. *J. Exp. Med.* **190**, 75–89 (1999).
119. Leins, H. et al. Aged murine hematopoietic stem cells drive aging-associated immune remodeling. *Blood* **132**, 565–576 (2018).
120. Goardon, N. et al. Coexistence of LMPP-like and GMP-like leukemia stem cells in acute myeloid leukemia. *Cancer Cell* **19**, 138–152 (2011).
121. Manz, M. G., Miyamoto, T., Akashi, K. & Weissman, I. L. Prospective isolation of human clonogenic common myeloid progenitors. *Proc. Natl Acad. Sci. USA* **99**, 11872–11877 (2002).

**Acknowledgements** We thank the members of the Weissman and Hasenkrug laboratories for advice and discussions; A. McCarty, T. Naik, L. Quinn and T. Raveh for technical and logistical support; A. Banuelos, G. Blacker, B. George, G. Gulati, J. Liu, R. Sinha, M. Tal, N. Womack and Y. Yiu for general help, advice and experimental support; C. Carswell-Crumpton, C. Pan, J. Pasillas and the staff at the Stanford Institute for Stem Cell Biology and Regenerative Medicine FACS Core for flow cytometry assistance; H. Maecker and I. Herschmann of the Stanford Human Immune Monitoring Center (HIMC) for assistance with immunoassays; and the members of the Rocky Mountain Veterinary Branch (RMVB), especially T. Wiediger, for excellent care of the aged mice. This work was partially funded by the Intramural Research Program of the National Institute of Allergy and Infectious Diseases, National Institutes of Health, USA; the NIH/NCI Outstanding Investigator Award (R35CA220434 to I.L.W.); the NIH NIDDK (R01DK115600 to I.L.W.); the NIH NIAID (R01AI143889 to I.L.W.); and the Virginia and D.K. Ludwig Fund for Cancer Research (to I.L.W.). J.B.R. was supported by the Stanford Radiation Oncology Kaplan Research Fellowship, the RSNA Resident/Fellow Research Grant, and the Stanford Cancer Institute

Fellowship Award and the Ellie Guardino Research Fund. This work was supported by the Stanford Cancer Institute, an NCI-designated Comprehensive Cancer Center. J.J.N. was supported by Stanford University Medical Scientist Training Program grant T32-GM007365 and T32-GM145402. E.D. was supported by grants from NIH NIDDK (5T32DK098132-09 and 1T1DK139565-01). The funders had no role in study design, data collection and analysis, decision to publish or preparation of the manuscript. Some illustrations were created using BioRender.

**Author contributions** J.B.R. and L.M.M. contributed equally to this work and they both have the right to be listed first in bibliographic documents. J.B.R. and L.M.M. conceived and performed experiments, analysed and interpreted all the data, and wrote the paper. J.J.N., M.M.C., A.B.C., R.J.M. and E.D. performed experiments and analysed data. L.M.M., M.M.C., A.B.C. and R.J.M. performed the Friend virus experiments. J.B.R. and E.D. designed and performed the RNA-seq and transplant experiments. I.L.W. and K.J.H. conceived experiments, supervised the research, interpreted results and wrote the paper. All of the authors reviewed, edited and approved the manuscript.

**Competing interests** I.L.W. is listed as an inventor on patents related to CD47 licensed to Gilead Sciences, but has no financial interests in Gilead; he is also a co-founder and equity holder of Bitterroot Bio, PHeast and 48 Bio; he is on the scientific advisory board of Appia. J.B.R. is a co-founder and equity holder of 48 Bio. I.L.W., K.J.H., J.B.R., L.M.M. and J.J.N. are listed as co-inventors on a pending patent application related to this work. The other authors declare no competing interests.

#### Additional information

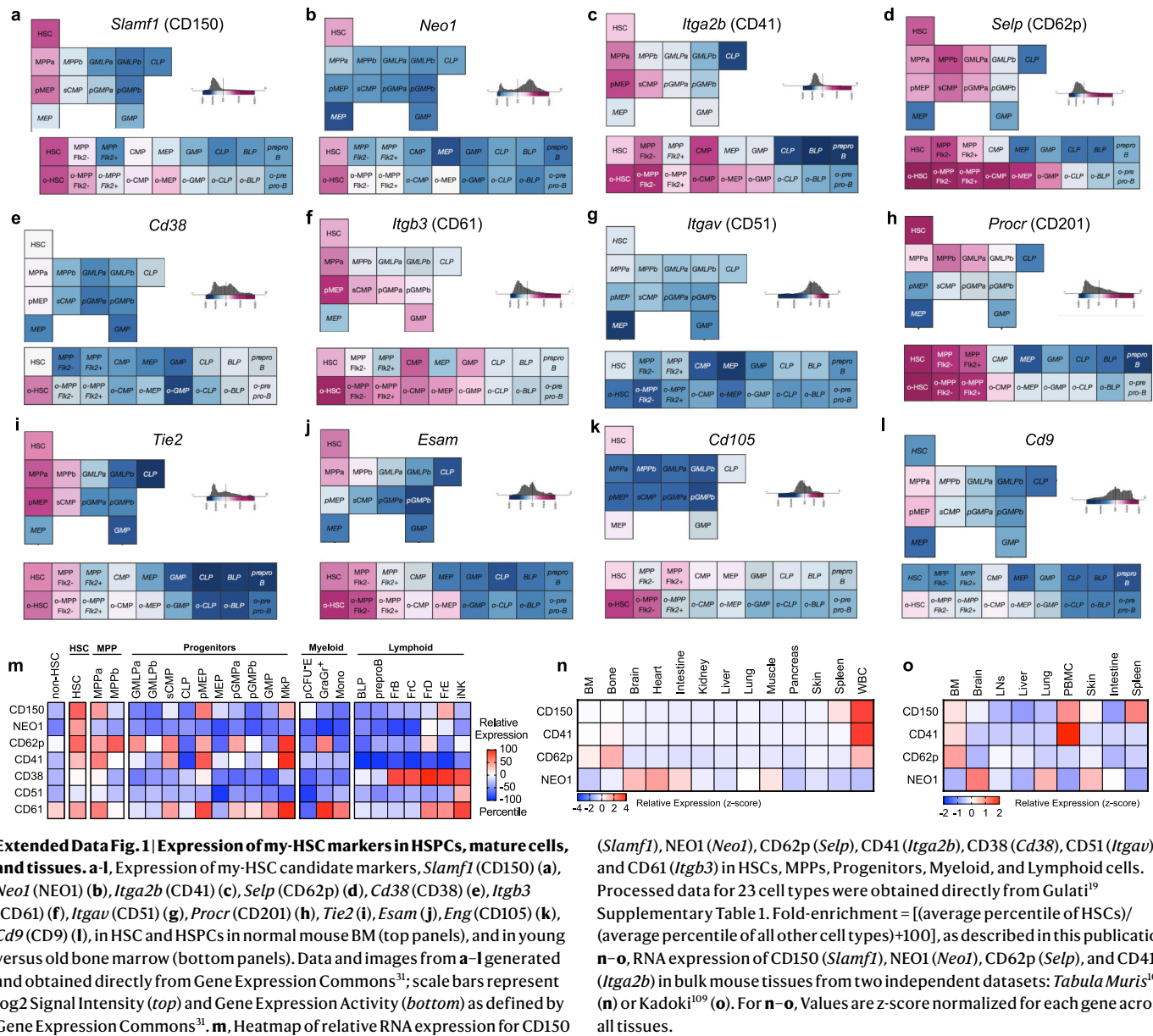
**Supplementary information** The online version contains supplementary material available at <https://doi.org/10.1038/s41586-024-07238-x>.

**Correspondence and requests for materials** should be addressed to Kim J. Hasenkrug or Irving L. Weissman.

**Peer review information** *Nature* thanks Jennifer Trowbridge and the other, anonymous, reviewer(s) for their contribution to the peer review of this work. Peer reviewer reports are available.

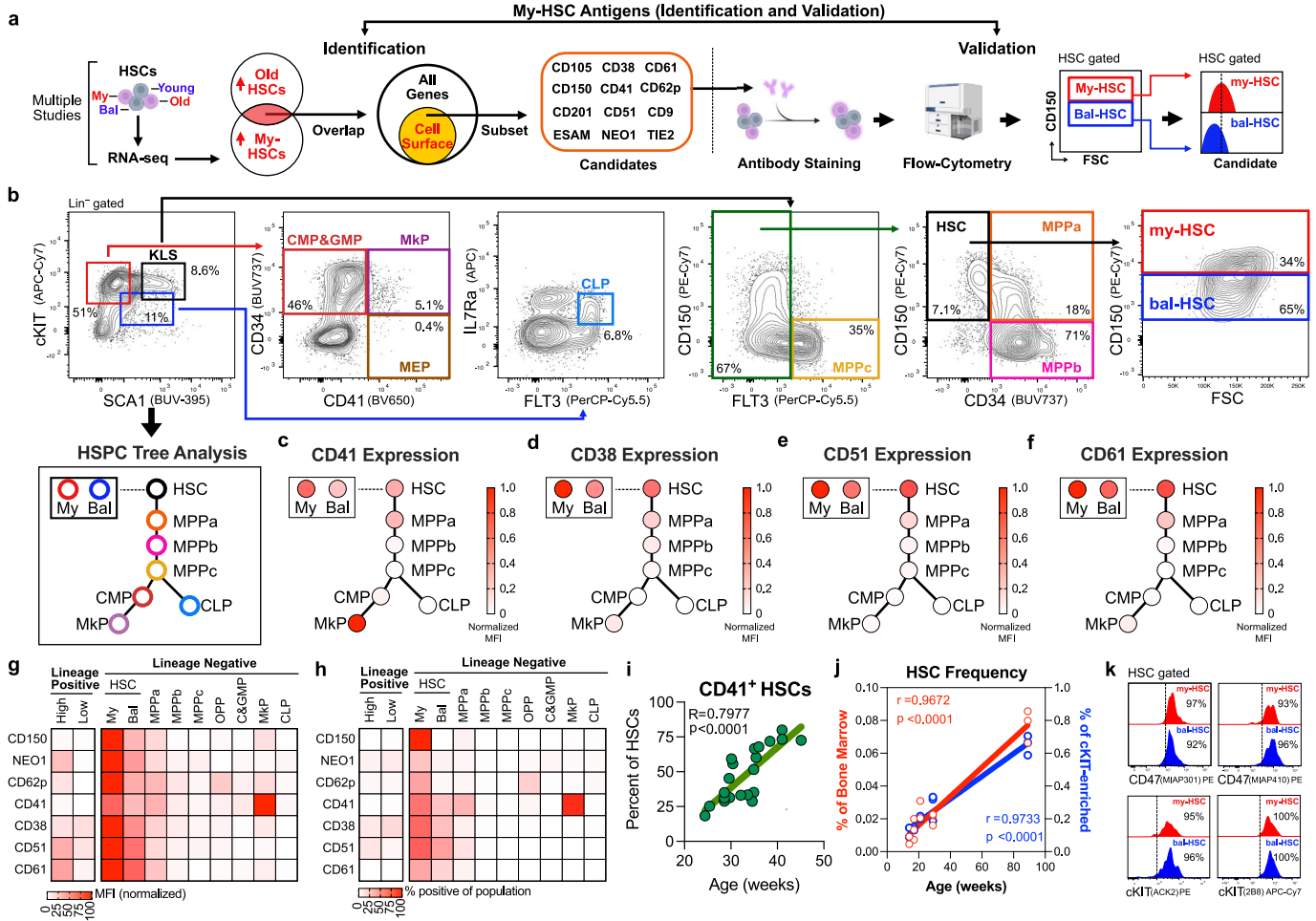
**Reprints and permissions information** is available at <http://www.nature.com/reprints>.

# Article



**Extended Data Fig. 1 | Expression of my-HSC markers in HSPCs, mature cells, and tissues.** **a–l**, Expression of my-HSC candidate markers, *Slamf1* (CD150) (**a**), *Neo1* (**b**), *Itga2b* (CD41) (**c**), *Selp* (CD62p) (**d**), *Cd38* (CD38) (**e**), *Itgb3* (CD61) (**f**), *Itgav* (CD51) (**g**), *Procr* (CD201) (**h**), *Tie2* (**i**), *Esam* (**j**), *Eng* (CD105) (**k**), *Cd9* (CD9) (**l**), in HSC and HSPCs in normal mouse BM (top panels), and in young versus old bone marrow (bottom panels). Data and images from **a–l** generated and obtained directly from Gene Expression Commons<sup>31</sup>; scale bars represent log2 Signal Intensity (*top*) and Gene Expression Activity (*bottom*) as defined by Gene Expression Commons<sup>31</sup>. **m**, Heatmap of relative RNA expression for CD150

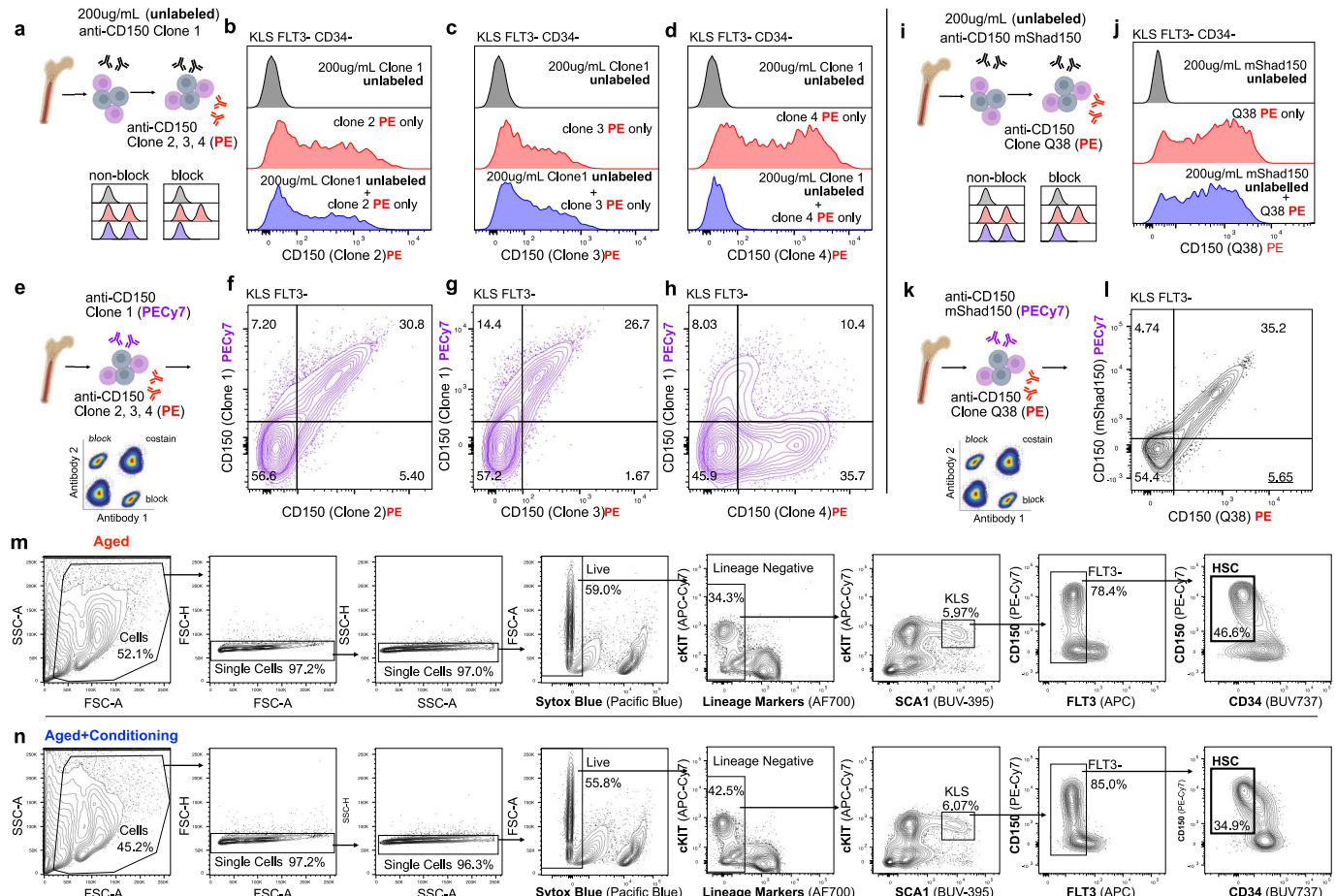
(*Slamf1*), NEO1 (*Neo1*), CD62p (*Selp*), CD41 (*Itga2b*), CD38 (*Cd38*), CD51 (*Itgav*), and CD61 (*Itgb3*) in HSCs, MPPs, Progenitors, Myeloid, and Lymphoid cells. Processed data for 23 cell types were obtained directly from Gulati<sup>19</sup>. **Supplementary Table 1.** Fold-enrichment = [(average percentile of HSCs)/(average percentile of all other cell types)+100], as described in this publication. **n–o**, RNA expression of CD150 (*Slamf1*), NEO1 (*Neo1*), CD62p (*Selp*), and CD41 (*Itga2b*) in bulk mouse tissues from two independent datasets: *Tabula Muris*<sup>108</sup> (**n**) or Kadoki<sup>109</sup> (**o**). For **n–o**, Values are z-score normalized for each gene across all tissues.



**Extended Data Fig. 2 | Gating strategy for total HSCs, my-HSCs, bal-HSCs, and HPCs.** **a**, Schematic to identify and validate my-HSC cell-surface antigens. The diagram was created using BioRender. **b**, Representative flow-cytometry gating of mouse BM to identify total HSC ( $\text{Lin}^- \text{cKIT}^+ \text{Sca1}^+ \text{FLT3}^- \text{CD34}^- \text{CD150}^+$ ), my-HSC ( $\text{Lin}^- \text{cKIT}^+ \text{Sca1}^+ \text{FLT3}^- \text{CD34}^- \text{CD150}^{\text{High}}$ ), bal-HSC ( $\text{Lin}^- \text{cKIT}^+ \text{Sca1}^+ \text{FLT3}^- \text{CD34}^- \text{CD150}^{\text{Low}}$ ), MPPs<sup>115</sup> [ $\text{Lin}^- \text{cKIT}^+ \text{Sca1}^+ \text{FLT3}^- \text{CD34}^+ \text{CD150}^+$ ], MPPb ( $\text{Lin}^- \text{cKIT}^+ \text{Sca1}^+ \text{FLT3}^- \text{CD34}^+ \text{CD150}^-$ ), MPPc ( $\text{Lin}^- \text{cKIT}^+ \text{Sca1}^+ \text{FLT3}^- \text{CD34}^+ \text{CD150}^-$ ]), OPP ( $\text{Lin}^- \text{cKIT}^+ \text{Sca1}^+$ ), CMP&GMP ( $\text{Lin}^- \text{cKIT}^+ \text{Sca1}^- \text{CD34}^+ \text{CD41}^+$ ), MkP ( $\text{Lin}^- \text{cKIT}^+ \text{Sca1}^- \text{CD34}^+ \text{CD41}^+$ ), MEP ( $\text{Lin}^- \text{cKIT}^+ \text{Sca1}^- \text{CD34}^- \text{CD41}^+$ ), CLP ( $\text{Lin}^- \text{cKIT}^+ \text{Sca1}^- \text{CD34}^- \text{CD41}^+$ ), IL7Ra<sup>+</sup>FLT3<sup>+</sup>). Panels are after excluding dead cells, doublets, and lineage-positive (CD3<sup>+</sup>, or Ly-6G<sup>+</sup>/C<sup>+</sup>, or CD11b<sup>+</sup>, or CD45R<sup>+</sup>, or Ter-119<sup>+</sup>) cells. Used for Fig. 1b–k, Fig. 2a–f, Fig. 3b–d, Fig. 4a, Extended Data Fig. 2c–k, Extended Data Fig. 3a–l, Extended Data Fig. 4a–s, Extended Data Fig. 5c–s, Extended Data Fig. 6a Extended Data Fig. 8c–h. Illustration of Hematopoietic Stem and Progenitor Cell (HSPC) Tree Analysis. CMP is combined CMP&GMP. Gate to define my-HSC vs. bal-HSC was set as described previously<sup>5</sup>. **c–f**, Relative expression of CD41 (c), CD38 (d), CD51 (e), CD61 (f), on HSC and HSPCs."/>

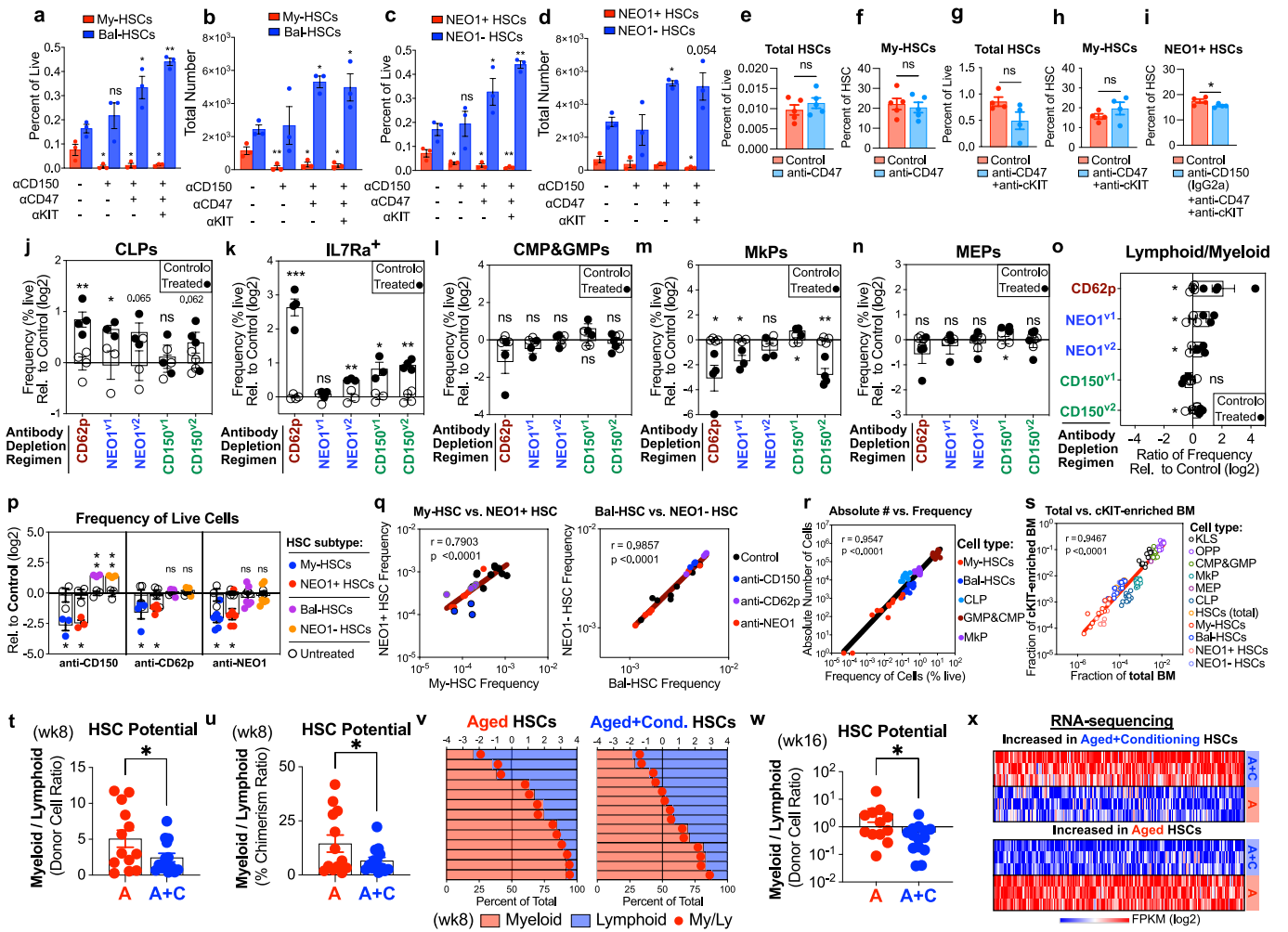
MFI values for each marker were obtained for each population and normalized from 0–1 based on the lowest to highest expression. **g–h**, Relative cell-surface levels (g) and percent-positive cells (h) for CD150, NEO1, CD62p, CD41, CD38, CD51, and CD61, on lineage-positive high and low cells, total HSCs, and HPCs in the BM. For cell-surface levels (g), MFI values for each marker were obtained for each population and normalized from 0–100 based on the lowest to highest expression. **i**, Percentage of total HSCs that are CD41<sup>+</sup> (y-axis) vs. mouse age in weeks (x-axis);  $n = 21$  mice. **j**, Mouse age (x-axis) vs. the frequency of total HSCs (my-HSC+bal-HSC) as a percentage of live cells in the (i) total BM (left y-axis, red) or (ii) cKIT-enriched BM (right y-axis, blue) in untreated mice;  $n = 13$  mice. **k**, Percent-positive of my-HSCs vs. bal-HSCs for CD47 (k, top) using independent anti-CD47 clones (MIAP301, left; MIAP410, right), and for cKIT (k, bottom) using independent anti-cKIT clones (ACK2, left; 2B8, right). Mouse ages: 4–6 months (b–i, k), 3–23 months (j). For **a–k**, BM was cKIT-enriched prior to analysis. For **j**, total BM (non cKIT-enriched) was also examined.  $p$ -values and  $r$  values calculated with one-tailed Pearson correlation coefficient (i–j).  $n$  represents independent mice.

# Article



**Extended Data Fig. 3 | Anti-CD150 non-masking antibodies and FACS gating to isolate HSCs.** **a**, Schematic to identify anti-CD150 antibodies not masked by anti-CD150 antibody clone 1 (TC15), used in panels **b–d**; BM cells were incubated with saturating concentrations of unlabelled anti-CD150 antibody clone 1 (TC15) and then stained with PE anti-CD150 clones 2, 3, 4 (Q38, 9D1, mShad150). **b–d**, Saturating concentrations of unlabelled anti-CD150 antibody clone TC15 blocks staining with PE anti-CD150 clone 4 (mShad150) (**d**), but does not block staining of PE anti-CD150 clones 2, 3 (Q38, 9D1) (**b–c**). **e**, Schematic to determine if anti-CD150 clones 2, 3, 4 (Q38, 9D1, mShad150) identify the same population as anti-CD150 clone 1 (TC15); used in panels **f–h**; BM cells were incubated with PECy-7 anti-CD150 antibody clone 1 (TC15) and with PE anti-CD150 clones 2, 3, 4 (Q38, 9D1, mShad150). **f–h**, Co-staining with anti-CD150 clones 2, 3 (Q38, 9D1) identifies the same population as anti-CD150 antibody clone TC15 (**f–g**). Co-staining with anti-CD150 clone 4 (mShad150) and anti-CD150 antibody clone 1 (TC15) is mutually blocked (**h**). **i**, Schematic to identify anti-CD150 antibodies that are not blocked by anti-CD150 clone mShad150, used in panel **j**; BM cells are incubated with saturating concentrations of unlabelled anti-CD150 antibody clone mShad150 and then stained with PE anti-CD150 clone 2 (Q38). **j**, Saturating

concentrations of unlabelled anti-CD150 antibody clone mShad150 does not block staining of PE anti-CD150 clone 2 (Q38) (**j**). **k**, Schematic to determine if co-staining with anti-CD150 clone 2 (Q38) identifies the same population as anti-CD150 antibody clone mShad150; used in panel **l**; BM cells are incubated with PECy-7 anti-CD150 antibody clone mShad150 and with PE anti-CD150 clone 2 (Q38). **l**, Co-staining with anti-CD150 clones 2 (Q38) identifies the same population as anti-CD150 antibody clone mShad150 (**l**). **m–n**, Representative FACS gating of mouse BM to sort total HSC (Lin<sup>-</sup>cKIT<sup>+/bright</sup>Sca1<sup>+</sup>FLT3CD34CD150) from aged (11 months) control mice (Aged, A) or aged (11 months) mice with my-HSC depletion (Aged+Conditioning, A + C), used to sort HSCs for RNA-seq experiment presented in Fig. 2g, h, Extended Data Fig. 4x, and used to sort HSCs for transplant experiments presented in Fig. 2i–k, Extended Data Fig. 4t–v. My-HSC depletion was performed with anti-NEO1+anti-CD62p+anti-cKIT+CD47 and cells were collected at day 9 post-treatment; n = 3 mice (A), n = 3 mice (A + C). The diagrams (**a, e, i, k**) were created using BioRender. Mouse ages approximately: 3 months (**a–h**), 5–8 months (**i–l**), 11 months (**m–n**). For (**a–n**), BM was cKIT-enriched prior to FACS analysis or sorting. n represents independent mice.



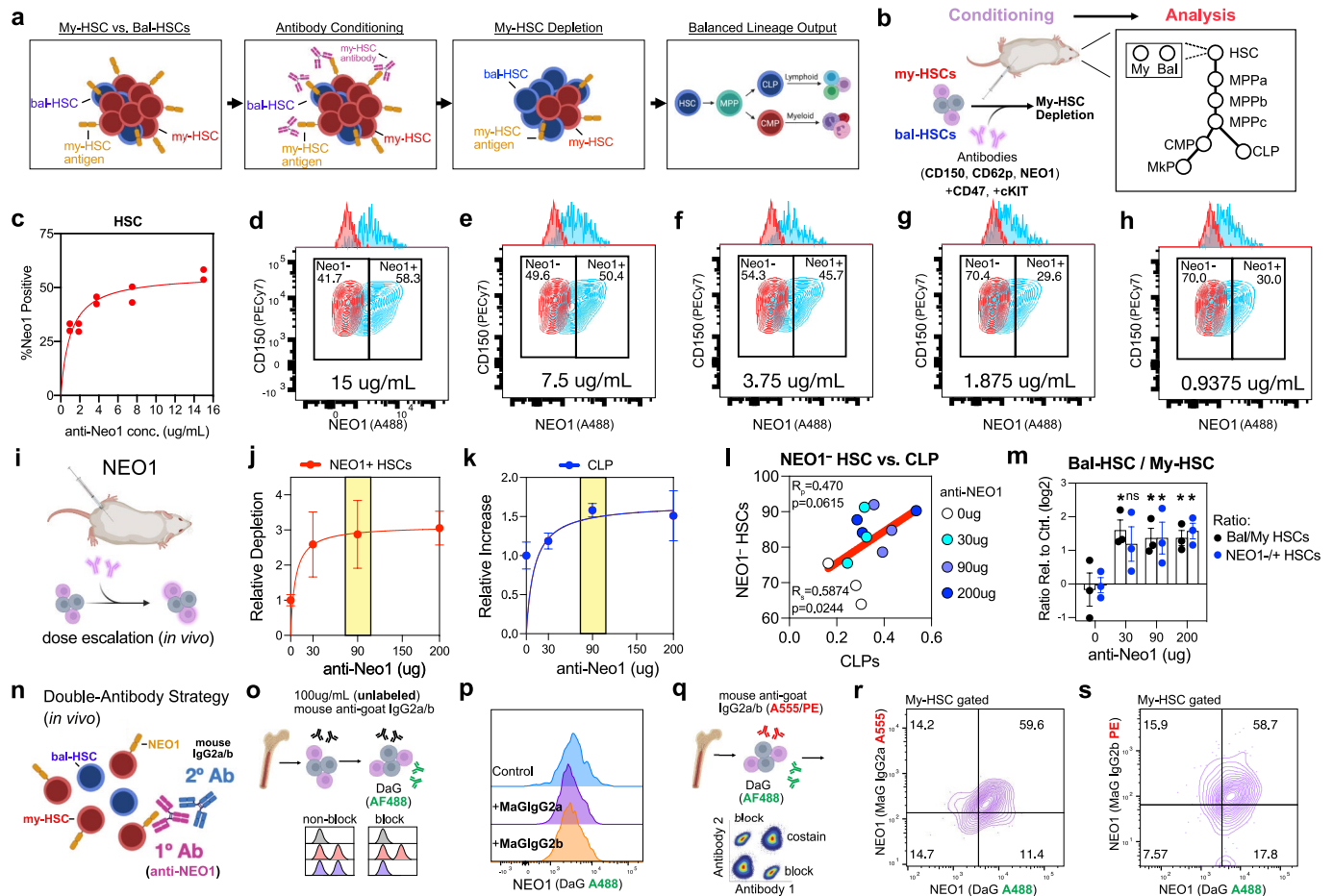
**Extended Data Fig. 4** | See next page for caption.

# Article

## Extended Data Fig. 4 | Antibody-mediated depletion of my-HSCs in vivo.

**a–d**, Frequency (% live) (**a**, **c**) or absolute number (**b**, **d**) of my-HSCs and bal-HSCs (**a–b**) or of NEO1<sup>+</sup> HSCs and NEO1<sup>+</sup> HSCs (**c–d**) after anti-CD150 conditioning (anti-CD150, anti-CD150+anti-CD47, or anti-CD150+anti-CD47+anti-cKIT);  $n = 3$  mice per group. **e**, Total HSCs (my-HSCs+bal-HSCs) as percent-live in mice receiving anti-CD47;  $n = 5$  mice per group;  $P = 0.3637$ . **f**, Percentage of total HSCs that are my-HSCs in mice receiving anti-CD47;  $n = 5$  mice per group;  $P = 0.6628$ . **g**, Total HSCs (my-HSCs+bal-HSCs) as a percent-live, in mice receiving anti-CD47+anti-cKIT;  $n = 4$  mice per group;  $P = 0.0973$ . **h**, Percentage of total HSCs that are my-HSCs in mice receiving anti-CD47+anti-cKIT;  $n = 4$  mice per group;  $P = 0.2805$ . **i**, Percentage of total HSCs that are NEO1<sup>+</sup> HSCs in mice receiving anti-CD150 (IgG2a)+anti-CD47+anti-cKIT (e.g., protocol CD150<sup>v2</sup>);  $n = 4$  mice per group; \* $P = 0.0353$ . **j–n**, Frequency (% live) of CLPs (**j**), IL7Ra<sup>+</sup> cells (**k**), CMPs&GMPs (**l**), MkPs (**m**), and MEPs (**n**), after anti-CD150, anti-CD62p, or anti-NEO1 conditioning protocols. Values relative to mean of untreated control mice and log2-transformed;  $n = 3$  mice per group (NEO1<sup>v1</sup>, NEO1<sup>v2</sup>, CD150<sup>v1</sup>);  $n = 4$  mice per group (CD62p, CD150<sup>v2</sup>). **o**, Ratio of frequency (% live) for Lymphoid to Myeloid Progenitors (CLP)/(CMP&GMP), after anti-CD150, anti-CD62p, or anti-NEO1 antibody protocols. Values relative to mean of untreated control mice and log2-transformed;  $n = 3$  mice per group (NEO1<sup>v1</sup>, NEO1<sup>v2</sup>, CD150<sup>v1</sup>);  $n = 4$  mice per group (CD62p, CD150<sup>v2</sup>). **p**, Frequency (% live) of my-HSCs, bal-HSCs, NEO1<sup>+</sup> HSCs, and NEO1 HSCs after treatment with anti-CD150, anti-CD62p, or anti-NEO1 protocols;  $n = 3$  mice per group (anti-CD150<sup>v1</sup>);  $n = 4$  mice per group (anti-CD62p);  $n = 3$  control mice and  $n = 6$  treated mice (anti-NEO1, combined 90 ug & 200 ug protocols). Values relative to mean of control mice and log2-transformed. For **j–p**, values for treated mice (filled circles); values for control mice (unfilled circles). **q**, Correlation of fraction of live cells for my-HSCs vs. NEO1<sup>+</sup> HSCs (left), and bal-HSCs vs. NEO1<sup>+</sup> HSCs (right), of control mice and mice receiving anti-CD150, anti-CD62p, or anti-NEO1 protocols, in cKIT-enriched BM;  $n = 3$  mice (anti-CD150<sup>v1</sup>);  $n = 4$  mice (anti-CD62p);  $n = 3$  control mice and  $n = 6$  treated mice (anti-NEO1, combined 90 ug & 200 ug protocols). **r**, Comparison of the absolute number of cells in total (non-cKIT-enriched) BM (y-axis) vs. frequency of cells as a percent-live (in cKIT-enriched) BM (x-axis), for my-HSCs, bal-HSCs, CLP,

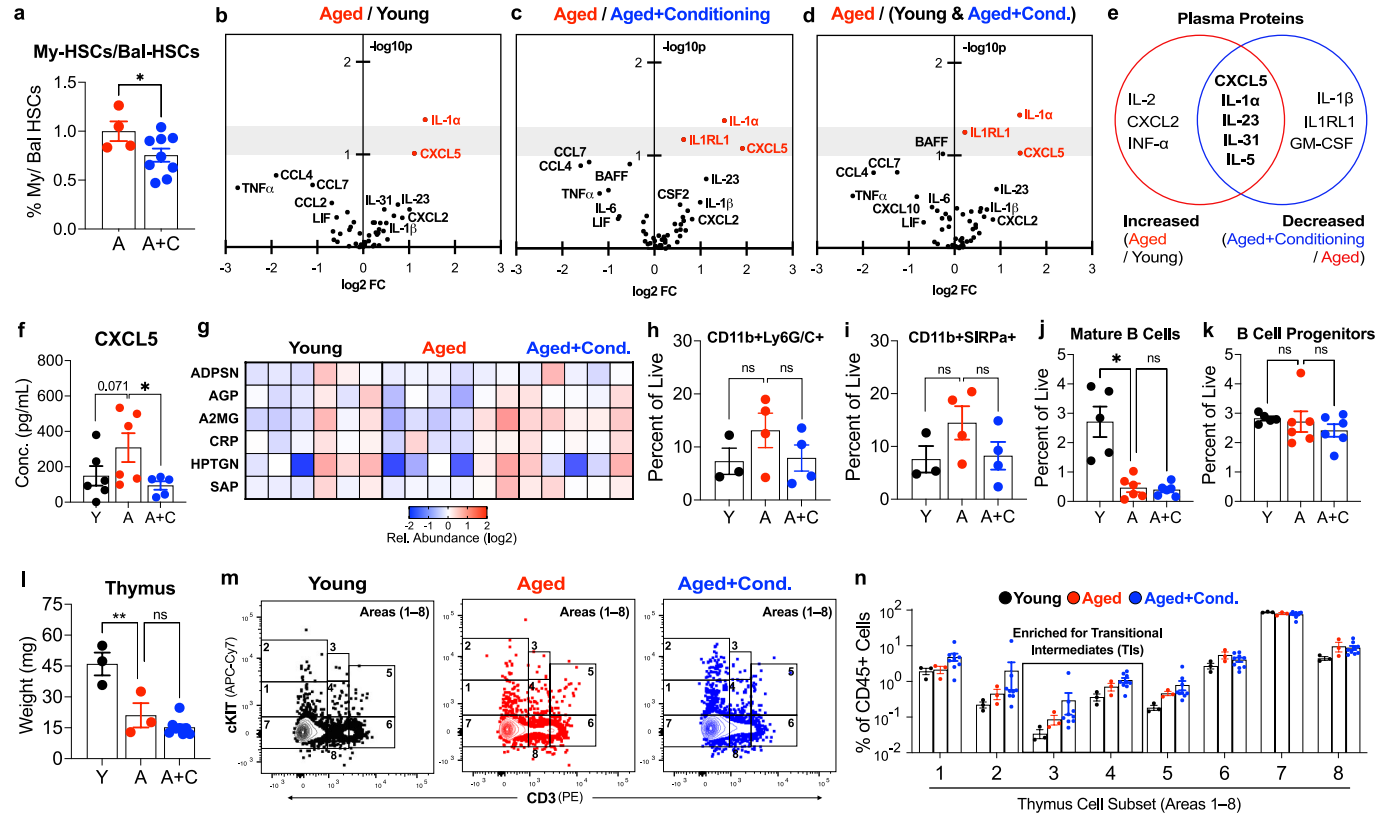
CMP&GMP, and MkP in control mice and mice receiving anti-CD150, anti-CD150+anti-CD47, or anti-CD150+anti-CD47+anti-cKIT;  $n = 3$  mice per condition. **s**, Comparison of the frequency of cells as a fraction of total (non-cKIT-enriched) BM (x-axis) vs. the frequency of cells as a fraction of cKIT-enriched BM (y-axis), for cell populations in control mice and mice receiving anti-CD150, anti-CD150+anti-CD47, or anti-CD150+anti-CD47+anti-cKIT;  $n = 3$  mice per condition. Data for **q–s** log10-transformed. **t–v**, HSC lineage potential 8-weeks after transplantation of 100 total HSCs FACS-sorted from CD45.2 aged mice without (A) or with my-HSC depletion (A + C) into CD45.1 recipients. Donor Myeloid to Lymphoid Ratio (**t**, \* $P = 0.0275$ ) and Percent-Chimerism Ratio (**u**, \* $P = 0.0340$ ). For each recipient (y-axis), % donor cells (bottom x-axis) that are Myeloid (red bars) or Lymphoid (blue bars) and the Myeloid/Lymphoid log2-ratio (red circles) (top x-axis) (**v**);  $n = 13$  recipient mice (A),  $n = 14$  recipient mice (A + C). **w**, Donor Myeloid/Lymphoid Ratio 16-weeks after transplantation of 100 total HSCs FACS-sorted from CD45.2 aged mice without (A) or with my-HSC depletion (A + C) into CD45.1 recipients;  $n = 12$  recipient mice (A),  $n = 14$  recipient mice (A + C); \* $P = 0.0232$ . **x**, Top 200 differentially expressed genes ranked by p-value for RNA-seq comparison between (A) vs. (A + C), based on Fragments Per Kilobase of transcript per Million mapped reads (FPKM); log2-transformed. Heatmap generated using Phantasia<sup>110</sup> (v1.21.5) with FPKM values as input and Limma<sup>112</sup> to define differentially expressed genes;  $n = 3$  mice (A),  $n = 3$  mice (A + C). Mouse ages approximately: 6–7 months (**a–d**, **r–s**), 7–9 months (**g–i**), 5–9 months (**j–q**), 11 months (donors, **t–w**), 2 months (recipients, **v**). For (**a**, **c**, **g–s**), BM was cKIT-enriched prior to analysis. For (**b**, **d**, **e–f**, **r–s**), total BM (non cKIT-enriched) was examined. P-values obtained by ordinary one-way ANOVA followed by one-tailed Dunnett's multiple comparisons test with non-treated as control (**a–d**), unpaired parametric one-tailed t-test (**i–k**, **p**, **t–u**), unpaired non-parametric one-tailed t-test (**w**), or unpaired parametric two-tailed t-test (**e–h**, **l–o**). p-values and R values calculated with one-tailed Pearson correlation coefficient (**q–s**). CD150<sup>v1</sup> is rat IgG2b anti-CD150 protocol; CD150<sup>v2</sup> is rat IgG2a anti-CD150 protocol; NEO1<sup>v2</sup> includes mouse IgG2a anti-goat; α, anti-; ns, not significant. Bars indicate mean +/- s.e.m. n represents independent mice; \* $P < 0.05$ , \*\* $P < 0.005$ , \*\*\* $P < 0.0005$ ; Exact P-values provided as source data.



**Extended Data Fig. 5 | Optimization of NEO1 depletion protocol in vitro and in vivo.** **a–b**, Strategy to restore balanced lineage output by depleting my-HSCs. **c–h**, Anti-NEO1 antibody saturation curve (**c**) determined from in vitro antibody dilution series (**d–h**). **i**, Schematic of in vivo saturation experiments with anti-NEO1 antibody; used in panels **j–m**. **j–m**, Dose-dependent relationship between anti-NEO1 antibody dose (0 ug, 30 ug, 90 ug, 200 ug), when combined with anti-CD47 and anti-cKIT, on the relative depletion of NEO1<sup>+</sup> HSCs (**j**), and increase in CLPs (**k**). Optimal concentration in yellow;  $n = 3$  mice per group. **l**, The increase in NEO1<sup>-</sup> HSCs after anti-NEO1 dose escalation (0 ug, 30 ug, 90 ug, 200 ug) is correlated with the increase in CLPs. **m**, Impact on the ratio of Bal-HSCs/My-HSCs (black) and NEO1<sup>-</sup> HSCs/NEO1<sup>+</sup> HSCs (blue) as a percentage of live cells after anti-NEO1 antibody dose-escalation (0 ug, 30 ug, 90 ug, 200 ug), when combined with anti-CD47 and anti-cKIT;  $n = 3$  per group. Values relative to mean value of control (0 ug) mice and log2-transformed. **n**, Schematic of double antibody strategy to target NEO1, whereby mouse IgG2a or IgG2b monoclonal anti-goat

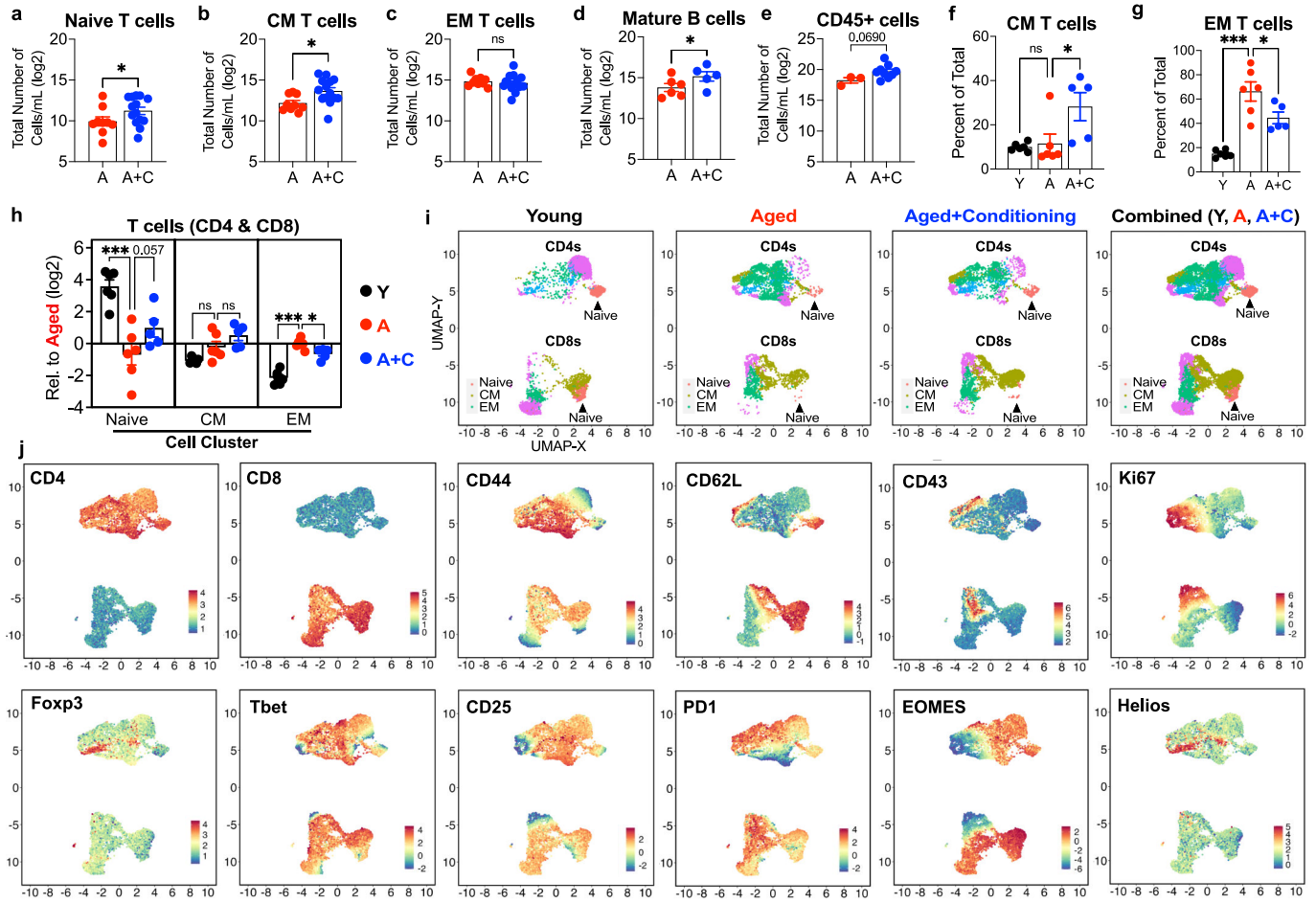
antibodies are administered 24 h after goat anti-NEO1<sup>93,94</sup>. **o–p**, Schematic (**o**) to demonstrate that saturating concentrations of mouse IgG2a or IgG2b anti-goat do not reduce ability of donkey anti-goat AF488 detect goat anti-NEO1 antibody (**p**). **q–s**, Schematic (**q**) of experiment demonstrating that mouse anti-goat IgG2a A555 (**r**) and IgG2b PE (**s**) antibodies identify the same population as donkey anti-goat AF488 by flow cytometry. The diagrams (**a, b, i, n, o, q**) were created using BioRender. Mouse ages approximately: 5–7 months (**c–h, n–s**), 6–9 months (**i–m**). For (**c–s**), BM was cKIT-enriched prior to analysis. For correlation  $p$ -values, one-tailed Pearson correlation coefficient ( $R_p$ ), and one-tailed Spearman correlation coefficient ( $R_s$ ) were calculated (**l**).  $p$ -values obtained by ordinary one-way ANOVA followed by one-tailed Dunnett's multiple comparisons test with 0 ug condition as control (**m**). MaG, mouse anti-goat; DaG, donkey anti-goat. Bars indicate mean  $\pm$  s.e.m.  $n$  represents independent mice; \* $P < 0.05$ , \*\* $P < 0.005$ , \*\*\* $P < 0.0005$ ; Exact  $P$ -values provided as source data.

# Article



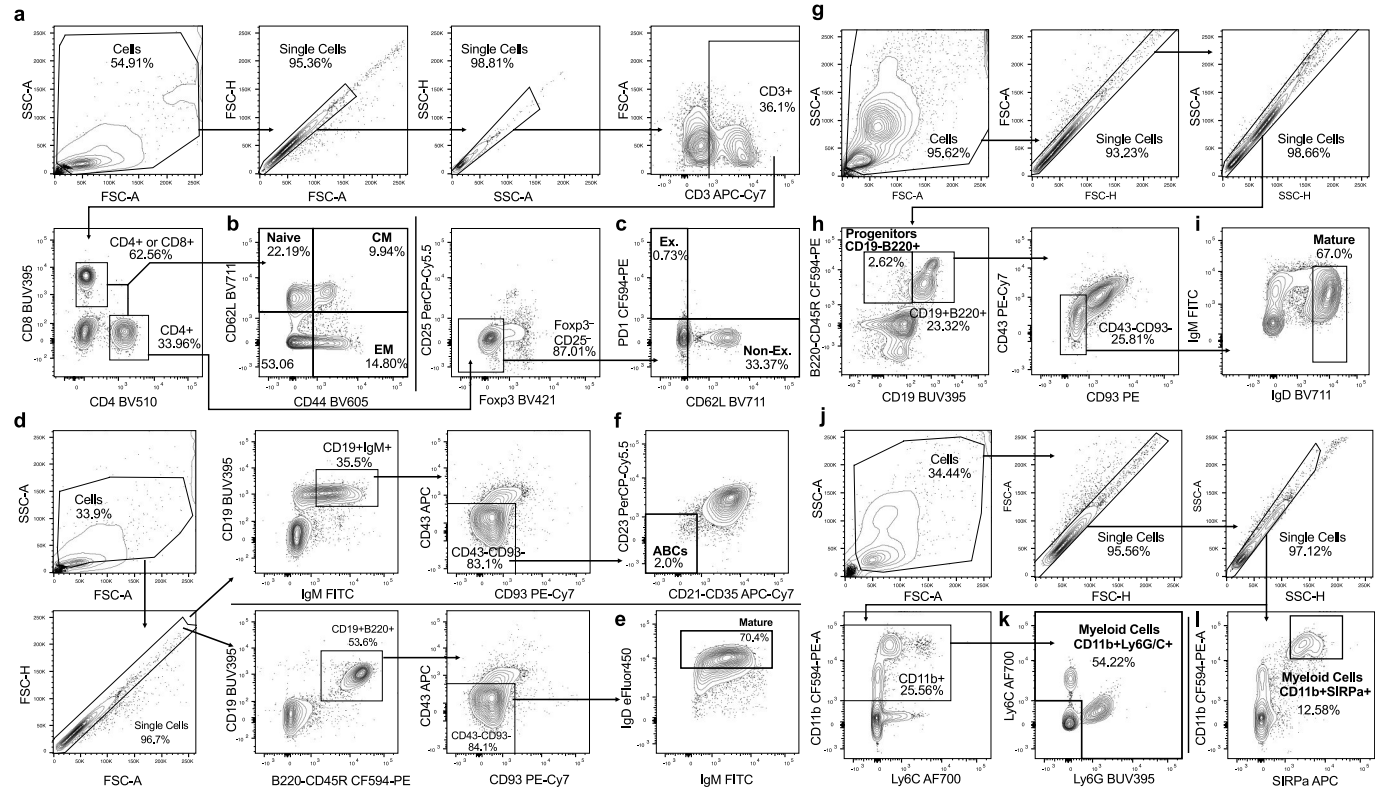
**Extended Data Fig. 6 | My-HSC depletion restores features of a youthful immune system.** **a**, Ratio of frequency of my-HSCs to bal-HSCs (% live) in aged (A), or aged+conditioning mice (A + C) after 8-weeks;  $n = 4$  (A),  $n = 9$  (A + C);  $P = 0.0346$ . **b-d**, Statistical significance (y-axis, -log10p) vs. fold-change (x-axis, log2-FC) of plasma protein levels at week 8 for (A)/(Y) (**b**), (A)/(A + C) (**c**), or (A)/(Y & A + C) (**d**) comparisons. Grey bar ( $y = 1-1.3$ ): values above grey bar  $p < 0.05$ ;  $n = 6$  (Y, A),  $n = 5$  (A + C). **e**, Overlap of top 17% of plasma proteins, ranked by statistical significance, increased in (A)/(Y) and decreased in (A + C)/(A). **f**, Estimated plasma concentration of CXCL5<sup>116</sup> at week 8;  $n = 6$  (Y, A),  $n = 5$  (A + C). **g**, Relative plasma abundance of inflammatory proteins at week 8;  $n = 6$  (Y, A),  $n = 5$  (A + C). Values relative to the mean for (Y) and log2-transformed. **h-i**, Frequency of CD11b<sup>+</sup>Ly6G/C<sup>+</sup> (**h**) and CD11b<sup>+</sup>SIRPa<sup>+</sup> (**i**) mature myeloid cells in the blood approximately 1-week after antibody-conditioning;  $n = 3$  (A),  $n = 4$  (A, A + C). **j-k**, Frequency of mature B cells (B220<sup>+</sup>CD19<sup>+</sup>CD43<sup>+</sup>CD93<sup>+</sup>IgM<sup>+</sup>IgD<sup>+</sup>) (**j**), and progenitor B cells (B220<sup>+</sup>CD19<sup>-</sup>B cells) (**k**), in the BM approximately 1-week after antibody-conditioning;  $n = 5$  (A),  $n = 6$  (A, A + C). Thymus weight (**l**) and frequency of thymic subsets 1–8 as defined by Akashi & Weissman<sup>117</sup>, as % of total CD45<sup>+</sup> cells in the thymus (**n**), 8-weeks after antibody-conditioning; representative FACS (**m**);  $n = 3$  (Y, A),  $n = 9$  (A + C). Populations enriched for transitional intermediate cells (areas 3&4)<sup>117</sup> highlighted in box (**n**). Mouse ages: Y (3–6 months); A & A + C (18–24 months). For (**a**), BM was cKIT-enriched prior to analysis.  $p$ -values obtained by unpaired parametric one-tailed t-test (**a**), ordinary one-way ANOVA followed by one-tailed Dunnett's multiple comparisons test using Aged as control (**f**), one-way ANOVA followed by Holm multiple comparisons test (**b-d**, **g**), ordinary one-way ANOVA followed by two-tailed Dunnett's multiple comparisons test using Aged as control (**h-i**, **l**, **n**), or Brown-Forsythe and Welch ANOVA tests followed by Dunnett's T3 multiple comparisons test using Aged as control (**j-k**). Bars indicate mean  $\pm$  s.e.m.  $n$  represents independent mice; \* $P < 0.05$ , \*\* $P < 0.005$ , \*\*\* $P < 0.0005$ ; Exact  $P$ -values provided as source data.

1-week after antibody-conditioning;  $n = 5$  (A),  $n = 6$  (A, A + C). Thymus weight (**l**) and frequency of thymic subsets 1–8 as defined by Akashi & Weissman<sup>117</sup>, as % of total CD45<sup>+</sup> cells in the thymus (**n**), 8-weeks after antibody-conditioning; representative FACS (**m**);  $n = 3$  (Y, A),  $n = 9$  (A + C). Populations enriched for transitional intermediate cells (areas 3&4)<sup>117</sup> highlighted in box (**n**). Mouse ages: Y (3–6 months); A & A + C (18–24 months). For (**a**), BM was cKIT-enriched prior to analysis.  $p$ -values obtained by unpaired parametric one-tailed t-test (**a**), ordinary one-way ANOVA followed by one-tailed Dunnett's multiple comparisons test using Aged as control (**f**), one-way ANOVA followed by Holm multiple comparisons test (**b-d**, **g**), ordinary one-way ANOVA followed by two-tailed Dunnett's multiple comparisons test using Aged as control (**h-i**, **l**, **n**), or Brown-Forsythe and Welch ANOVA tests followed by Dunnett's T3 multiple comparisons test using Aged as control (**j-k**). Bars indicate mean  $\pm$  s.e.m.  $n$  represents independent mice; \* $P < 0.05$ , \*\* $P < 0.005$ , \*\*\* $P < 0.0005$ ; Exact  $P$ -values provided as source data.



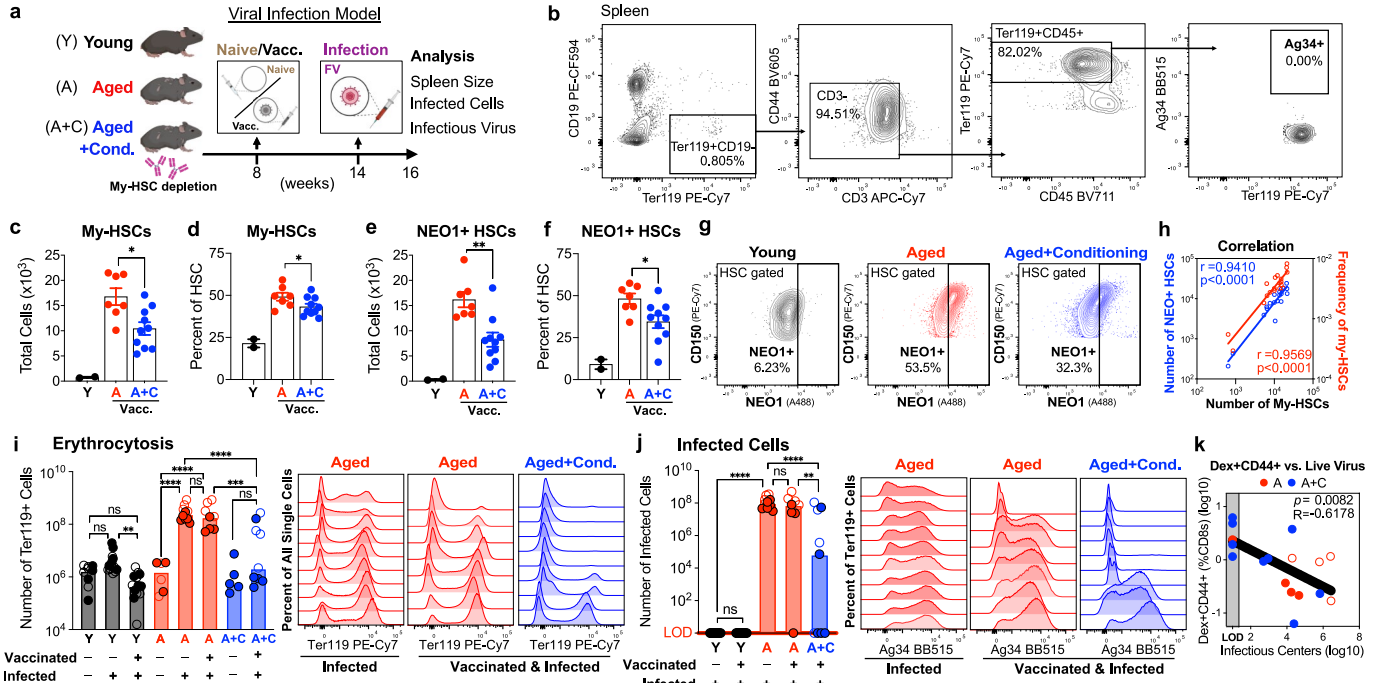
**Extended Data Fig. 7 | My-HSC depletion increases naïve T cells and B cells in aged mice.** **a–c**, Absolute numbers of (**a**) naïve (CD44<sup>+</sup>CD62L<sup>+</sup>); \*P = 0.0430, (**b**) central memory (CM: CD44<sup>+</sup>CD62L<sup>+</sup>); \*P = 0.0177, or (**c**) effector memory (EM: CD44<sup>+</sup>CD62L<sup>+</sup>); P = 0.576, T cells (CD4 & CD8), per mL of blood, approximately 8-weeks post-treatment. Values log<sub>2</sub>-transformed; n = 9 (A), n = 14 (A + C), mice pooled from 2 independent experiments. **d**, Absolute numbers of mature B cells (IgM<sup>+</sup>IgD<sup>+</sup>) per mL of blood, approximately 8-weeks post-treatment; \*P = 0.0498. Values log<sub>2</sub>-transformed; n = 6 (A), n = 5 (A + C). **e**, Absolute numbers of CD45+ cells per mL of blood, approximately 8-weeks post-treatment. Values log<sub>2</sub>-transformed; n = 3 (A), n = 9 (A + C); P = 0.069. **f–g**, Percentage of CM (**f**) and EM (**g**) subsets per total T cells (CD4 & CD8), 8-weeks post-treatment; n = 6 (Y, A),

n = 5 (A + C). **h–j**, Frequency relative to Aged mice of T cell (CD4 & CD8) subsets 8-weeks after antibody treatment (**h**). Naive, CM, and EM subsets were defined by 12-marker cluster-based analysis (**i–j**); n = 6 (Y, A), n = 5 (A + C). Values relative to mean for Aged control mice and log<sub>2</sub>-transformed. Mouse ages: Y (3–6 months); A & A + C (18–24 months). P-values obtained by unpaired parametric one-tailed t-test (**a**, **d**), unpaired parametric two-tailed t-test (**b–c**, **e**), or ordinary one-way ANOVA followed by two-tailed (**f–g**) or one-tailed (**h**) Dunnett's multiple comparisons test using Aged as control. Bars indicate mean ± s.e.m. n represents independent mice; \*P < 0.05, \*\*P < 0.005, \*\*\*P < 0.0005; Exact P-values provided as source data.



**Extended Data Fig. 8 | Flow-cytometry gating strategy for T cells, B cells, and myeloid cells. a–c.** Gating strategy to identify: (b) naïve (CD44<sup>-</sup>CD62L<sup>+</sup>), central memory (CD44<sup>+</sup>CD62L<sup>+</sup>), and effector memory (CD44<sup>+</sup>CD62L<sup>-</sup>) T cells (combined CD4 & CD8), or (c) CD4 T cells that are PDI<sup>+</sup>CD62L<sup>-</sup> or PDI<sup>-</sup>CD62L<sup>+41</sup> in the blood, used for Fig. 3e,g, Extended Data Fig. 7a-c, Extended Data Fig. 7f-g.

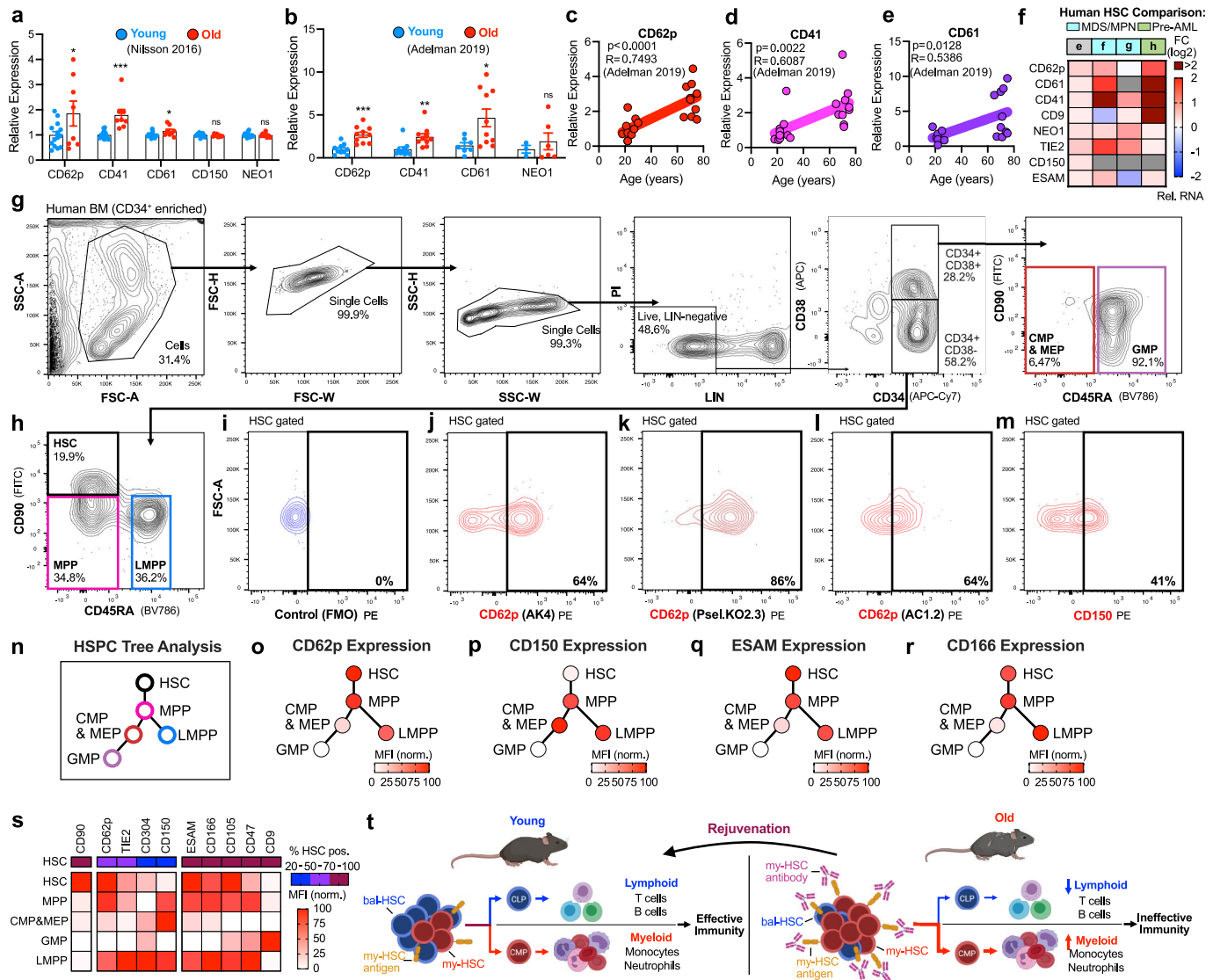
**d–f** Gating strategy to identify: (e) mature B cells (CD19<sup>+</sup>B220<sup>+</sup>IgM<sup>+</sup>IgD<sup>+</sup>)<sup>118</sup>, or (f) Aged B Cells ABCs<sup>119</sup> (CD19<sup>+</sup>IgM<sup>+</sup>CD93<sup>-</sup>CD43<sup>-</sup>CD21/CD35<sup>-</sup>CD23<sup>-</sup>)<sup>42</sup> in the blood, used for Fig. 3f,h, Extended Data Fig. 7d. **g–i.** Gating strategy to identify (h) progenitor B cells (B220<sup>+</sup>CD19<sup>-</sup>), or (i) mature B cells (B220<sup>+</sup>CD19<sup>+</sup>CD43<sup>-</sup>CD93<sup>-</sup>IgM<sup>+</sup>IgD<sup>+</sup>) in the bone-marrow, used for Extended Data Fig. 6j,k. **j–l.** Gating strategy to identify (k) CD11b<sup>+</sup>Ly6G/C<sup>+</sup> myeloid cells, or (l) CD11b<sup>+</sup>SIRPa<sup>+</sup> myeloid cells in the blood, used for Extended Data Fig. 6h,i.



**Extended Data Fig. 9 | Antibody-conditioning enhances functional immunity to infection.** **a**, Schematic of model to determine the impact of antibody-conditioning on functional immunity. The diagram was created using BioRender. **b**, Gating to identify Ter119<sup>+</sup> cells (Ter119<sup>+</sup>CD19<sup>-</sup>CD3<sup>-</sup>CD45<sup>+lo</sup>) and antigen-infected cells (Ag34<sup>+</sup>Ter119<sup>+</sup>) in mouse spleens, used for Extended Data Fig. 9i,j. **c–h**, My-HSC and NEO1<sup>+</sup> HSC absolute numbers in total BM (**c**,**e**), or as percentage of total HSCs (**d**,**f**), with correlations (**h**), 10-weeks after anti-NEO1<sup>v2</sup> conditioning. Representative FACS on total HSCs (**g**). A and A + C mice received vaccination at Week 8;  $n = 2$  (Y),  $n = 7$  (A),  $n = 10$  (A + C). **i**, Total number of Ter119<sup>+</sup> cells per mouse spleen in mice that were Naive, Infected, or Vaccinated & Infected with FV. Representative FACS histograms for Ter119 expression, gated on all single cells. Each row represents an independent mouse.  $n = 9$  (Y, naïve),  $n = 13$  (Y, FV infected),  $n = 13$  (Y, vaccinated & FV infected),  $n = 6$  (A, naïve),  $n = 10$  (A, FV infected),  $n = 8$  (A, vaccinated & FV infected),  $n = 5$  (A + C, naïve),  $n = 9$  (A + C, vaccinated & FV infected). Data log10-transformed. **j**, Total number of antigen-infected (Ag34<sup>+</sup>Ter119<sup>+</sup>) cells per spleen in mice that were: Infected, or Vaccinated & Infected with FV. Representative FACS histograms for Ag34 expression, gated on Ter119<sup>+</sup> cells. Each row represents an independent mouse;  $n = 13$  (Y, FV infected),  $n = 13$  (Y, vaccinated & FV infected),  $n = 10$  (A, FV infected),

$n = 8$  (A, vaccinated & FV infected),  $n = 9$  (A + C, vaccinated & FV infected). Data  $\log_{10}(x+1)$ -transformed. **k**, Correlation of Infectious virus levels (Infectious Centres; x-axis) vs. Dextramer<sup>+</sup>CD44<sup>+</sup> cells (Percent of splenic CD8<sup>+</sup>T cells; y-axis) in Vaccinated & FV-infected mice;  $n = 8$  (A, vaccinated & FV-infected),  $n = 9$  (A + C, vaccinated & FV-infected). Data  $\log_{10}$ -transformed. For **i–k**, data from experiments using the anti-NEO1<sup>v1</sup> protocol (open circles) or the anti-NEO1<sup>v2</sup> protocol (closed circles) were combined. Mouse ages: Y (3–6 months); A & A + C (21–22 months). For (**c–f**), BM was cKIT-enriched prior to analysis. For (**c**,**e**,**h**), total BM (non-cKIT-enriched) was also analysed to calculate total numbers of cells.  $p$ -values obtained by one-tailed unpaired parametric t-test (**c–f**), two-tailed Pearson correlation coefficient (**h**,**k**), or ordinary one-way ANOVA followed by Tukey's multiple comparisons test (**i–j**). NEO1<sup>v2</sup> protocol is NEO1<sup>v1</sup> protocol (anti-NEO1+ anti-CD47+anti-cKIT)+mouse (IgG2a) anti-goat. Inf., FV infected without vaccination; Vacc. & Inf., FV infected with vaccination; Vacc. & Inf., FV infected with vaccination; LOD, limit of detection; n.s., not significant.  $n$  represents independent mice. Bars indicate mean  $\pm$  s.e.m. (**c–f**) or bars depict median (**i–j**). \* $P < 0.05$ , \*\* $P < 0.005$ , \*\*\* $P < 0.0005$ ; Exact  $P$ -values provided as source data.

# Article



**Extended Data Fig. 10 | Mouse my-HSC markers are enriched in aged human HSCs.** **a**, Relative mRNA expression of CD62p (*Selp*,  $P = 0.0243$ ), CD41 (*Itga2b*,  $P = 0.0001$ ), CD61 (*Itgb3*,  $P = 0.0135$ ), CD150 (*Slamf1*,  $P = 0.179$ ), and NEO1 (*Neol*,  $P = 0.433$ ) in human HSCs isolated from young (age 20–26) and old (age >70) donors; data obtained from Nilsson<sup>54</sup>, GSE69408. **b**, Relative mRNA expression of CD62p (*Selp*,  $P = 0.0001$ ), CD41 (*Itga2b*,  $P = 0.0027$ ), CD61 (*Itgb3*,  $P = 0.0116$ ), and NEO1 (*Neol*,  $P = 0.274$ ) in human HSCs isolated from young (age 18–30) or old (age 65–75) donors; data obtained from Adelman<sup>53</sup> (GSE104406). **c–e**, Correlation of relative mRNA expression of CD62p (**c**), CD41 (**d**), and CD61 (**e**) in human HSCs as compared to donor age; data obtained from Adelman<sup>53</sup> (GSE104406). For **a–e**, values relative to mean of young samples. **f**, Heatmap depicting expression of candidate markers in independent datasets of human: HMGA2<sup>+</sup> vs. HMGA2<sup>-</sup> CD34<sup>+</sup> cells ( $e^{104}$ ), MPN ( $f^{56}$ ) or MDS ( $g^{57}$ ) vs. normal HSCs, and Pre-AML vs. normal HSCs ( $h^{58}$ ). **g–h**, Representative FACS to identify human HSCs (Lin<sup>-</sup>CD34<sup>+</sup>CD38<sup>-</sup>CD45RA<sup>-</sup>CD90<sup>+</sup>)<sup>59</sup>, MPPs (Lin<sup>-</sup>CD34<sup>+</sup>CD38<sup>-</sup>CD45RA<sup>-</sup>CD90<sup>-</sup>)<sup>59</sup>, LMPPs (Lin<sup>-</sup>CD34<sup>+</sup>CD38<sup>-</sup>CD45RA<sup>-</sup>)<sup>120</sup>, CMPs & MEPs (Lin<sup>-</sup>CD34<sup>+</sup>CD38<sup>-</sup>CD45RA<sup>-</sup>)<sup>121</sup>, and GMPs (Lin<sup>-</sup>CD34<sup>+</sup>CD38<sup>-</sup>CD45RA<sup>-</sup>)<sup>121</sup> in normal human BM<sup>59</sup>, used for Fig. 5f–i, Extended Data Fig. 10i–s. Samples are post CD34<sup>+</sup>-enrichment.

**i–m**, FACS of human HSCs depicting fluorescence-minus-one (FMO) control (**i**), anti-CD62p clone AK4 (**j**), anti-CD62p clone Psel.KO2.3 (**k**), anti-CD62p clone AC1.2 (**l**), and anti-CD150 (**m**); representative for  $n = 3$  donors (**j**);  $n = 2$  donors (**k–m**). **n**, Illustration of human Hematopoietic Stem and Progenitor Cell (HSPC) Tree Analysis (**n**). **o–s**, Relative expression of CD62p (**o**), CD150 (**p**), ESAM (**q**), and CD166 (**r**), on human HSPCs, with summary (**s**), showing percent positive HSCs, and normalized MFI for each marker on HSPCs. For **o–s**, FACS median fluorescent intensity (MFI) values for each marker were obtained for each population, divided by the MFI for the FMO control, and then normalized from 0–100 based on the lowest to highest expression. Red colour scale corresponds to normalized MFI values. Blue, purple, maroon scale corresponds to bins for HSC positivity (20–50%, 51–70%, and 71–100%). **t**, Model to rejuvenate aged immune systems by depleting myeloid-biased hematopoietic stem cells. The diagram was created using BioRender.  $p$ -values obtained by unpaired parametric one-tailed t-test (**a–b**), or  $p$ -values and R values calculated with one-tailed Pearson correlation coefficient (**c–e**). MDS, myelodysplastic syndrome; MPN, myeloproliferative neoplasms. Bars indicate mean  $\pm$  s.e.m. \* $P < 0.05$ , \*\* $P < 0.005$ , \*\*\* $P < 0.0005$ ; Exact  $P$ -values provided as source data.

## Reporting Summary

Nature Portfolio wishes to improve the reproducibility of the work that we publish. This form provides structure for consistency and transparency in reporting. For further information on Nature Portfolio policies, see our [Editorial Policies](#) and the [Editorial Policy Checklist](#).

### Statistics

For all statistical analyses, confirm that the following items are present in the figure legend, table legend, main text, or Methods section.

n/a Confirmed

- The exact sample size ( $n$ ) for each experimental group/condition, given as a discrete number and unit of measurement
- A statement on whether measurements were taken from distinct samples or whether the same sample was measured repeatedly
- The statistical test(s) used AND whether they are one- or two-sided  
*Only common tests should be described solely by name; describe more complex techniques in the Methods section.*
- A description of all covariates tested
- A description of any assumptions or corrections, such as tests of normality and adjustment for multiple comparisons
- A full description of the statistical parameters including central tendency (e.g. means) or other basic estimates (e.g. regression coefficient) AND variation (e.g. standard deviation) or associated estimates of uncertainty (e.g. confidence intervals)
- For null hypothesis testing, the test statistic (e.g.  $F$ ,  $t$ ,  $r$ ) with confidence intervals, effect sizes, degrees of freedom and  $P$  value noted  
*Give P values as exact values whenever suitable.*
- For Bayesian analysis, information on the choice of priors and Markov chain Monte Carlo settings
- For hierarchical and complex designs, identification of the appropriate level for tests and full reporting of outcomes
- Estimates of effect sizes (e.g. Cohen's  $d$ , Pearson's  $r$ ), indicating how they were calculated

*Our web collection on [statistics for biologists](#) contains articles on many of the points above.*

### Software and code

Policy information about [availability of computer code](#)

Data collection	Flow cytometry data was collected using FACSDiva Software (BD) and using FACS Aria II (BD Biosciences) or FACS Symphony (BD Biosciences) instruments. Plasma immunoassay data was collected by instruments at the Stanford Human Immune Monitoring Center (HIMC).
Data analysis	All graphs were generated and analyzed statistically with GraphPad Prism version 9.4.1 for macOS (GraphPad Software) or with SPSS Statistics version 28.0.0.1 (IBM). The flow cytometry results were analyzed using FlowJo v10.8 Software (BD Life Sciences). Flow-cytometry computational analysis was conducted with the Spectre package (PMID: 33840138) using R version 4.2.2. Publicly available gene-expression data was analyzed using Microsoft Excel applied to pre-processed data or data processed by GREIN (PMID: 31110304), GEO2R (PMID: 11752295), or Phantasmus (doi: 10.18129/B9.bioc.phantasmus). For RNA-sequencing of purified mouse HSCs, libraries were prepared using Takara SMART-Seq v4 Ultra low Input RNA kit and sequencing was performed with NovaSeq with approximately 20 million paired reads per sample by MedGenome Inc. Differential gene expression was performed using DESeq2 (PMID: 25516281) with fold change shrinkage. Heatmaps were generated using Phantasmus v1.21.5 (doi:10.1101/2022.12.10.519861) with FPKM values as input and Limma (PMID: 25605792) to define differentially expressed genes. GSEA was conducted on genes ranked by DESeq2 test statistic using WEB-based GEne SeT Analysis Toolkit (WebGestalt 2019, PMID: 31114916) with default parameters using a custom list of curated gene-signatures.

For manuscripts utilizing custom algorithms or software that are central to the research but not yet described in published literature, software must be made available to editors and reviewers. We strongly encourage code deposition in a community repository (e.g. GitHub). See the Nature Portfolio [guidelines for submitting code & software](#) for further information.

## Data

Policy information about [availability of data](#)

All manuscripts must include a [data availability statement](#). This statement should provide the following information, where applicable:

- Accession codes, unique identifiers, or web links for publicly available datasets
- A description of any restrictions on data availability
- For clinical datasets or third party data, please ensure that the statement adheres to our [policy](#)

Data for all graphical representations in figures is provided in Source Data files. HSC RNA-seq data has been deposited at the Gene Expression Omnibus at GSE252062 and at the Sequence Read Archive (SRA) with BioProject ID: PRJNA1054066. The following publicly available datasets were used, with web links provided in the manuscript: GSE4372924, GSE3955334, GSE4889335, GSE10954636, GSE2768637, GSE4492338, GSE12805039, GSE4781940, GSE13050427, GSE11276932, E-MEXP-393531, GSE327192, GSE104406108, GSE69408150, GSE115348151, GSE107594152, GSE11141093, GSE5568994, GSE7424695, GSE132040156, GSE87633157, GSE10042826.

## Research involving human participants, their data, or biological material

Policy information about studies with [human participants or human data](#). See also policy information about [sex, gender \(identity/presentation\), and sexual orientation](#) and [race, ethnicity and racism](#).

### Reporting on sex and gender

**Sex or gender was not considered in study design.** Bone marrow mononuclear cells were from young-adult male donors that were commercially obtained from AllCells, Inc. All donors were male, but this was determined by sample availability and not predetermined.

### Reporting on race, ethnicity, or other socially relevant groupings

**Race, ethnicity, or other socially relevant groupings was not considered in study design.** Bone marrow mononuclear cells were from young-adult male donors that were commercially obtained from AllCells, Inc.

### Population characteristics

Bone marrow mononuclear cells were from male young-adult donors. All donors were male, but this was determined by sample availability and not predetermined.

### Recruitment

Participants were not recruited for this study. Bone marrow mononuclear cells from young-adult donors (ages 26-33) were commercially obtained from AllCells, Inc. All donors were male, but this was determined by sample availability and not predetermined.

### Ethics oversight

All human samples were commercially obtained from AllCells, Inc.

Note that full information on the approval of the study protocol must also be provided in the manuscript.

## Field-specific reporting

Please select the one below that is the best fit for your research. If you are not sure, read the appropriate sections before making your selection.

Life sciences

Behavioural & social sciences

Ecological, evolutionary & environmental sciences

For a reference copy of the document with all sections, see [nature.com/documents/nr-reporting-summary-flat.pdf](https://nature.com/documents/nr-reporting-summary-flat.pdf)

## Life sciences study design

All studies must disclose on these points even when the disclosure is negative.

### Sample size

The sample size for in vivo experiments, including antibody-depletion, viral infection, and transplantation was decided based on prior publications with similar experiments by our laboratories or others, including PMID: 27510901; PMID: 31204177; PMID: 18033883; PMID: 31754028; PMID: 20304793; PMID: 9930867; PMID: 9658099; PMID: 10873767.

### Data exclusions

For plasma immunoassay analysis, MFI average values were compared after removal of statistical outliers using the extreme studentized deviate (ESD) Grubbs statistical test ( $\alpha=0.0001$ ). For animal experiments, sick or diseased mice were excluded from the analysis.

### Replication

All attempts at replication were successful. Replicated experiments were identically or similarly designed. Some experiments were replicated at independent institutions (Stanford or Rocky Mountain Labs) with independent mouse strains. Data depicts combined results of at least 2 independent experiments (Fig. 1b–c, Fig. 1i–k, Fig. 3b, Fig. 4b–e, Fig. 5h–5i, Ex. Fig. 2g–j, Ex. Fig. 4j–q, Ex. Fig. 7a–c, Ex. Fig. 9b, Ex. Fig. 9i–k, Ex. Fig. 10s), or is representative of four or more experiments (Fig. 1d–h, Ex. Fig. 2b–c), three experiments (Fig. 2c, Fig. 2f, Fig. 5f–g, Ex. Fig. 10g–j, Ex. Fig. 10o), two experiments (Fig. 3c–e, Fig. 3g, Ex. Fig. 7f–j, Ex. Fig. 8a–c, Ex. Fig. 10k–m, Ex. Fig. 10p), or one experiment (2a–b, Fig. 2d–e, Fig. 2g–k, 3f, 3h–j, 4a, Ex. Fig. 2d–f, Ex. Fig. 2k, Ex. Fig. 3a–n, Ex. Fig. 4a–i, Ex. Fig. 4r–x, Ex. Fig. 5c–s, Ex. Fig. 6a–n, Ex. Fig. 7d–e, Ex. Fig. 8d–l, Ex. Fig. 9c–h, Ex. Fig. 10q–r). Biological replicates (n = individual mice) are reported in the figure legends.

### Randomization

For all experiments, allocation of mice into experimental groups was randomized after matching for age and sex.

Investigators were not blinded during data collection or analysis as all experiments involved internal control groups. Experimental and control animals were treated equally.

# Reporting for specific materials, systems and methods

We require information from authors about some types of materials, experimental systems and methods used in many studies. Here, indicate whether each material, system or method listed is relevant to your study. If you are not sure if a list item applies to your research, read the appropriate section before selecting a response.

## Materials & experimental systems

n/a	Involved in the study
<input type="checkbox"/>	<input checked="" type="checkbox"/> Antibodies
<input type="checkbox"/>	<input checked="" type="checkbox"/> Eukaryotic cell lines
<input checked="" type="checkbox"/>	<input type="checkbox"/> Palaeontology and archaeology
<input type="checkbox"/>	<input checked="" type="checkbox"/> Animals and other organisms
<input checked="" type="checkbox"/>	<input type="checkbox"/> Clinical data
<input checked="" type="checkbox"/>	<input type="checkbox"/> Dual use research of concern
<input checked="" type="checkbox"/>	<input type="checkbox"/> Plants

## Methods

n/a	Involved in the study
<input checked="" type="checkbox"/>	<input type="checkbox"/> ChIP-seq
<input type="checkbox"/>	<input checked="" type="checkbox"/> Flow cytometry
<input checked="" type="checkbox"/>	<input type="checkbox"/> MRI-based neuroimaging

## Antibodies

### Antibodies used

HSPC FACS analysis: anti-FLT3 APC 1:50 (ThermoFisher; 17-1351-82) or anti-FLT3 PerCP-eFluor710 1:50 (eBioscience; 46-1351-82), goat anti-mouse NEO1 15ug/mL (R&D; AF1079), anti-CD150 PE-Cy7 1:50 (BioLegend; 115914; clone TC15-12F12.2), anti-IL7Ra PE-Cy5 1:25 (ThermoFisher; 15-1271-82 or BioLegend; 135016) or anti-IL7Ra APC 1:25 (BioLegend; 135012), anti-CD16/32 BV510 1:50 (BioLegend; 101308), anti-cKit APC-eFluor780 1:50 (ThermoFisher; 47-1171-82), anti-mouse Lineage Cocktail (includes anti-CD3, anti-Ly-6G/C, anti-CD11b, anti-CD45R, anti-Ter-119) AF700 1:10 (BioLegend; 133313), anti-CD48 BV711 1:50 (BD; 740687), anti-CD41 BV650 1:50 (BD; 740504), anti-CD34 biotin 1:50 (ThermoFisher; 13-0341-85), anti-SCA1 BUV395 1:50 (BD; 744328), followed by Streptavidin BUV737 1:50 (BD; 612775) and donkey anti-goat IgG H&L AF488 1:100 (abcam; ab150129). In some instances, anti-CD150 clone mShad150 PE 1:50 (eBioscience; 12-1502-80) or PE-Cy7 (eBioscience; 25-1502-82), anti-CD150 clone 9D1 PE 1:50 (eBioscience; 12-1501-80), anti-CD150 clone Q38-480 PE 1:50 (BD; 562651), anti-CD62p PE 1:50 (BioLegend; 148308), or anti-Ly6D PE 1:50 (eBioscience; 12-5974-80), were included. For testing of candidate my-HSC markers, the following antibodies were used: anti-CD51 PE 1:50 (12-0512-81; ThermoFisher), anti-CD61 PE 1:50 (561910; BD), anti-CD31 PE 1:50 (561073; BD), anti-CD38 PE 1:50 (12-0381-81; ThermoFisher), anti-CD47 clone MIAP301 PE 1:50 (127507; BioLegend), anti-CD47 clone MIAP410 PE 1:50 (LS-C810701-25; LSBio), anti-CD62p PE 1:50 (148305; BioLegend), anti-ALCAM PE 1:50 (12-1661-82; ThermoFisher), anti-CD9 PE 1:50 (124805; BioLegend), anti-ESAM PE 1:50 (136203; BioLegend), anti-TIE2 PE 1:50 (124007; BioLegend), anti-CD201 PE 1:50 (141503; BioLegend), or anti-cKIT clone ACK2 PE 1:50 (135105; BioLegend). Isotype control rat IgG 1mg/mL (ab37361; abcam) was used as a blocking antibody control.

T cell analysis: anti-Helios AF647 1:200 (BD; 563951), anti-CD3 APC-Cy7 1:200 (BioLegend; 100222), anti-Ki67 R718 1:150 (BD; 566963), anti-CD43 AF488 1:400 (BioLegend; 121210), anti-CD8 BUV395 1:400 (BD; 563786), anti-Foxp3 eFl450 1:150 (Invitrogen; 48-5773-82), anti-CD4 BV510 1:400 (BioLegend; 100559), anti-CD44 BV605 1:400 (BD; 563058), anti-CD62L BV711 1:1,000 (BioLegend; 104445), anti-EOMES PE 1:200 (Invitrogen; 12-4875-82), anti-PD1 PE-CF594 1:200 (BD; 562523), anti-Tbet PE-Cy7 1:200 (Invitrogen; 25-5825-82), anti-CD25 PerCP-Cy5.5 1:200 (BioLegend; 102030). FV-specific CD8+ T cells were identified using H-2Db/Abu-Abu-L-Abu-LTVFL APC- or PE-DbgagL-MHC Dextramer (Immudex, Copenhagen, Denmark) at 1:25 during surface staining. B cell analysis: anti-CD43 APC 1:400 (BioLegend; 121214), anti-CD21/CD35 APC-Cy7 1:400 (BioLegend; 123418), anti-CD5 AF700 1:200 (BioLegend; 100636), anti-IgM FITC 1:400 (Invitrogen; 11-5790-81), anti-CD19 BUV395 1:400 (BD; 563557), anti-IgD eFluor450 1:400 (eBioscience; 48-5993-82), anti-CD11b BV510 1:400 (BioLegend; 101245), anti-MHCII BV605 1:400 (BD; 563413), anti-CD40 BV711 1:400 (BD; 740700), anti-PDL1 PE 1:200 (Invitrogen; 12-5982-82), anti-CD93 PE-Cy7 1:400 (BioLegend; 136506), anti-CD23 PerCP-Cy5.5 1:200 (BioLegend; 101618), and anti-CD45R/B220 PE-CF594 1:800 (BD; 562290).

Peripheral blood chimerism analysis: anti-CD8a Spark UV387 1:50 (BioLegend; 100797), anti-CD4 BUV737 1:200 (BD, 612843), anti-Gr1 Pacific Blue 1:100 (BioLegend, 108429), anti-CD3 BV711 1:100 (BioLegend, 100241), anti-CD44 BV785 1:300 (BioLegend, 103059), anti-CD45.2 AF488 1:100 (BioLegend, 109815), anti-Foxp3 PE 1:100 (eBioscience, 12-5773-82), anti-CD62L PE/Dazzle™ 594 1:200 (BioLegend, 104447), anti-CD19 PE-Cy7 1:100 (BioLegend, 115519), anti-CD45.1 APC 1:50 (BioLegend 110713), anti-CD11b APC-Cy7 1:100 (BioLegend, 101225). Intracellular staining was performed with Foxp3 Transcription Factor Staining Buffer Set (eBioscience, 00-5523-00) per manufacturer's protocol. Red blood cells were removed with ACK lysis buffer (Gibco, a1049201). Non-specific binding was prevented with TruStain FcX PLUS (BioLegend cat# 156604). To determine viability of fixed cells, cells were incubated in buffer containing LIVE/DEAD™ Fixable Aqua Dead Cell (ThermoFisher; L34957).

For erythroid cell analysis, spleen cells were first incubated for 30 min with mAb 34, a mouse IgG2b specific for the FV glycoGag protein expressed on infected cells (PMID: 6787798), then stained with anti-mouse IgG2b FITC (BD; 553395) and anti-Ter119 PE-Cy7 (Invitrogen; 25-5921-82).

Human HSC analysis: anti-lineage panel PE-Cy5: [anti-CD3 1:200 (BD; 555341), anti-CD4 1:200 (BD; 555348), anti-CD8 1:200 (BD; 555368), anti-CD11b 1:200 (BD; 555389), anti-CD14 1:200 (ThermoFisher; MHCD1406), anti-CD19 1:200 (BD; 555414), anti-CD20 1:200 (BD; 555624), anti-CD56 1:200 (BD; 555517), anti-CD235a 1:200 (BD; 559944)], anti-CD34 APC-Cy7 1:25 (343514; Biolegend), anti-CD45RA BV-785 1:25 (304139; Biolegend), anti-CD38 APC 1:10 (555462; BD), anti-CD90 FITC 1:50 (328107; Biolegend), and one of anti-human PE: anti-CD62P clone AK4 1:20 (304905; Biolegend), anti-CD62P clone Psel.KO2.3 1:20 (12-0626-82; eBioscience), anti-

CD62P clone AC1.2 1:5 (550561; BD), anti-CD150 1:20 (306307; Biolegend), anti-TIE2 1:20 (CD202b, 334205; Biolegend), anti-ESAM 1:10 (408519; Novus), anti-CD166 1:20 (ALCAM, 343903; Biolegend), anti-CD9 1:20 (312105; Biolegend), anti-CD105 1:20 (Endoglin, 800503; Biolegend), or anti-CD304 1:20 (Neuropilin-1, 354503; Biolegend).

**In vivo experiments:** Isotype control antibodies: mouse IgG1 (clone MOPC-21, Bio X Cell), rat IgG2b (clone LTF-2, Bio X Cell), or rat IgG2a (clone RTK2758, BioLegend). Experimental antibodies: rat IgG2a anti-CD150 (clone TC15-12F12.2, BioLegend), rat IgG2b anti-CD150 (clone mShad150, eBioscience), anti-CD62p (clone RMP-1, BioLegend), goat anti-NEO1 (polyclonal cat# AF1079, R&D), mouse IgG2a anti-goat (SB115d; SouthernBiotech), mouse IgG2b anti-goat (SB115h; SouthernBiotech), mouse IgG1 anti-CD47 (clone MIAP410, Bio X Cell), rat anti-cKIT (clone ACK2, Bio X Cell).

## Validation

All antibodies used in this study have been previously validated by commercial manufactures, previous publications, and/or this study.

All antibodies used for mouse HSC, HSPC, T & B cells analysis were validated by commercial manufacturer or have been cited in the literature:

anti-FLT3 APC (ThermoFisher; 17-1351-82), reported to recognize mouse FLT3 (manufacturer's website)  
 anti-FLT3 PerCP-eFluor710 (eBioscience; 46-1351-82), reported to recognize mouse FLT3 (manufacturer's website)  
 goat anti-mouse NEO1 (R&D;AF1079), reported to recognize mouse Neogenin (manufacturer's website). See additional validation details below.  
 anti-CD150 PE-Cy7 (BioLegend; 115914; clone TC15-12F12.2), reported to recognize mouse CD150 (manufacturer's website)  
 anti-IL7Ra PE-Cy5 (ThermoFisher; 15-1271-82), reported to recognize mouse IL-7 receptor (manufacturer's website)  
 anti-IL7Ra PE-Cy5 (BioLegend; 135016), reported to recognize mouse IL-7Ra (manufacturer's website)  
 anti-IL7Ra APC (BioLegend; 135012), reported to recognize mouse IL-7Ra (manufacturer's website)  
 anti-CD16/32 BV510 (BioLegend; 101308), reported to recognize mouse CD16/32 (manufacturer's website)  
 anti-cKit APC-eFluor780 (ThermoFisher; 47-1171-82), reported to recognize mouse c-Kit (manufacturer's website)  
 anti-mouse Lineage Cocktail (includes anti-CD3, anti-Ly-6G/C, anti-CD11b, anti-CD45R, anti-Ter-119) AF700 (BioLegend; 133313), reported to recognize mouse CD3, mouse Ly-6G/Ly-6C, mouse CD11b, mouse CD45R/B220, mouse TER-119 (manufacturer's website)  
 anti-CD48 BV711 (BD; 740687), reported to recognize mouse CD48 (manufacturer's website)  
 anti-CD41 BV650 (BD; 740504), reported to recognize mouse CD41 (manufacturer's website)  
 anti-CD34 biotin (ThermoFisher; 13-0341-85), reported to recognize mouse CD34 (manufacturer's website)  
 anti-SCA1 BUV395 (BD; 744328), reported to recognize mouse SCA1 (manufacturer's website)  
 Streptavidin BUV737 (BD; 612775)  
 donkey anti-Goat IgG H&L AF488 (abcam; ab150129), reported to recognize goat IgG (manufacturer's website)  
 anti-CD150 clone mShad150 PE (eBioscience; 12-1502-80), reported to recognize mouse CD150 (manufacturer's website)  
 anti-CD150 clone mShad150 PE-Cy7 (eBioscience; 25-1502-82), reported to recognize mouse CD150 (manufacturer's website)  
 anti-CD150 clone 9D1 PE (eBioscience; 12-1501-80), reported to recognize mouse CD150 (manufacturer's website)  
 anti-CD150 clone Q38-480 PE (BD; 562651), reported to recognize mouse CD150 (manufacturer's website)  
 anti-CD62p PE (BioLegend; 148308), reported to recognize mouse CD62p (manufacturer's website)  
 anti-Ly6D PE (eBioscience; 12-5974-80), reported to recognize mouse Ly-6D (manufacturer's website)  
 anti-CD51 PE (12-0512-81; ThermoFisher), reported to recognize mouse CD51 (manufacturer's website)  
 anti-CD61 PE (561910; BD), reported to recognize mouse CD61 (manufacturer's website)  
 anti-CD31 PE (561073; BD), reported to recognize mouse CD31 (manufacturer's website)  
 anti-CD38 (12-0381-81; ThermoFisher), reported to recognize mouse CD38 (manufacturer's website)  
 anti-CD47 clone MIAP301 PE (127507; BioLegend), reported to recognize mouse CD47 (manufacturer's website)  
 anti-CD47 clone MIAP410 PE (LS-C810701-25; LSBio), reported to recognize mouse CD47 (manufacturer's website)  
 anti-CD62p PE (148305; BioLegend), reported to recognize mouse CD62p (manufacturer's website)  
 anti-ALCAM PE (12-1661-82; ThermoFisher), reported to recognize mouse ALCAM (manufacturer's website)  
 anti-CD9 (124805; BioLegend), reported to recognize mouse CD9 (manufacturer's website)  
 anti-ESAM (136203; BioLegend), reported to recognize mouse ESAM (manufacturer's website)  
 anti-TIE2 (124007; BioLegend), reported to recognize mouse TIE-2 (manufacturer's website)  
 anti-CD201 (141503; BioLegend), reported to recognize mouse CD201 (manufacturer's website)  
 anti-cKIT clone ACK2 (135105; BioLegend), reported to recognize mouse c-KIT (manufacturer's website)  
 anti-Helios AF647 (BD; 563951), reported to recognize mouse Helios (manufacturer's website)  
 anti-CD3 APC-Cy7 (BioLegend; 100222), reported to recognize mouse CD3 (manufacturer's website)  
 anti-Ki67 R718 (BD; 566963), reported to recognize mouse Ki-67 (manufacturer's website)  
 anti-CD43 AF488 (BioLegend; 121210), reported to recognize mouse CD43 (manufacturer's website)  
 anti-CD8 BUV395 (BD; 563786), reported to recognize mouse CD8a (manufacturer's website)  
 anti-Foxp3 eFluor450 (Invitrogen; 48-5773-82), reported to recognize mouse FOXP3 (manufacturer's website)  
 anti-CD4 BV510 (BioLegend; 100559), reported to recognize mouse CD4 (manufacturer's website)  
 anti-CD44 BV605 (BD; 563058), reported to recognize mouse CD44 (manufacturer's website)  
 anti-CD62L BV711 (BioLegend; 104445), reported to recognize mouse CD62L (manufacturer's website)  
 anti-EOMES PE (Invitrogen; 12-4875-82), reported to recognize mouse EOMES (manufacturer's website)  
 anti-PD1 PE-CF594 (BD; 562523), reported to recognize mouse PD-1 (manufacturer's website)  
 anti-Tbet PE-Cy7 (Invitrogen; 25-5825-82), reported to recognize mouse T-bet (manufacturer's website)  
 anti-CD25 PerCP-Cy5.5 (BioLegend; 102030), reported to recognize mouse CD25 (manufacturer's website)  
 anti-CD43 APC (BioLegend; 121214), reported to recognize mouse CD43 (manufacturer's website)  
 anti-CD21/CD35 APC-Cy7 (BioLegend; 123418), reported to recognize mouse CD21/CD35 (manufacturer's website)  
 anti-CD5 AF700 (BioLegend; 100636), reported to recognize mouse CD5 (manufacturer's website)  
 anti-IgM FITC (Invitrogen; 11-5790-81), reported to recognize mouse IgM (manufacturer's website)  
 anti-CD19 BUV395 (BD; 563557), reported to recognize mouse CD19 (manufacturer's website)  
 anti-IgD eFluor450 (eBioscience; 48-5993-82), reported to recognize mouse IgD (manufacturer's website)  
 anti-CD11b BV510 (BioLegend; 101245), reported to recognize mouse CD11b (manufacturer's website)  
 anti-MHCII BV605 (BD; 563413), reported to recognize mouse MHC II (manufacturer's website)  
 anti-CD40 BV711 (BD; 740700), reported to recognize mouse CD40 (manufacturer's website)  
 anti-PDL1 PE (Invitrogen; 12-5982-82), reported to recognize mouse PD-L1 (manufacturer's website)  
 anti-CD93 PE-Cy7 (BioLegend; 136506), reported to recognize mouse CD93 (manufacturer's website)

anti-CD23 PerCP-Cy5.5(BioLegend; 101618), reported to recognize mouse CD23 (manufacturer's website)  
 anti-CD45R/B220 PE-CF594 (BD; 562290), reported to recognize mouse B220/CD45R (manufacturer's website)  
 anti-CD8a Spark UV 387 (BioLegend; 100797), reported to recognize mouse CD8a (manufacturer's website)  
 anti-CD4 BUV 737 (BD, 612843), reported to recognize mouse CD4 (manufacturer's website)  
 anti-Gr1 Pacific Blue (BioLegend, 108429), reported to recognize mouse Gr-1 (manufacturer's website)  
 anti-CD3 BV 711 (BioLegend, 100241), reported to recognize mouse CD3 (manufacturer's website)  
 anti-CD44 BV785 (BioLegend, 103059), reported to recognize mouse CD44 (manufacturer's website)  
 anti-CD45.2 AF488 (BioLegend, 109815), reported to recognize mouse CD45.2 (manufacturer's website)  
 anti-Foxp3 PE (eBioscience, 12-5773-82), reported to recognize mouse Foxp3 (manufacturer's website)  
 anti-CD62L PE/Dazzle™ 594 (BioLegend, 104447), reported to recognize mouse CD62L (manufacturer's website)  
 CD19 PE-Cy7 (BioLegend, 115519), reported to recognize mouse CD19 (manufacturer's website)  
 anti-CD45.1 APC (BioLegend 110713), reported to recognize mouse CD45.1 (manufacturer's website)  
 anti-CD11b APC-Cy7 (BioLegend, 101225), reported to recognize mouse CD11b (manufacturer's website)

All antibodies for erythroid cell analysis or infectious analysis were validated by commercial manufacturer or have been cited in the literature: mAb 34 (PMID: 6787798), F-MuLV envelope-specific Mab 72015 (PMID: 1744218).  
 goat anti-mouse (H+L) HRP (EMD Millipore; AP308P), reported to recognize mouse IgG (manufacturer's website)  
 anti-mouse IgG2b FITC (BD; 553395), reported to recognize mouse IgG2b (manufacturer's website)  
 anti-Ter119 PE-Cy7 (Invitrogen; 25-5921-82), reported to recognize mouse Ter119 (manufacturer's website)

All antibodies used for human HSC analysis were validated by commercial manufacturer or have been cited in the literature:  
 anti-lineage panel PE-Cy5:

anti-CD3 (BD; 555341), reported to recognize human CD3 (manufacturer's website)  
 anti-CD4 (BD; 555348), reported to recognize human CD4 (manufacturer's website)  
 anti-CD8 (BD; 555368), reported to recognize human CD8 (manufacturer's website)  
 anti-CD11b (BD; 555389), reported to recognize human CD11b (manufacturer's website)  
 anti-CD14 (ThermoFisher; MHCD1406), reported to recognize human CD14 (manufacturer's website)  
 anti-CD19 (BD; 555414), reported to recognize human CD19 (manufacturer's website)  
 anti-CD20 (BD; 555624), reported to recognize human CD20 (manufacturer's website)  
 anti-CD56 (BD; 555517), reported to recognize human CD56 (manufacturer's website)  
 anti-CD235a (BD; 559944), reported to recognize human CD235a (manufacturer's website)

anti-CD34 APC-Cy7 (343514; Biolegend), reported to recognize human CD34 (manufacturer's website)  
 anti-CD45RA BV-785 (304139; Biolegend), reported to recognize human CD45RA (manufacturer's website)  
 anti-CD38 APC (555462; BD), reported to recognize human CD38 (manufacturer's website)  
 anti-CD90 FITC (328107; Biolegend), reported to recognize human CD90 (manufacturer's website)  
 anti-CD62P PE clone AK4 (304905; Biolegend), reported to recognize human CD62p (manufacturer's website)  
 anti-CD62P PE clone Psel.KO2.3 (12-0626-82; eBioscience), reported to recognize human CD62p (manufacturer's website)  
 anti-CD62P PE clone AC1.2 (550561; BD), reported to recognize human CD62p (manufacturer's website)  
 anti-CD150 PE (306307; Biolegend), reported to recognize human CD150 (manufacturer's website)  
 anti-TIE2 PE (334205; Biolegend), reported to recognize human Tie2 (manufacturer's website)  
 anti-ESAM PE (408519; Novus), reported to recognize human ESAM (manufacturer's website)  
 anti-CD166 (ALCAM) PE, (343903; Biolegend), reported to recognize human CD166 (ALCAM) (manufacturer's website)  
 anti-CD9 PE (312105; Biolegend), reported to recognize human CD9 (manufacturer's website)  
 anti-CD105 Endoglin PE (800503; Biolegend), reported to recognize human CD105 (manufacturer's website)  
 anti-CD304 (Neuropilin-1) PE (354503; Biolegend), reported to recognize human CD304 (manufacturer's website)

All antibodies used for in vivo antibody conditioning experiments were validated by commercial manufacturer or have been cited in the literature:

#### Isotype control antibodies:

mouse IgG1 (clone MOPC-21, Bio X Cell), reported to be a non-reactive isotype-matched control for mouse IgG1 antibodies (manufacturer's website)  
 rat IgG2b (clone LTF-2, Bio X Cell), reported to recognize keyhole limpet hemocyanin, which is not expressed by mammals, so useful for isotype-matched control for rat IgG2b antibodies (manufacturer's website)  
 rat IgG2a (clone RTK2758, BioLegend), reported to recognize KLH and tested as chosen as an isotype control on resting, activated, live, and fixed mouse tissues (manufacturer's website)

#### Experimental antibodies:

rat IgG2a anti-CD150 (clone TC15-12F12.2, BioLegend), reported to recognize mouse CD150 (manufacturer's website)  
 rat IgG2b anti-CD150 (clone mShad150, eBioscience), reported to recognize mouse CD150 (manufacturer's website)  
 anti-CD62p (clone RMP-1, BioLegend), reported to recognize mouse CD62p (manufacturer's website)  
 mouse IgG2a anti-goat (SB115d; SouthernBiotech), reported to recognize goat IgG (manufacturer's website)  
 mouse IgG2b anti-goat (SB115h; SouthernBiotech), reported to recognize goat IgG (manufacturer's website)  
 mouse IgG1 anti-CD47 (clone MIAP410, BioX Cell), reported to recognize mouse CD47 (manufacturer's website)  
 rat anti-cKIT (clone ACK2, Bio X Cell), reported to recognize mouse c-KIT (manufacturer's website)

goat anti-NEO1 (polyclonal cat# AF1079, R&D): Reported to recognize mouse Neogenin (manufacturer's website). Specificity for mouse Neogenin validated by loss of staining in NEO1-KO mice, comparing Nestin-Cre:Neogenin-f/f mice to control mice (Neuron 2020. PMID: 32562661); validated by FACS by labeling mouse HSCs by flow-cytometry that express higher NEO1 mRNA compared to unlabeled cells (PMID: 31754028); in vivo/in vitro functional neutralization (PMID: 22412855; PMID: 30479344; PMID: 35186922; PMID: 25029243; PMID: 31042165); validated by detecting mouse Neogenin by Western and IHC (R&D Systems); IHC (PMID: 33740419; PMID: 23457482); in vitro FACS antibody titration (this study, Extended Data Fig. 5c-h), FACS secondary antibody co-labeling on HSCs (this study, Extended Data Fig. 5n-s), and in vivo functional dose-response relationship (this study, Extended Data Fig. 5i-m).

Extensive additional characterization of antibodies was performed in this study: To identify anti-CD150 antibodies that are not blocked by anti-CD150 antibody clone 1 (TC15-12F12.2, TC15), bone-marrow HSPC stained cells were incubated with saturating concentrations (200ug/mL) of unlabeled anti-CD150 antibody clone TC15 and then stained with PE-conjugated anti-CD150 clones 2 (Q38), 3 (9D1), or 4 (mShad150); PE-Cy7 conjugated anti-CD150 clone TC15 was used as a control. To confirm if any anti-CD150 clones identify the same population of cells as anti-CD150 antibody clone 1 (TC15) by flow-cytometry, bone-marrow HSPC stained cells were incubated with PE-Cy7 anti-CD150 antibody clone 1 (TC15) and with either PE-conjugated anti-CD150 clone 2 (Q38), 3 (9D1), or 4 (mShad150). To confirm that anti-CD150 antibody clone 4 (mShad150) does not block anti-CD150 clone 2 (Q38), bone-marrow cells were incubated with saturating concentrations (200ug/mL) of unlabeled anti-CD150 clone mShad150 and then stained with PE-conjugated anti-CD150 clone Q38; PE-Cy7 conjugated anti-CD150 clone mShad150 was used as a control. To confirm that anti-CD150 clone mShad150 and clone Q38 identify the same populations by flow-cytometry, bone-marrow cells were incubated with PE-Cy7 anti-CD150 clone mShad150 and with PE anti-CD150 clone 2 (Q38).

To confirm that mouse IgG2a (SB115d; SouthernBiotech) and IgG2b (SB115h; SouthernBiotech) anti-goat antibodies do not block donkey anti-goat IgG AF488 (abcam; ab150129), bone-marrow HSPC stained cells were incubated with saturating concentrations (100ug/mL) of unlabeled mouse IgG2a (6158-01; SouthernBiotech) or IgG2b (6157-01; SouthernBiotech) anti-goat antibodies and then stained with donkey anti-goat AF488. To confirm that mouse IgG2a and IgG2b anti-goat antibodies identify the same populations as donkey anti-goat IgG AF488 by flow-cytometry, bone-marrow HSPC stained cells were incubated with mouse IgG2a AF555 (6158-32; SouthernBiotech) or IgG2b PE (6157-09; SouthernBiotech) anti-goat antibodies, and with donkey anti-goat AF488.

## Eukaryotic cell lines

Policy information about [cell lines and Sex and Gender in Research](#)

Cell line source(s)	Mus dunni cells, originally derived from an adult female <i>M. dunni</i> animal (PMID: 6092693), were used for in vitro experiments. The Mus dunni cells used in this study were obtained from ATCC (American Type Culture Collection).
Authentication	The Mus dunni cells were obtained from American Type Culture Collection (ATCC) and were not independently authenticated beyond the identity provided by ATCC.
Mycoplasma contamination	The Mus dunni cells used in this study tested negative for mycoplasma contamination upon receipt from ATCC.
Commonly misidentified lines (See <a href="#">ICLAC</a> register)	No commonly misidentified cell lines were used in this study.

## Animals and other research organisms

Policy information about [studies involving animals; ARRIVE guidelines](#) recommended for reporting animal research, and [Sex and Gender in Research](#)

Laboratory animals	All mice were C57BL/6 or (C57BL/10×A.BY)F1 (H-2b/b, Fv1b, Rfv3r/s) and between 8-weeks to 120-weeks old. For transplant experiments, C57BL/6J (Jackson Labs, Strain #000664) CD45.2 mice were donors and B6.SJL-Ptprca Pepcb/BoyJ (Jackson Labs, Strain #002014) CD45.1 mice were recipients. Mice were bred and maintained at Stanford University's Research Animal Facility or at the Rocky Mountain Laboratories. All animal experiments were performed according to guidelines established by the Administrative Panel on Laboratory Animal Care of Stanford University or on an Animal Study Proposal approved by the Animal Care and Use Committee of the Rocky Mountain Laboratories (RML 2018-058, RML 2021-046) and carried out by certified staff in an Association for Assessment and Accreditation of Laboratory Animal Care International-accredited facility according to the institution's guidelines for animal use, the basic principles in the NIH Guide for the Care and Use of Laboratory Animals, the Animal Welfare Act, and the United States Department of Agriculture and the United States Public Health Service Policy on Humane Care and Use of Laboratory Animals. Mice were housed in individually ventilated cages, same-sex, on a 12-hour light cycle, with temperature and humidity control, enrichment material, and ab libitum rodent chow and water.
Wild animals	No wild animals were used in this study.
Reporting on sex	All experiments were conducted with sex-matched animals, without bias to either sex. Sex-based analysis was not performed.
Field-collected samples	No field-collected samples were used in this study.
Ethics oversight	All animal experiments were performed according to guidelines established by the Administrative Panel on Laboratory Animal Care of Stanford University or on an Animal Study Proposal approved by the Animal Care and Use Committee of the Rocky Mountain Laboratories.

Note that full information on the approval of the study protocol must also be provided in the manuscript.

# Flow Cytometry

## Plots

Confirm that:

- The axis labels state the marker and fluorochrome used (e.g. CD4-FITC).
- The axis scales are clearly visible. Include numbers along axes only for bottom left plot of group (a 'group' is an analysis of identical markers).
- All plots are contour plots with outliers or pseudocolor plots.
- A numerical value for number of cells or percentage (with statistics) is provided.

## Methodology

### Sample preparation

Mouse bone marrow cells: mice were euthanized and bone marrow harvested following one of two methods. The unilateral or bilateral femurs, tibias, and pelvises were dissected, cleaned, and collected in a mortar bowl containing PBS supplemented with 2% FBS (FACS-buffer) and 1mg/mL DNase-I (LS002007; Worthington). Bones were crushed, and the resulting cell suspension was passed through a 40um filter. Alternatively, the femurs and tibias were dissected, cleaned, and cut at the joints and the bone marrow was flushed using an inserted 25-gauge needle and phosphate-buffered balanced salt solution (PBBS) with cells passed through a 100um filter. Cells were collected by centrifugation and washed with FACS-buffer multiple times. Red blood cells were depleted by ACK-lysis or by cKIT enrichment. For ACK-lysis, cells were resuspended in 1mL ACK Lysing Buffer (A1049201; ThermoFisher) and incubated for 10 minutes at room-temperature for 10 min. For cKIT enrichment, cells were Fc-blocked by incubation with 1mg/mL rat IgG (ab37361; abcam) for 30 minutes on ice, followed by the addition of anti-cKIT APC-eFluor780 (47-1171-82; ThermoFisher) for 30 minutes. Cells were collected by centrifugation and resuspended in FACS-buffer containing 10uL anti-APC MicroBeads (130-090-855; Miltenyi Biotec) and incubated for 20 minutes on ice. Cells were then washed and isolated with LS Columns (130-042-401; Miltenyi Biotec) using a MACS Separator (Miltenyi Biotec) according to manufacturer instructions, and then stained for flow cytometry as indicated in the methods section. For erythroid cell analysis, spleen cells were first incubated for 30 min with mAb 34, a mouse IgG2b specific for the FV glycoGag protein expressed on infected cells, then stained with anti-mouse IgG2b FITC (BD; 553395) and anti-Ter119 PE-Cy7 (Invitrogen; 25-5921-82).

For HSC transplant experiments, 100 total HSCs (KLS FLT3–CD34–CD150+) were FACS-sorted from CD45.2 aged control mice, or CD45.2 aged mice that received antibody-conditioning 9 days earlier and injected retro-orbitally into 2-month-old recipient CD45.1 mice together with 1x106 whole-bone marrow CD45.1 support cells in 100uL PBS. Recipient mice received split-dose irradiation 24 hours prior to transplantation with 2 doses of 4.5Gy 4 hours apart. For chimerism analysis, peripheral blood was collected from the facial vein. HSC-derived donor cells were identified based on CD45.2 expression and host recipient cells were identified based on CD45.1 expression.

Human bone marrow cells: bone marrow mononuclear cells from young-adult donors (ages 26-33) were commercially obtained (AllCells, Inc.). CD34-positive cells were enriched with CD34 MicroBead Kit (130-046-702; Miltenyi Biotec) according to manufacturer instructions, and then stained for flow cytometry as indicated in the methods section.

Mouse blood cell isolation: mouse peripheral blood was collected in EDTA tubes after removal of cells through centrifugation at 500 RCF for 10 min and red blood cells were depleted with ACK-lysis, followed by a PBS wash, and then stained for flow cytometry as indicated in the methods section.

### Instrument

Flow-cytometry was performed on a FACS Aria II (BD Biosciences) or FACS Symphony (BD Biosciences) at Stanford University or at the Rocky Mountain Labs.

### Software

Flow cytometry data was collected using FACSDiva Software (BD) and analyzed with FlowJo v10.8 Software (BD Life Sciences). Flow-cytometry computational analysis was conducted with the Spectre package (PMID: 33840138) using R version 4.2.2.

### Cell population abundance

Cell population abundances are provided in the figures depicting gating strategies. For RNA-seq of purified HSCs, cells were directly sorted into lysis buffer. To evaluate sort purity, independent pilot experiments using the same gating strategies were conducted with post-sort purity of approximately 90%.

### Gating strategy

FACS gating strategies for analysis are supplied in Extended Data Fig. 2a (mouse HSPCs), Extended Data Fig. 8a–c (T cells), Extended Data Fig. 8d–e (B cells), Extended Data Fig. 8g–i (mature/progenitor B cells), Extended Data Fig. 8j–l (mature myeloid cells), Extended Data Fig. 9b (Ter119+ and Ag34-infected cells), and Extended Data Fig. 10g–h (human HSCs and HPCs). FACS gating strategies for cell sorting are supplied in Extended Data Fig. 3m–n (total HSC: Aged vs. Aged +Conditioning). Population definitions are stated in the manuscript main text or methods. For analysis of human HSCs, for some antibodies the gating was determined by fluorescence-minus-one (FMO). For analysis of candidate mouse or human myeloid cells, fluorescence-minus-one (FMO) controls were used to define gates. For erythroid/infected cell analysis, cells from uninfected controls were used for gating strategy. Previously published gating strategies were used and referenced to define and analyze mouse HSCs and HPCs (PMID: 33236985; PMID: 31754028; PMID: 26863982; PMID: 22123971), T cells (PMID: 31457092), B cells (PMID: 10429672; PMID: 21562046; PMID: 23410004; PMID: 33639971), and human HSCs (PMID: 22123971; PMID: 19180077). For peripheral blood chimerism analysis, donor cells were identified based on CD45 expression and host recipient cells were identified based on CD45.1 expression; Myeloid cells were defined as CD11b+CD19-CD3- cells and Lymphoid cells were defined as CD19+ or CD3+ (PMID: 31754028)

- Tick this box to confirm that a figure exemplifying the gating strategy is provided in the Supplementary Information.